JCU ePrints

This file is part of the following reference:

Villarreal Albitres, William F. (2005)
An experimental investigation into the effect of interface friction on bagasse compaction between grooved steel platens.
Masters (Research) thesis, James Cook University.

Access to this file is available from:

http://eprints.jcu.edu.au/2113

JCU
JAMES COOK UNIVERSITY

An Experimental Investigation into the Effect of Interface Friction on Bagasse Compaction between Grooved Steel Platens

Thesis submitted by

William F. Villarreal Albitres

BE (Mech.), Universidad Nacional de Trujillo, Perú

in May 2005

for the degree of Master of Engineering Science
in the School of Engineering (Mechanical Engineering)
James Cook University

Statement of Access

I, the undersigned, author of this work, understand that James Cook University will make this thesis available for use within the University Library and, via the Australian Digital Theses network or other means, for use elsewhere. All users consulting this thesis will have to sign the following statement:

> *In consulting this thesis I agree not to copy or closely paraphrase it*
> *in whole or in part without the written consent of the author; and*
> *to make proper public written acknowledgement for any assistance*
> *that I have obtained it*

Beyond this, I do not wish to place any restriction on access to this thesis

04 May, 2005

_____   _____

William F. Villarreal A.   *Date*

Statement of Sources

DECLARATION

I declare that this thesis is my own work and has not been submitted in any other form for another degree or diploma at any university or other institution of tertiary education. Information derived from the published or unpublished work of others has been acknowledged in the text and a list of reference is given

04 May, 2005

_____   _____

William F. Villarreal A.   *Date*

Acknowledgements

Abstract

Modern factory crushing units process prepared sugar cane through sets of counter-rotating grooved rolls. A typical unit in Australia would process in excess of 600 tonnes of material per hour. Throughput and extraction performance is strongly dependent on material behaviour, the geometry and surface condition at the roll bagasse interface. Factories use welding procedures to arc roughen the tips of grooves in an effort to increase friction. Although industry procedures appear ad hoc it is clear that some level of roughness is crucial to performance. A similar statement can be made in respect to roll grooving given the wide variation in adopted practice. This project involved an experimental investigation into the effects of interface friction on bagasse compaction between grooved steel platens. An apparatus was developed for use in the SOE MTS testing facility. A factorial design experiment involving 105 tests randomised in blocks was conducted to discover the interaction between friction (the dependent variable) and groove angle, compaction, and roughness (independent variables). The results indicate that roughness, groove angle and compaction significantly affect friction coefficient. While roughness and groove angle contribute to increase friction coefficient, compaction causes a marked decrease. Observations on samples of bagasse exhibiting pure shear suggest that the frictional forces generated at the interface cannot be sustained by the shear strength of bagasse. Comparisons between friction coefficient and shear coefficient showed that the friction coefficient values approach the shear coefficient values under particular geometric and loading conditions. An empirical model was developed to explore variables. The effect of groove angle, degree of roughness (location and size of roughened asperity) and sample compaction on friction has been ascertained.

Contents

Tables

Figures

Symbols

A	Cross-sectional area
A_a	Apparent area
A_t	true area
C	Variable compaction
C_c	Compression ratio
C_f	Filling ratio
D	Roller diameter
D_m	Mean Diameter
E	Elastic modules
F	Force
F_c	Compressive force, yield function in cap region
F_n	Normal force
FR	filling ratio
F_s	Yield function in Drucker-Prager shear region
F_t	Tangential force, yield function in transition region
G	Variable groove angle
G_b	Bagasse shear modules
H	Height of bagasse penetration
K	Bulk modulus
K_o	Plasticity constant
L	Length
M	Mass
N	Reacting normal force
N_s	Number of responses
N_x, N_y	Reacting normal force components
R	Variable roughness, experimental parameter
R_a	Average roughness
R_q	Root mean square
R_x, R_y	Reacting forces components

T	Time
V_f	Volume of fibre
V_j	Volume of juice
V_o	Initial no gas volume of cane
W	Gravitational force
c	Cohesion coefficient
c_w	Cohesion coefficient on the wall
d	material cohesion
$d_{\tau'}$	Shear stress differential
d_{γ}	Shear strain differential
$d_{\sigma'}$	Normal stress differential
d_{ε_v}	Volumetric strain differential
$d\tau'$	Differential of shear strain
$d\sigma'$	Differential of normal stress
$\dot{e}$	Shear strain of liquid film
f	Fibre fraction
f_a	Friction force due to adhesion
f_f	Frictional force
g	Acceleration due to gravity
h	Height of asperity
h_d	Hardness
h_m	Height of bagasse blanket
i	initial condition
k	Number of levels
m_f	Final mass of prepared cane or bagasse
m_i	Initial mass of prepared cane or bagasse
p	Hydrostatic pressure
q	Von Mises equivalent stress
s_t	Tangential speed
υ	Peripheral speed
w	Work opening
α	Angle of nip, cap transition parameter

α_a Asperity angle

α_i Initial contact angle

$\hat{a}$ Treatment number

β Neutral plane angle, internal friction coefficient

λ Specific density

γ Compaction

γ_{bss} Bagasse shear strain

γ_{zx} Engineer's strain

$\dot{\gamma}_f$ Liquid film shear strain

δ Displacement differential

ε_e Elastic strain

ε_p Plastic strain

ε_v Volumetric strain

$\varepsilon_{xz}, \varepsilon_{zx}$ Pure shear strain

ζ Asperity tip radius

η Angle of an inclined wall

θ Groove angle

θ_s Shear plane angle

μ Friction coefficient

μ_{pp} Porous pressure

μ_s Static friction

μ_w Friction coefficient on the wall

v Specific volume

π Dimensional product

ρ_c Density of cane

ρ_f Density of fibre

ρ_j Density of juice

ρ_o No gas density of prepared cane

σ Total normal stress

σ' Normal effective stress

σ_Y Yield stress

$\sigma_x, \sigma_y, \sigma_z$ Normal stress components

$\sigma_1, \sigma_2, \sigma_3$ Normal stress components

σ_{sd} Standard deviation of asperities heights

τ, τ' Shear stress

τ_1, τ_2, τ_3 Shear stress components

τ_w Shear stress on the wall

τ_{xy}, τ_{yx} Internal shear stress

ϕ Angle of friction

ϕ_w Angle of wall

ϕ' Effective angle of internal friction

ψ Plasticity index.

1

INTRODUCTION

Abstract: This chapter presents the nature and scope of the problem being investigated. The existing literature and the recent investigations into the mechanics of cane crushing suggest that interface friction is an important parameter influencing mill feeding and dewatering. This chapter provides an overview of the rolling process, an introduction to the possible ways in which friction might influence rolling behaviour, the potential significance of the research, the aims and objectives, and the thesis layout.

1.1 Overview

Over recent years researchers have developed a more thorough understanding of the underlying mechanisms governing the dewatering of prepared cane and bagasse. It has been found that to dewater bagasse efficiently between grooved rolls, it is important to minimise the shear strain while maximizing the volumetric strain within the bagasse. This suggests that roll groove geometry maybe important to milling. Roll roughness (hard asperities on the top and flank of the grooves) is used as a routine practice by the majority of modern factory crushing units to improve mill feeding into the entry region of the roll and maximise the dewatering process of the crushed material. This means that in a rolling environment if the roll surface does not have enough friction, the crushing rate might not be achieved or energy from the roll might not transfer to the blanket in order to carry out the process of dewatering. This process of expression of liquid through grooved rolling involves complicated fibro-porous mechanics. The compressive force applied through a pair of rollers to a material undergoing a reduction process not only generates complex frictional forces acting on the grooved roller surface, but the compressive force also generates stresses and strain in the material. In the last forty years, many investigators (Bullock, 1957; Murry, 1960; Cullen, 1965; and Plaza, 1994) have conducted experiments into interface friction using smooth platens with bagasse. The important variables in their experiments were level of preparation, pressure on the material, and rubbing speed. However, no research has been undertaken on the surface texture of the groove profile. Clearly, this would seem to be important to the effectiveness of the frictional interface. In practice there are a multitude of groove profiles used by industry across the world but no clear adoption strategy for roll roughness. It is worth noting that when saturated bagasse penetrates radially into a grooved roller, juice escapes from a region of high pressure deep inside the bagasse to a region of lower pressure near the roots of the grooves (Kauppila, 2003). Hence, during the rolling process the boundary condition between the bagasse and the roll surface evolves as a function of spatial position. The classical friction coefficient equation given by Coulomb (Williams, 1994) is insufficient to evaluate acting frictional forces at roll groove interface, as shown Figure 1.1. To improve the performance of the mill from the viewpoint of interface friction, an exploration and measurement of frictional stresses in a roughened grooved rolling environment is required. Bullock (1957) and Murry (1960) compressed bagasse samples uniaxially against a smooth rubbing steel surface. Cullen

(1965) adopted a conventional soil shear box to undertake similar experiments. More recently, Plaza (1994) conducted experiments to determine the effect of the texture of a groove surface on the friction coefficient, using small asperities. Despite this progress in the identification of the variables involved at the interface friction, none of the researchers have determined the effect of the compacted bagasse between grooved surfaces. Bagasse compaction changes along the compressive arc of the roller. Furthermore, there is a need to understand in depth the behaviour of roughened groove surface extending Plaza's (1994) work by including texture of wider dimensions and groove angles.

1.2   Description of the rolling process

Prepared sugar cane or bagasse consists of insoluble fibro-vascular bundles and pith (fibre or fibrous skeleton), liquid in broken and unbroken cells, and a small amount of colloidal water, which is chemically adhered to the fibre. All of these components are assumed to be randomly distributed within the prepared cane or bagasse, and are fed into the crushing unit (Figure 1.1).
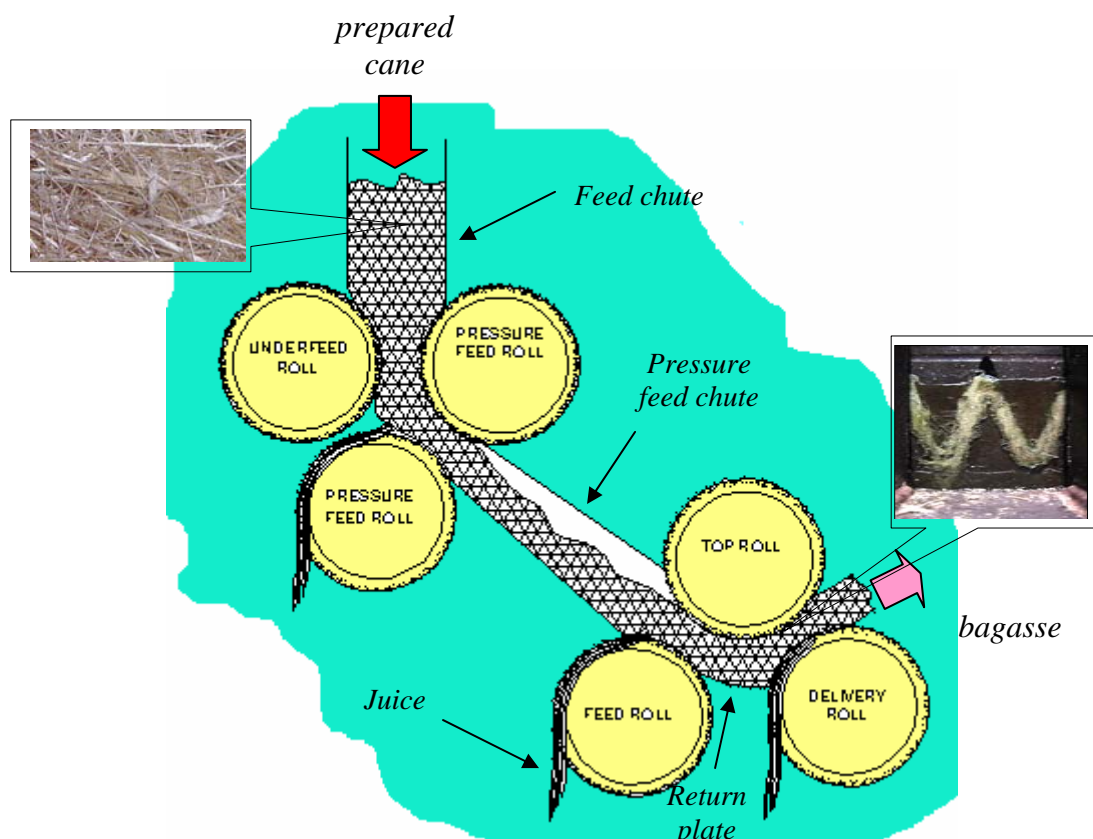
Figure 1.1 *Typical arrangement of a roughened six-roll mill of a crushing unit.*

The material is compressed between counter rotating grooved rolls forcing liquid expression. The compression process is dynamic and violent and some rupturing of unbroken cells may also occur. The liquid expelled is called juice, which is composed of water, sucrose and other insoluble solids. The fibre and cells, which form a porous medium, move forward due to tangential frictional forces generated on the grooved roller. Not all the extracted liquid from the solid fibrous medium is drained away; part of it adheres to the fibre and intact cells. Some flow of liquid through the minimum opening between the rolls may also take place. The material leaving the rollers, the bagasse, is semi-saturated, composed of fibre, soluble solid and liquid (mechanically attached to the fibre). Water or diluted juice is added to the exiting bagasse to assist with removal of the juice attached to the fibre. This process occurs in grooved multi-roller mills and is repeated at five or six milling units along the milling train, extracting roughly up to 97% of the sucrose in the prepared cane.

1.3   Grip and deformation of bagasse by grooved rollers

Bagasse can be defined as a soft, deformable and highly compressible fibrous material which contacts with a rigid surface in the presence of liquid and voids. When bagasse is gripped by the rollers, it quickly becomes saturated and undergoes high volumetric strain resulting in changes in shape and volume. As crushing continues, radial forces cause the material to penetrate deep into the grooved surface. Figure 1.2 shows a photograph of a uniaxial experiment undertaken by Kauppila (2003) in which he attempted to simulate the rolling process. It can be seen that the bagasse is tightly packed against the tips of the teeth and loosely distributed in and around the root region. Juice drainage will be clearly affected by local compaction, which in turn might be influenced by flank friction.

1.4   Contact mechanism between surfaces

When two engineering surfaces, which take load come into contact some distortions occur on each of them. These distortions may be elastic or may involve some additional plastic, with a consequent change in shape. When the surfaces are subjected to traction load, in addition to normal load, this load may reach a value causing gross sliding to

take place. When this happens the bodies in contact have reached the situation of limiting friction. Internally, two points within the contact zone will undergo tangential displacement relative to points distant from the surface, which move tangentially through an effectively rigid body.
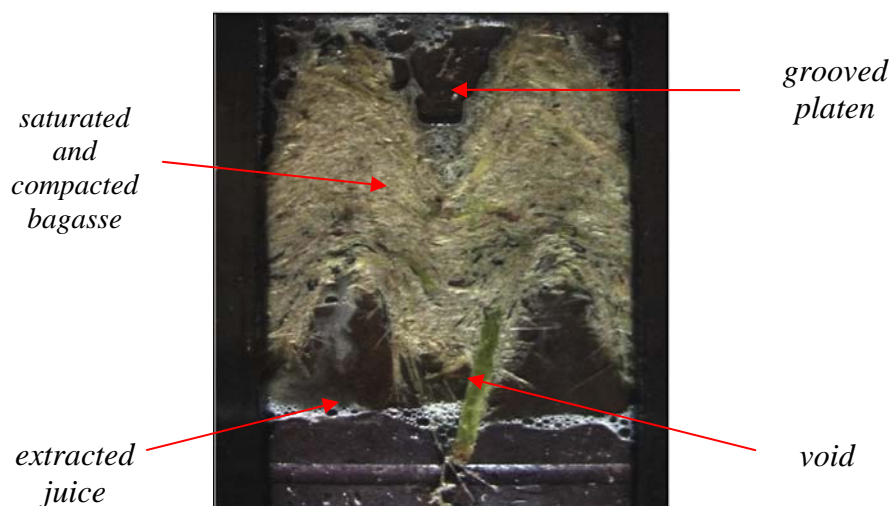
Figure 1.2 *Aspect of the interface friction between bagasse and grooved surfaces (after Kauppila, 2003).*

The sliding mechanism between two bodies in contact has been described by tribologists, among them Williams (1994) and Ludema (1996). They refer to a process of plastic flow and ploughing fracturing of junctions that a soft material experiences in respect to a hard material. The traction values applied to a body will depend on the maximum shear stress at any point of contact, so that some slip is expected if any point cannot sustain that load. From the tribology point of view, the contact mechanism between any two bodies constitutes the basis to describe contact between bagasse and a roller. In a rolling environment, this contact occurs when frictional force generated by compressive load of the roller is of a magnitude greater or at least equal to the its opposite component of the reactive normal force. No limiting friction is reached that the material to drag into the rollers. When bagasse, which is the weaker material in respect to the rollers and with compressible characteristics, is moving towards the exit plane, a combination of normal and shear stresses are presented not only internally, but at the contacted surface. The effect on contact interface between bagasse and a roller have been reported by Murry (1967) and Cullen (1965) with differing opinions. For example, Murry postulated that as the material is moving towards the exit plane, high normal

stresses support the material. At a plane within the compaction region the material experiences sliding due to the fact that it is moving faster. This faster movement causes opposing frictional forces at the interface. On the contrary, Cullen believed that shear strength of bagasse cannot sustain shear forces when the material is under high pressure, accordingly the bagasse fails due to internal stress. This position was supported by Plaza (1994), who reported similar findings.

1.5   The necessity of friction

When prepared cane or bagasse is fed into a mill, the flow of the material is not smooth and this material experiences a retention process as it heads towards the exit. This retention has been attributed to the fact that slipping occurs at the interface. The frictional forces produced are not sufficient to drag the material into the rollers. Furthermore, the mass of material per unit of volume being fed is decreased to the degree that the transference of load through the material is low, causing a decrease in the reduction of bagasse volume. This problem gives rise to a fall both in the capacity of the crushing unit and the dewatering of bagasse.

Bagasse feeding can be increased if friction forces are increased. Frictional forces, under normal stress, depend directly on the friction coefficient generated at the contact surface, without considering the surface area sustaining itself. The methods practised to increase frictional forces have been varied, from the use of chevrons (Hugot, 1986) to artificial roughness on the contact surface (Kroes, 1999). This last method has become a routine practice nowadays, even though its application has not been explained.

1.6   Statement of the problem

Over the last 50 years the majority of Australian sugar mills have largely increased their crushing rate from 65 ton/hr in 1950, to over 550 ton/hr in 2001. This remarkable increase was due not only to the introduction of the roll pressure feeders, but also to the continued increase in friction at the interface, between the bagasse and the grooved roll surface. Up to the present time, Coulomb's laws of friction remain the best engineering parameter to describe the friction coefficient between two perfectly smooth and clean bodies in contact with each other. Coulomb's concepts allow a useful approximation

and give numerical answers when pure sliding is possible. At a macroscopic level, however, Coulomb's laws do not adequately explain interface friction in a typical sugar mill-rolling environment, where the interface between the roller and bagasse depends on factors such as the geometry of the groove, surface topography, prepared cane, and operational condition of the rollers. For example, Coulomb predicts an increment of frictional forces as reactive normal forces increase. This prediction, however, is poor for bagasse and roller contact, because these frictional forces actually decrease (Cullen, 1965).

So effectively Coulomb's model is not able to describe the relation between the friction coefficient and the variables involved when bagasse makes contact with the rollers. This has motivated researchers to investigate the relevant variables involved at the interface friction. When the feeding material does not move smoothly along the compression region between the rollers, but undergoes a hold-up at any plane, this gives rise to less mass being fed into the crushing unit. It has been reported that pressure exerted on the material, rubbing, the groove angle and the degree of comminution are variables which influence the friction coefficient (Bullock, 1958; Cullen, 1965). Although important progress has been made in determining the variables causing the friction coefficient changes, no investigation has been conducted to determine the effect of the compacted bagasse between grooved surfaces. The compaction of the material changes from the time it is gripped until it escapes. For example, compaction level of the order of 400-500 kg/m^3 is developed at the feed nip, and 800-900 kg/m^3 at the delivery nip (Plaza, 2003).

The effect of the groove angles has been investigated by Cullen (1965). He tested smooth groove angles of 45°, 55° and 180° and low depth. Today, there is no study which describes the response of the friction coefficient between 55° and 180°, therefore further investigation is required in order to determine a response of the friction coefficient in a wider range. The routine practice of roughening the roller surface motivated Plaza (1994) to undertake experiments to determine the effect of roughness on the friction coefficient. He reported that there was no significant influence with respect to the size of the roughness on the friction coefficient. This finding is opposite to the generalised belief that roughening the roller surface increases the friction coefficient, a fact reflected in a greater grip of the feeding material. Therefore, Plaza's results need to be extended using grooved platens at different angles and greater depth of the groove. Nonetheless, progress has been achieved modelling the friction

coefficient. For example, the model developed by Bullock (Hugot, 1986) has been used to predict friction to the present day. This model, however, only relates friction as a function of the rubbing speed in a lineal manner. More recently Adam (2004) developed a model of the friction coefficient incorporating pressure on the material and the angle of the roller groove. In spite of this, there is still a need to describe the interface friction by developing a model which relates the texture of the surface and compaction of the material, variables which have not been investigated.

1.7　The significance of this research

The investigation into the interface friction will not only permit a better understanding of the mechanism governing frictional forces between bagasse and a grooved surface, but will have direct application to both the sugar industry and computational and experimental modelling. For example, a proper combination of the variables at the interface may lead to maximising the friction coefficient value. Maximising the friction coefficient value will improve gripping of the feeding material without requiring additional machinery and, consequently, improve throughput at the crushing station. Furthermore, the development of an empirical model which relates the texture, geometry of grooved surface and bagasse compaction may allow the prediction of the friction coefficient for engineering design.

1.7.1　The requirement for the sugar industry

An investigation of the main factors affecting the friction forces at the boundary between prepared cane or bagasse and a roughened grooved surface will enable us to:

1. Determine the variable or variables which significantly affect the interface friction, and the course of the action to take to improve the grip of feed material into the roll nip.

2. Identify the type of asperity needed to roughen the flank of a grooved surface in order to improve throughput and reduce maintenance costs.

3. Maximise the friction coefficient by optimising the main factors affecting the interface friction.

4. Maximise the dewatering of bagasse, thereby identifying the type of grooved surface to be used in the milling units.

1.7.2 The requirement for computational and experimental modelling of cane crushing

Using computer modelling to establish the relationship between numerical and empirical modelling, researchers at James Cook University (JCU) and the Sugar Research Institute (SRI) have investigated the fundamental properties of bagasse between grooved surfaces, to numerically reproduce observed responses in a two-roll mill. Numerical reproduction of the observed responses in a two roll-mill can be carried out without having to resort to expensive and many times difficult collection of data. The modelling of the interface friction will enable researchers to:

1. Validate the mathematical models of the contact surface, in order to simulate movement of the material along the compression region and measure the stresses generated.

2. Solve problems involved with throughput, extraction performance, and experimental modelling.

3. Simulate the alignment of fibres of the compressed material along the profile of the teeth as a function of the friction coefficient, particularly on roughened grooved elements.

4. Predict, for engineering design, the energy required to drag the material into the roller, as a function of the texture and geometry of the roller surface.

1.8 Thesis objectives

The importance of friction on mill feeding and dewatering can not be understated. This thesis will explore a range of variables expecting to directly influence friction at the boundary between bagasse and steel platens.

The specific objectives are as follows:

1. To determine the effect of roughness, compaction, and groove angle on the frictional forces at the boundary between grooved steel platens and compacted bagasse.

2. To quantify the magnitude of the static and kinetic friction coefficients at the boundary between grooved steel platens and bagasse.

3. To identify the size of asperity to roughen the flank or grooved surface, which will minimise maintenance costs.

4. To develop an empirical model which correlates the dependency of the frictional forces with the geometry of the groove and the level of compaction of the material.

5. To conduct observations of the directional properties of fibre in the vicinity of the grooved flank which is affected by the roughened groove surface.

1.9   Thesis outline

This thesis is laid out in the following manner:

Chapter 2 is devoted to reviewing the fundamental mechanisms affecting conventional sliding in a rolling environment. The frictional forces acting at a contact surface and stresses generated when bagasse is compacted are explained. A brief description of the nature of a surface is also given. The method used to determine roughness on a grooved surface is described. The last part of Chapter 2 contains a dimensional analysis of variables which has been included, even though the results of the analysis are not used in the rest of this thesis. It is anticipated, however, that the results may be of use to other researchers in this general field.

In Chapter 3, a literature review of experimental investigations into interface friction between bagasse and grooved steel platen is presented. This Chapter also deals with the specification of a suitable empirical model.

The research method used in this investigation is detailed in Chapter 4. Firstly, the materials and apparatus are described. Secondly, the factorial experiment design and the

restrictions found to randomise the experiment are outlined. In the last section of Chapter 4 the method and design used to develop the empirical model is explained.

Chapter 5 contains the experimental results. These results correspond to both the friction coefficient and dewatering of bagasse. Furthermore, this chapter presents the empirical model developed and the simulations for maximising the friction coefficient value by optimising the three independent variables.

Chapter 6 is mainly devoted to interpretation and discussion of the results.

Finally, Chapter 7 provides conclusions and makes recommendations for future research in the field.

2

LITERATURE REVIEW

Abstract: Friction in a rolling environment is essentially concerned with frictional forces on contact surfaces and stresses produced inside the feeding material being compressed. This chapter deals with the revision of the physical structure and the nature of prepared cane bagasse, respectively. The basic principle of the friction coefficient, its generation, and distribution at the interface between bagasse and a grooved surface are also mentioned. A brief description of topology of a surface is described to quantify the texture of a roughened roller surface. This chapter also includes the theory of dimensional analysis as a tool to determine a priori the likely relation between the friction coefficient and factors affecting the interface.

2.1 The physical structure of prepared sugar cane and bagasse

For the purpose of this thesis sugar cane is defined as chopped cane or billets between 20-50 mm in diameter and 150-300 mm in length. The material is assumed to be free of dirt and other foreign debris.

2.1.1 The nature of prepare cane

Prior to crushing the cane billets are processed through a heavy swing-hammer shredder which fragments the material into filaments between 0.2-1.0 mm in width and 20-50 mm in length. The shredded material is called prepared cane and can be defined as a quasi-three phase material consisting of a fibrous skeleton (solid phase), separated by spaces or voids which are filled with liquid and air. The skeleton is highly compressible and saturated (Owen, 1994). The level of comminution is considered an important factor which influences the cane crushing process. Several investigators have attempted to quantify the level of comminution of prepared cane. For example Murry (1960) measured the bulk density under a light axial pressure. Loughran (Kannapiran, 2003) extended Murry's techniques by accounting for the fibre effect on bulk density. Loughran's model correlates the compression ratio, C, at 50kPa in a precompressor with the fibre, f. The empirical relation is

$$\bar{a} = \frac{1}{C} - 6.3f \qquad (2.1)$$

where

$\bar{a}$ is the treatment number

C is compression ration, kPa, and

f is the fibre content.

and a treatment number of 0.4 corresponds to finely prepared cane and 1.1 very coarse material. While Loughran's treatment number appears to fit the experimental data reasonably well, the technique has not been adopted by Australian factories because it is too tedious. The industry method to quantify prepared cane in Australia factories involves measurement of the percentage of Pol (sucrose) in broken cells, termed

proportion of open cells (POC) (Cullen, 1986). This method suffers from poor repeatability (Loughran, 1990) but it is practical.
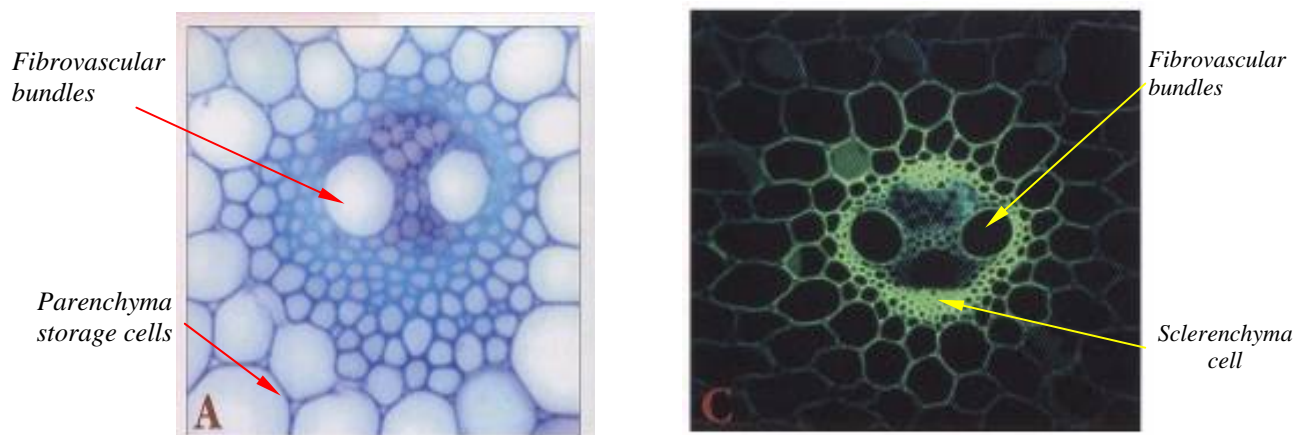
Figure 2.1 *Microscopic view of a vascular bundle in a sugar cane stem (Gambley, 2003).*

Solid fibre consists of fibro-vascular bundles and pith (Figure 2.1). The fibrous skeleton is considered very compressible, but individual fibro-vascular bundles are "quite" incompressible. The average dry density of the fibre is 1530 kg/m^3. Fibre represents 11-16 % of the mass of cane. The liquid is composed of water and soluble solids. It constitutes 74 - 89 % by mass of the prepared cane. The average density of the juice is 1080 kg/m^3. The remaining percentage of bagasse is made of soluble and insoluble solids.

2.1.2 The nature of bagasse

Bagasse is the fibrous residue leaving a crushing unit. Characteristic constituents of bagasse are moisture (46-52%), fibre (43-52 %) and soluble solids (0.9-4 %) and the particle size of fibre varies in a similar way to prepared cane. The true fibre (the cylindrical cell of the vascular tissue) and the pith (parenchymatous cells of the inner stalk) have a similar chemical composition, but are morphologically different. The ratio of fibre to pith is roughly 2.5:1. The length is almost 70 times its diameter (Figure 2.2). It can be assumed that the solid phase of bagasse maintains its structural integrity after compression. This implies that there is no inherent damage. However, the fibrous

skeleton is elasto-plastic and suffers significant irreversible damage during compression.
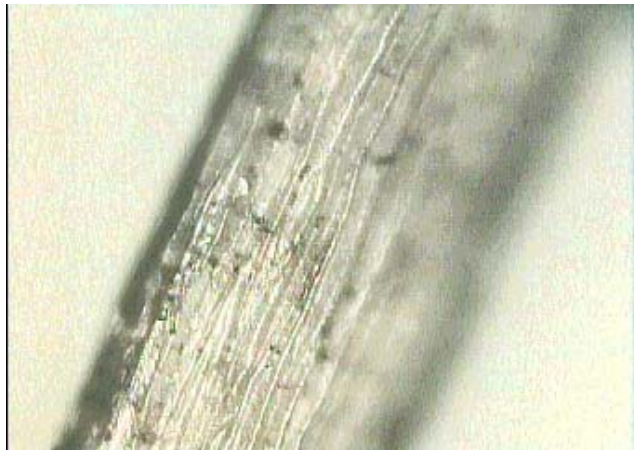
Figure 2.2 Magnification of a fibre element and its surface texture

2.2 The basic physical properties of bagasse

The solid, liquid and gas phases of prepared cane or bagasse have been related in terms of mass and volume as shown in Figure 2.3. The fibre content, *f* is the ratio of the final mass at zero moisture (m_f) to the initial mass (m_i), i.e.

$$f = \frac{m_f}{m_i} \tag{2.2}$$
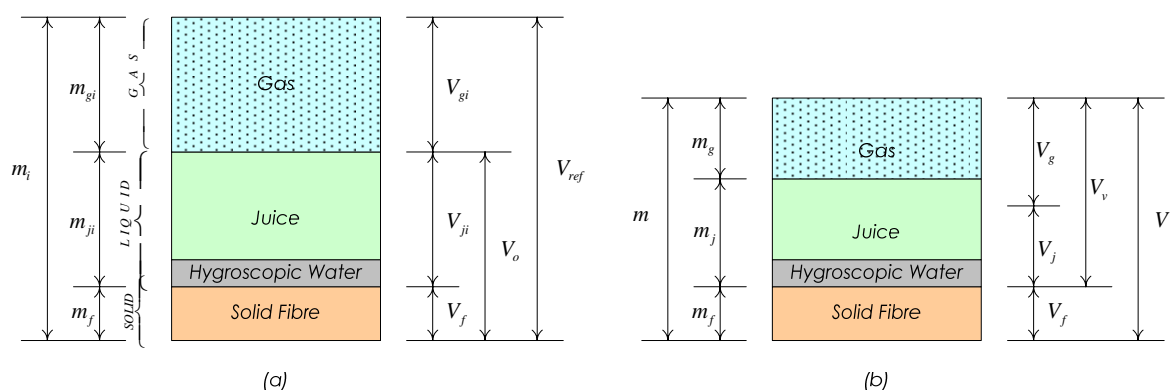
Figure 2.3 Mass and volume components of a prepared cane or bagasse sample:
(a) prior to juice expression at time t=0; (b) at any time during a
compression test (Leitch, 1996).

The initial no gas volume of cane (V_o) is

$$V_o = V_f + V_{ji} \qquad (2.3)$$

where V_f is the volume of fibre (constant), and V_{ji}, initial juice volume in sample. The no gas void density of prepared cane (ρ_o) is expressed by

$$\rho_o = \frac{m_i}{V_o} = \frac{1}{\dfrac{f}{\rho_f} + \dfrac{(1-f)}{\rho_j}} \qquad (2.4)$$

Following Bullock (1957) the compression ratio (C_c) is defined as the ratio of the no-void volume (V_o) to the instantaneous volume (V) at any time, i.e.

$$C_c = \frac{V_o}{V} \qquad (2.5)$$

The volumetric strain (ε_v) is

$$\varepsilon_v = \frac{V_{ref} - V}{V_{ref}} \qquad (2.6)$$

where, V_{ref} is the sample volume at initial zero strain reference and V is the total volume of prepared cane or bagasse. The ratio of the total volume at any time to the volume of fibre is called the specific volume (v)

$$v = \frac{V}{V_f} = \frac{1}{C_c}\left[1 + \frac{\rho_f}{\rho_j}\frac{(1-f)}{f}\right] \qquad (2.7)$$

where

$$\rho_f = \frac{m_f}{V_f}; \qquad (\rho_f \cong 1530 \ kg/m^3) \qquad (2.8)$$

and

$$\rho_j = \frac{m_j}{V_j}; \qquad (\rho_j \cong 1080 \ kg/m^3) \qquad \textbf{(2.9)}$$

The fibre compaction (γ) is given by

$$\gamma = \frac{m_f}{V} = \frac{1530}{v} \qquad \textbf{(2.10)}$$

where

v is the specific volume.

Some researchers prefer to use the term filling ratio C_F which is defined as the ratio of the compaction to the density of the fibre.

$$C_F = \frac{\gamma}{\rho_f} = \frac{1}{v} \qquad \textbf{(2.11)}$$

Over recent years there has been a considerable research effort applied to understanding of the large strain deformation of prepared cane (Owen, 1994; Leitch, 1996; Adam, 1997; Downing, 1999; Plaza, 2002; Kent, 2004). This research was based on porous media mechanics and the application of isotropic elasto-plastic models for the fibrous skeleton and Darcy's Law for liquid flow. While a great deal of work has been done and researchers now have a better understanding of the governing mechanisms, there is still fundamental question pertaining to the constitutive behaviour of the fibrous material. For example, the saturated fibrous material layers under uniaxial loading, and the assumption of material isotropy is clearly flawed (Adam, 1997).

2.3 Friction theory

2.3.1 The classical definition of friction

The first attempt to understand what friction is dates from the early Egyptians who used liquid lubricants to help slide stones used in their monuments. Early Greek scholars wrote about friction, but did not establish any models or rules to deal with it. Leonardo da Vinci was the first one who in 1495 looked at friction in a scientific manner. He

documented the testing devices he used to conduct studies on friction. These same procedures are used by researchers today. Interestingly, it was Amontons in 1699 and Coulomb in 1785 (Ludema, 1996) who rediscovered and formulated the dry friction laws based on experimental observation. Amontons essentially postulated the first law of friction: friction is proportional to the force applied to an object which has been set in motion. The force applied is independent of its plan contact area. Coulomb investigated the variables affecting friction. He observed that among the variables analysed, the velocity impinged to one of the body in contact did not exert influence on the friction coefficient. The present definition of friction is given as the resisting force tangential to the interface between two bodies when, under the action of an external force, one body moves or tends to move relative to the other. The model developed by Coulomb is

$$F = \mu N \qquad \qquad \textbf{(2.12)}$$

where

F = friction force

μ = proportional constant (friction coefficient), and

N = the reacting normal or downward force on the object to be moved.

If an arbitrary body rests on a flat horizontal surface and there is no motion there will be no friction. The friction coefficient statement represents the one-third relationship proposed by Amontons (Ludema, 1996). It is usually credited as the mathematical expression of the first law of friction; that is, the friction force is proportional to the applied force and independent of the contact area. The resistant force and true contact areas of two bodies in contact are shown in Figure 2.4, when a force is applied. More than 200 years after Coulomb, numerous theories and models have been released in order to express the factors acting at the interface between two bodies in contact. Tribologists (people who deal with the study of the interacting surfaces in relative motion) have claimed that the frictional properties of a given material do not depend only on its intrinsic properties, but also on the manner in which the material is used. They have ascribed the causes of friction to several mechanisms, such as: ploughing of the asperities (peaks), adhesion (atomic bounding between the two surfaces), the nature of the sliding system, and weak film. The latter assumes that sliding occurs between two bodies when the film fails by shear (Budinski, 2002).
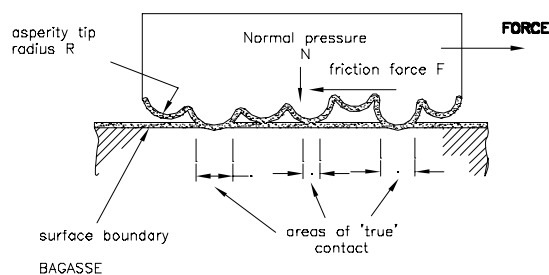
Figure 2.4 *Reacting force generated at the interface of two bodies due to a force applied to one of them (Blencoe & Williams, 1997).*

The friction coefficient, as was formulated by Coulomb, is used routinely today in the engineering profession, despite being affected by the sliding conditions, the geometry of the bodies in contact, lubricant, surface treatment, and environmental conditions.

2.3.2   A description of the contact area between two bodies A and B

There are no topographically smooth surfaces in engineering practice. The problem of relating friction to surface topography, in most cases, is simplified for the determination of the real area of contact and the study of the mechanism of mating micro contacts. The real area of contact between two engineering surfaces constitutes the sum of all micro-contacts created by individual asperities. This area is a tiny fraction of the apparent geometrical areas of contact. Asperities of the bodies are actually the true contact elements on which frictional forces are generated, as shown in the Figure 2.5.
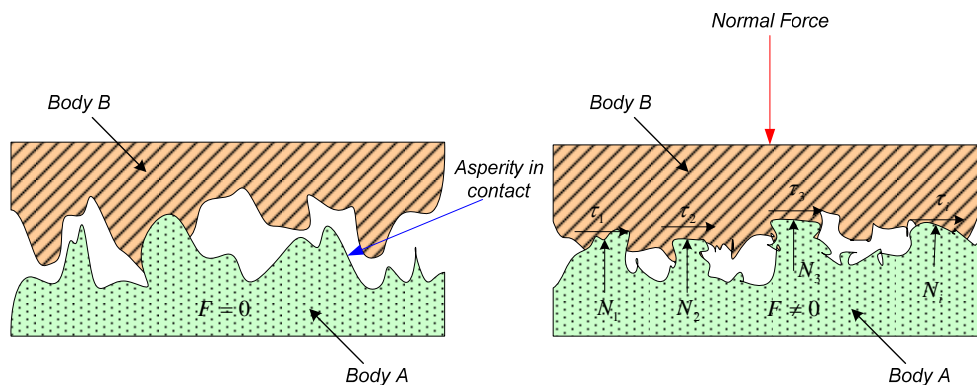
Figure 2.5 *Real contact areas of two bodies before and after the action of a compressive load.*

The contact pressure on the asperities may be so high that plastic deformation may occur in the peaks and valleys of the softer surface, while elastic deformation may occur on the hard surface. The real area of contact will increase as the normal load increases, because of the large strain deformation of the asperities. The usual assumption that the local plastic yield pressure, σ_y, is constant gives the real area of contact for one asperity under a load N_i ($A_i = N_i/\sigma_y$). For metallic materials, the real area of contact is proportional to the load and independent of size. Two bodies will slide if the tangential force acting on the surface of the asperities is enough to cause the shear breaking strength to be unable to sustain such a force. The tangential force is model as

$$f = \frac{\tau A}{\sigma} = \mu N \tag{2.13}$$

where

A = contact area

τ = shear stress

σ = normal stress

N = reacting normal force

f = tangential force, and

μ = the friction coefficient.

Stolarsky (1990) suggests that the magnitude of the real contact area of two metallic bodies under a given normal load is defined through the deformation properties of the material and its surface topography. He developed a model as a function of the hardness, shape, and roughness of the material. According to Stolarsky (1990) the mode of deformation that the material undergoes depends on its mechanical properties and surface topology. Equation (2.14) expresses such a relationship:

$$\psi = \frac{E}{p}\left(\frac{\sigma_{sd}}{\beta}\right)^{\frac{1}{2}} \tag{2.14}$$

where

ψ = plasticity index

E = elastic modules

β = asperity tip radius

p = yield pressure, and

σ_{sd} = standard deviation of asperity heights.

Figure 2.6 suggests that the coefficient of friction for two surfaces in contact is a function of:

- the material properties of the two surfaces in contact
- the relative speed
- the presence of foreign material
- the temperature, and
- the dryness between bodies.

This diversity of values makes the prediction of friction coefficient by a model complex.
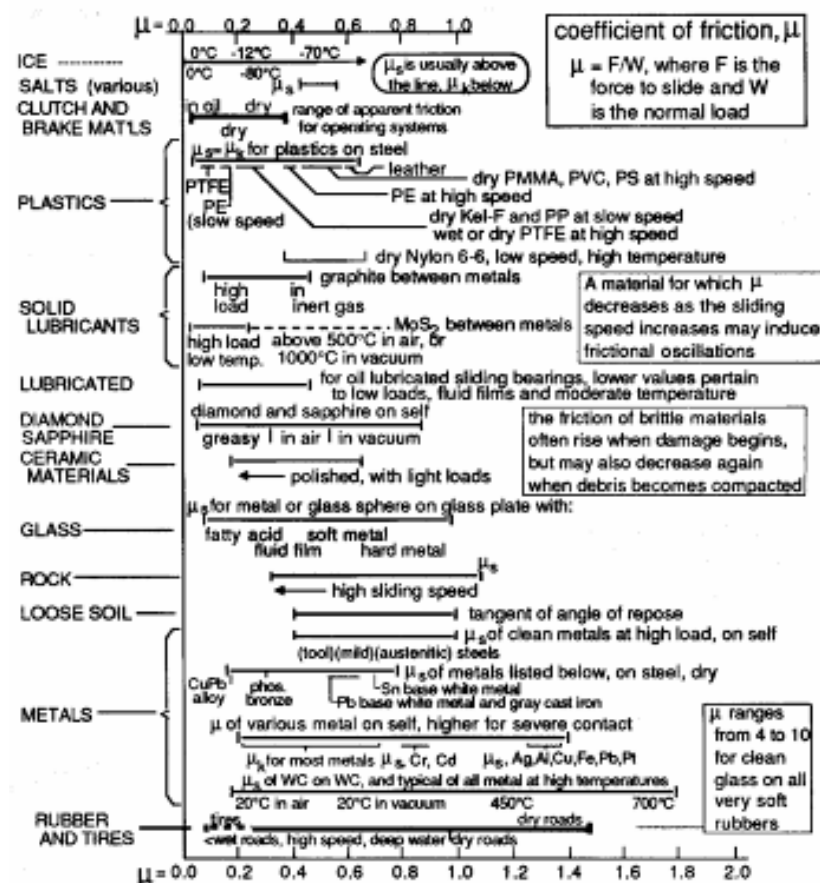
Figure 2.6 *Diversity of friction coefficient values for different materials*

(Ludema, 1996).

2.3.3 The concept of friction angle

Figure 2.7 depicts a body supporting a load F and free to slide on a body B bounded by a stationary horizontal force. Suppose the motion of body A is produced by a tangential force F_t so that the forces exerted by A and B are F_t and the load F_n. Conversely, the forces exerted by B on A are the frictional resistance, f, opposing the motion and the normal reaction N. Then, at the instant when sliding begins, we have by definition.

$$\textit{Static friction coefficient} = \mu = \frac{f}{N} \qquad \textbf{(2.15)}$$

where

μ is the friction coefficient

f is the tangential force, and

N is the normal force.

By combining f with N, and F_t with F_n, and since $f = F_t$ and $N = F_n$, the inclination of the resultant force exerted by body A and body B or vice versa, to the common normal line is given by

$$\tan \phi = \frac{f}{N} = \frac{F_t}{F_n} = \mu \qquad \textbf{(2.16)}$$

The angle $\phi = \tan^{-1} \mu$ is called the angle of friction or more correctly the limiting angle of friction, since it represents the maximum possible value of ϕ at the beginning of motion. The value of ϕ, increases in proportion to the force applied to the body up to its maximum value, a critical point, where it begin to slide. This maximum value represents the limit of the magnitude of static friction, sometimes referred to as starting friction. After sliding has commenced the dynamic force (F_t) required to keep the system in equilibrium is somewhat lower than f. The relation for a minimum possible value is given as

$$\phi_{min} = \tan^{-1} \cdot \mu_{min} \qquad \textbf{(2.17)}$$
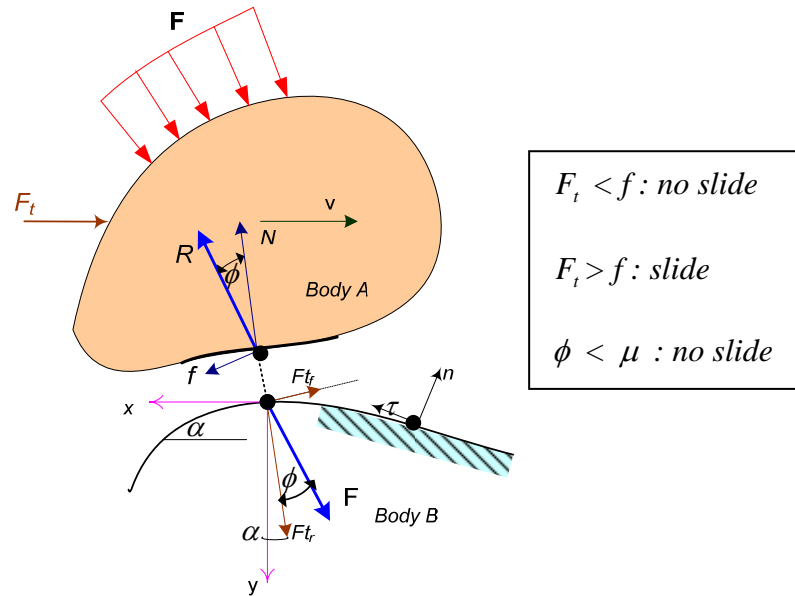
Figure 2.7 *Definition of friction angle.*

2.3.4 Sliding friction

Extensive theoretical and experimental studies have been conducted to explain the nature of the friction mechanism. The most current theories for sliding friction are based on the work performed by Bowden and Tabor (Ludema, 1996). Their friction model assumes that frictional forces have two main sources: adhesion and ploughing. Adhesion is due to the atomic forces acting at the areas of real contacts between surfaces (asperity junction). Ploughing is due to intimate contact between asperities. The asperities penetrate the softer material when a load is applied to one of the bodies. Plastic deformation is initiated when a tangential motion is maintained. Hence the required tangential force to displace material depends on the depth of penetration and the pressure applied. The adhesive interaction, particularly with clean metallic surfaces, is the frictional contact due to the electronic structure of the bodies. Attractive forces at the contact zone cause the cohesive strength of a solid. The adhesion component of friction, μ_a, is given as the ratio of the interfacial shear strength of the adhesive junction, τ , to the yield strength of the asperity material, σ_y , i.e.,

$$\mu_a = \frac{f_a}{N} = \frac{\tau}{\sigma_y} \qquad\qquad (2.18)$$

One of the limitations of the adhesion theory is that it has not been particularly useful for the prediction of real values of μ. For example, adhesion theory does not explain the effect of the surface roughness in friction. The general impression in the technical world is that friction increases when surface roughness increase beyond about 100 micro-inches. Another limitation of this theory is that the load applied to the bodies in contact is light. Friction due to a ploughing mechanism is considered to have occurred when two bodies in contact have a different hardness. The asperity of the harder surface may penetrate into the softer surface and produce grooves if a relative motion occurs. The friction coefficient due to ploughing is modelled as a function of the angle that an embedded asperity makes with a flat surface, i.e., $\mu_{def} = \cot\alpha$. Ploughing may be caused by surface asperities and hard wear particles present in the contact zone. Ploughing has received much attention because of its practical importance; the frictional force produced by ploughing is very sensitive to: the ratio of the radius of curvature of the particle to the depth of penetration.

2.4   Friction in a rolling environment

2.4.1   The bagasse compression mechanism

Figure 2.8 shows the contact mode occurring between a pair of rollers and a fibrous material during crushing. As the material approaches the axial plane, the individual fibro vascular bundles (fibres) in the solid matrix tend to align in a direction orthogonal to the maximum principal compressive stress. At the same time, the material becomes denser causing a marked decrease in its permeability. The solid matrix experiences high stress with fibres being held together by fibre to fibre friction. Deformation of the solid is characterised as elasto-plastic. As far as the liquid phase is concerned, the liquid moves from zones of high compaction to low compaction, dictated by the positive pressure gradient (Adam, 1997). As the compression progresses liquid motion is hindered by the local densification of the fibrous solid matrix.
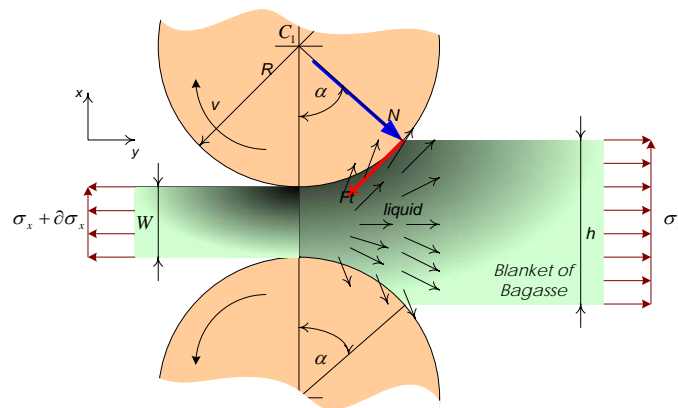
Figure 2.8 *Compression process between fibrous material and a pair of rollers.*

2.4.2 Contact between fibrous material and grooved roller

Rollers are manufactured with circumferential grooves to assist with liquid drainage and frictional grip (Hugot, 1986). Contact between bagasse and the rollers starts on the apex of the groove as shown in Figure 2.9(a). A volume reduction is experienced by the material due to the normal stresses applied. As the pressure increases, the material reduces further in volume. The deformation process is complex and largely irreversible. The compressed material becomes saturated. The fibre undergoes shear and displacement along the profile of the tooth up to the point where the entire flank of the tooth form is embedded in the bagasse (Figures 2.9(b), 2.9(c)).

(a)   *(b)*   *(c)*
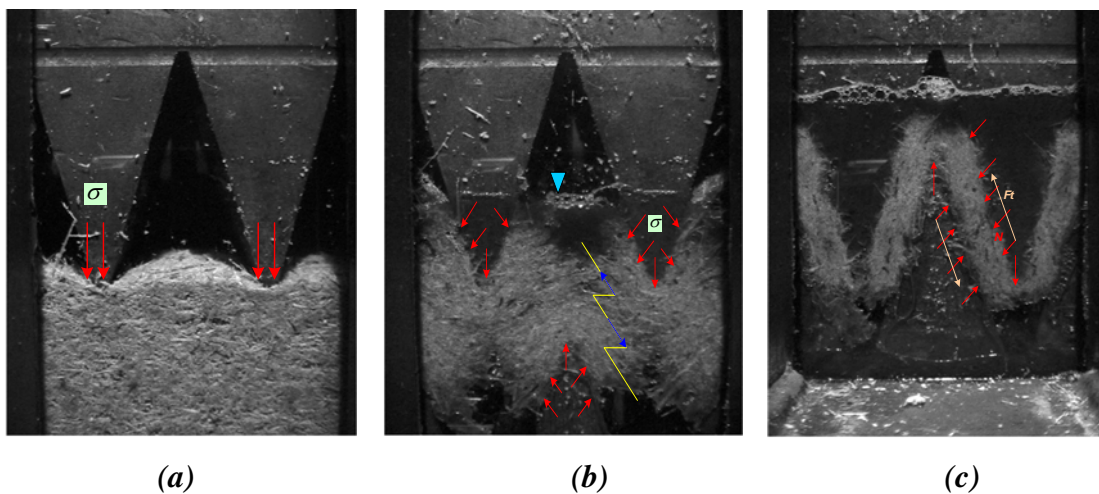
Figure 2.9 *Potential void reduction of bagasse between grooved surfaces*
(after Briton, 2001).

2.4.3 Frictional stress at the interface between bagasse and roller

The total deformation at any spatial position within the fibre depends on both mechanical loading and juice loading in accordance with Terzaghi's principle, if the bagasse is saturated (Yong, 1966). Hence the deformation mechanics for saturated bagasse can be assumed as fully coupled (solid-liquid coupling). The spatial deformation is strongly affected by the evolving boundary conditions (displacement and velocity). Further, the "effective" porosity of the groove flank is not well defined in terms of traditional modelling parlance (i.e., Direchlet or Newman). Clearly, in a fully saturated environment the resistance to liquid flow at the tooth flank will influence the evolution of stress state at the interface. Researchers have not resolved this issue and have tended to simplify the problem by modelling the crushing process as two dimensional plane strains with porous boundary conditions. Consider the 2D schematic shown in Figure 2.10. In a global sense both the compressive load N and the stress σ_x represent the external variables which produce deformation of the material during its passage through the pair of rollers. The distribution of forces acting on the blanket, due to the compressive load of the rollers, permits the analysis of the frictional forces on the rollers.
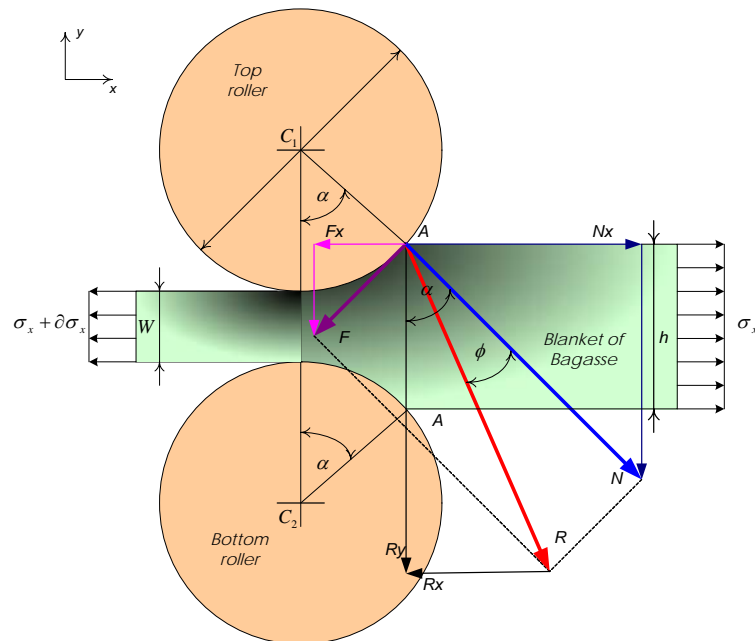
Figure 2.10 *Frictional forces acting in a rolling environment.*
A mean roller diameter is assumed.

It can be deduced that when the horizontal component F_x of the frictional force F is greater or at least equal to the horizontal component N_x of the normal forces, i.e. $N_x < F_x$ positive feeding results. Therefore, the condition required for feeding is $\tan \alpha < \mu$. Murry (1967) theorised that during steady-state crushing conditions, the frictional force F, which acts in the entry zone *AC* of the arc of contact, drags the blanket towards the axial exit of the rollers, as shown in Figure 2.11. At this zone no relative movement of the bagasse occurs in respect to the roller, because the circumferential speed of the roller is higher than the bagasse. As the bagasse moves towards zone CB, the frictional force starts to reduce because the bagasse is moving faster than the speed of roller. The plane at which the two speeds become equal was defined as the neutral plane (Murry, 1967). Cullen (1965) believed that this reduction occurs because the bagasse is sheared by shear stresses rather than slipping on the roll surface. A closer look at the interface between bagasse and a grooved boundary represented by Figure 2.12 allows one to see that frictional forces are acting in spatial dimension during the deformation process. Radial forces, *N*, which are due to the pressure of the bagasse, are responsible for the penetration of the material into the groove root.
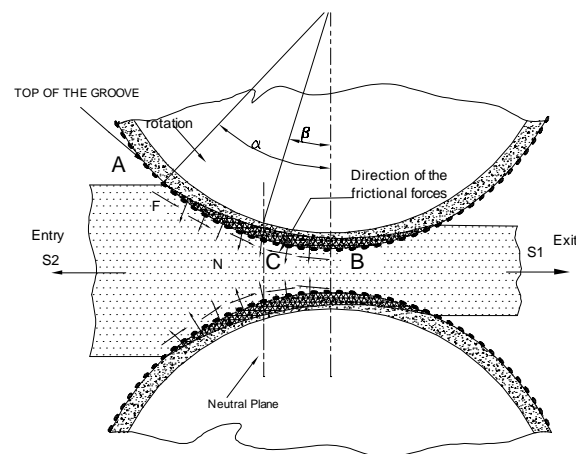
Figure 2.11 Schematic showing a plane strain view of two roughened rollers.

The groove angle and surface topology will determine the level of radial frictional forces, f_r, generated on the flank. On the other hand, tangential forces, f_t, are responsible for mill feeding. Tangential forces are measurable using traditional procedures. Radial forces in the vicinity of the flank are complex and difficult to measure.
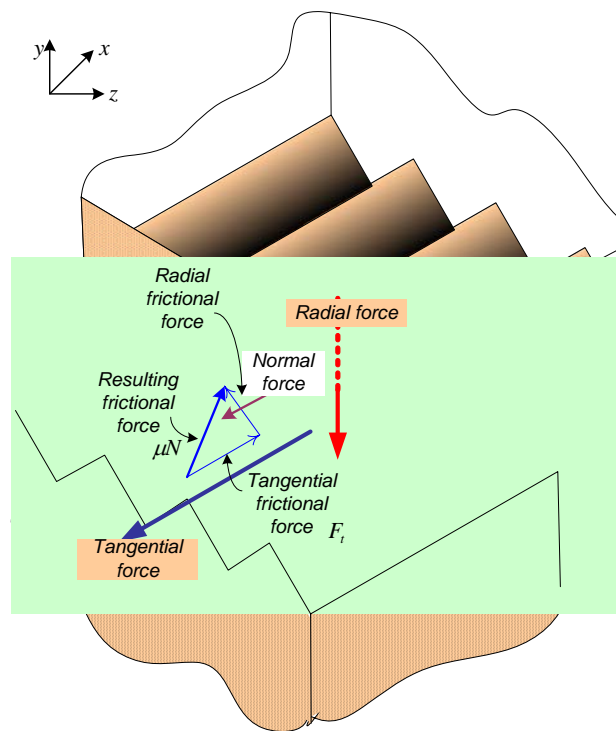
Figure 2.12 *Equilibrium of forces on grooved roller surfaces*

2.4.4 Failure criterion at an interface plane

When a material receiving a compressive load is in contact with something retaining it, the material will form frictional forces and a potential slip plane both at the interface (the surface wall, container) and within it. The criterion for the existence of potential slip along a wall is based on the same principle as that for forming an internal slip plane (Aysen, 2002; Nedderman, 1992). The shear stress on the wall or interface depends on the normal stress applied to the material that is, $\tau_w = f(\sigma_w)$. The wall yield locus determined by the Coulomb failure criterion is expressed in the form

$$\tau_w = \mu_w \sigma_w + c_w \tag{2.19}$$

where μ_w is the friction coefficient of the wall and c_w is the adhesion. The angle of wall friction can be defined by:

$$\tan \phi = \mu_w = \frac{d\tau_w}{d\sigma_w} \qquad \textbf{(2.20)}$$

Shear stresses can cause potential slip at the interface and within the material. Figure 2.13 shows the possible positions of a wall plane. If the material is failing internally, Mohr's circle must touch the internal yield locus (IYL), but if the wall yield loci (WYL) is within the internal yield loci, they will cut the circle at the four points A, B, C and D. If I is a point which corresponds to the interface or wall lies on the circle, then the relationship $|\tau_w| < \mu_w \sigma_w + c_w$ will define when I lies within the arcs BC and AD. It is expected that no slip occurs along the interface. If, however, I lies at A, B, C or D then $\tau_w = \mu_w \sigma_w + c_w$, and the material could be in a state about to slip along the interface. The point I will not be able to lie in the arcs AB and CD because the magnitudes of the wall shear would not exceed $\mu_w \sigma_w + c_w$.
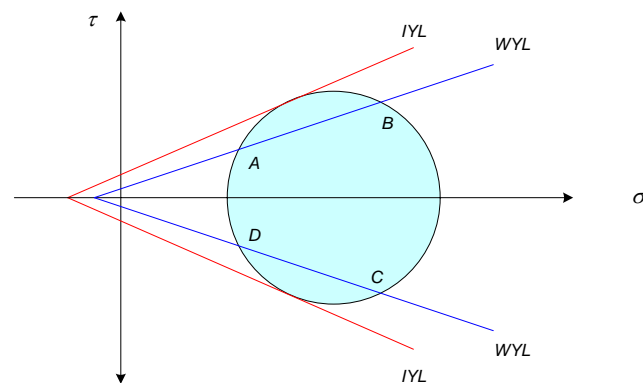
Figure 2.13 *Potential failure planes of a material subjected to shear stress*

The above analysis could imply that the yield loci are both at the wall and within the material since the shear stress behaves differently on its respective planes. The internal yield locus reduces the shear stress on any plane; while wall yield loci impose limits on the shear stress on the wall plane. Figure 2.13 shows schematically potential planes of a material subjected to shear stress. For example, if the material fails internally and also slipping occurs along the interface, it implies that the Mohr's circle could be touching the internal yield locus line and the wall plane would be either I or I'.

2.4.5 Drucker-Prager /Cap (DPC) plasticity model

The Drucker-Prager/Cap constitutive model represents one of the pioneering extensions of metal plasticity theory to soil plasticity. This model was an extension of the Von Mises yield criterion proposed by Drucker and Prager to account for confinement strengthening of granular materials. The developed model attempted to couple the deviatoric and volumetric deformation behaviours of porous materials. DPC model consists of a fixed plastic surface that defines the shear strength of the material and a work hardening cap which determines its yield surface (Figure 2.14). Equations describing shear failure line, transition surface, and hardening caps, respectively, are given in (2.21) to (2.23).

$$F_s = q - p \tan \beta - d = 0 \qquad (2.21)$$

$$F_c = \sqrt{\left[p - p_a\right]^2 + \left[\frac{Rq}{1 + \alpha - \alpha/\cos \beta}\right]^2} - R\left(d + p_a \tan \beta\right) = 0 \qquad (2.22)$$

$$F_t = \sqrt{\left[p - p_a\right]^2 + \left[q - \left(1 - \alpha/\cos \beta\right)\left(d + p_a \tan \beta\right)\right]^2} - \alpha\left(d + p_a \tan \beta\right) = 0 \quad (2.23)$$

where,

α = cap transition parameter

q = Von Mises equivalent stress

p = hydrostatic pressure

F_c = yield function in cap region

F_s = yield function in Drucker-Prager shear region

F_t = yield function in transition region

Despite a variety of alternative strain hardening plasticity models have been developed, the Drucker-Prager/Cap plasticity model is widely used not only for studying compaction of metallic materials but porous materials (Adam, 1997; Kannapiran 2003). It accounts for:

1. Stronger compact in compression than tension

2. Cohesion, internal friction angle, and their dependence on relative density (RD).

3. Shear failure and cap surface.
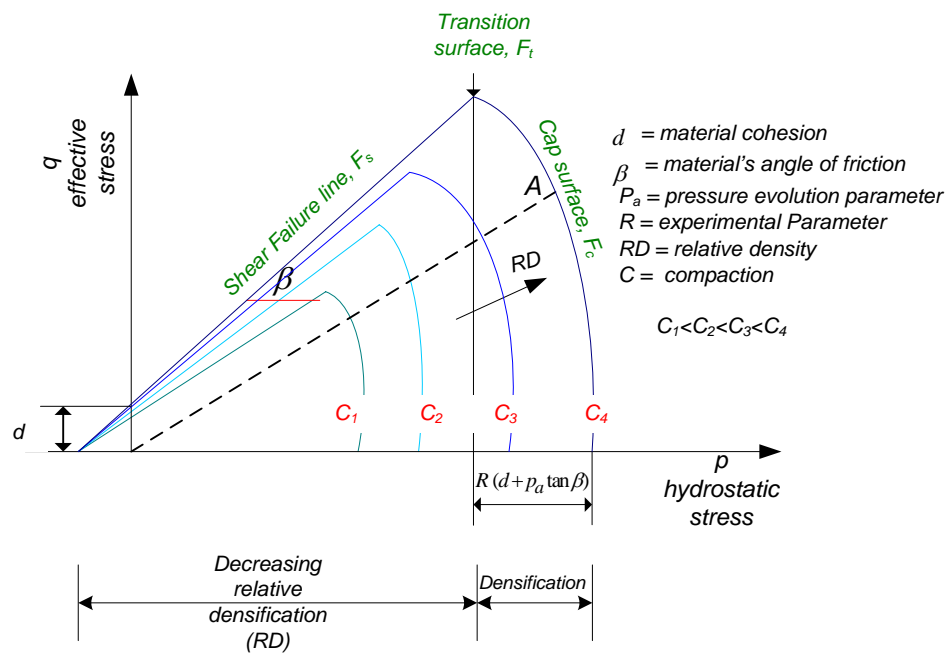
Figure 2.14 *A family of conventional DPC yield limits for different levels of relative density.*

An isotropic DPC model has been applied in bagasse compaction modelling for over a decade, because it contains some features that are in accordance with the noted physical response (Adam 1997, Kannapiran, 2003; Kent, 2004). The DPC model (Figure 2.14) indicates that when the material is at low compaction its response depends on the magnitude of the confining pressure. At low compaction, the allowable shear stress is proportional to the normal pressure applied to the material. The shear strength may be predicted by the Mohr-Coulomb shear failure criteria. This means that the material fails in shearing when the frictional stress at the interface is equal to or greater than the effective stress of the bagasse. In reality, bagasse is a fibrous material which undergoes significant spatial redistribution of fibres during compaction (Adam, 1997; Vass, 1999).
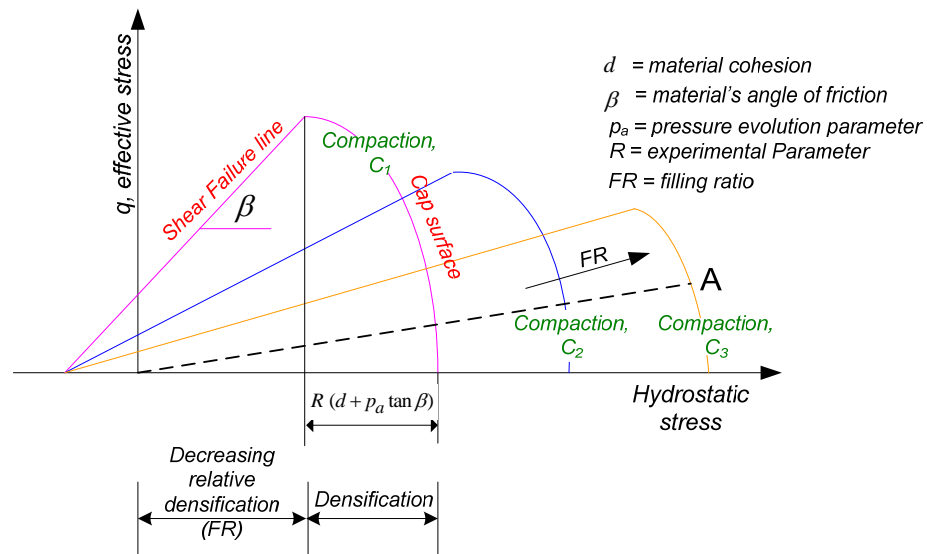
Figure 2.15 *The non-conventional DPC model parameters including a family of DPC yield limits for different levels of bagasse compaction (relative densities) over a range of compression.*

Clearly the material may be heterogeneous, but it is far from isotropic and one might argue that an anisotropic DPC model would better capture the observed response. However, such a model would be mathematically complex, difficult to code, and require a large number of coefficients for calibration

2.4.6   Coulomb wedge analysis

The Coulomb wedge analysis is a method based on the force equilibrium of a wedge to obtain the critical value of the sliding angle α (assuming a failure plane for the material) and the corresponding passive and active thrust that a material exerts when is retained by a wall. This method is employed in granular material (Nedderman, 1992) and soils (Aysen, 2003 and may have limited application with prepared cane despite the fibrous nature of the material. The Coulomb wedge analysis assumes that motion of the wedge (Figure 2.16) is downwards and the frictional forces act both on the wedge and the rest of material (cohesionless), and between the wedge and the wall. This response causes the frictional forces to act on the wall in an upward direction. The shear stress generated on the slip plane will be μ times the normal stress, so that the resulting force R will be inclined to the normal plane by the angle ϕ as depicted in Figure 2.16. The force N on

the wall will be inclined to the normal by the angle of the wall ϕ_w. For straight walls the force exerted on the wall gives the following relationship:

$$N\cos\phi = \frac{\lambda h^2}{2}\frac{\cot\alpha}{\tan\phi + \cot(\alpha-\phi)} = \frac{\lambda h^2}{2}f(\alpha) \tag{2.24}$$
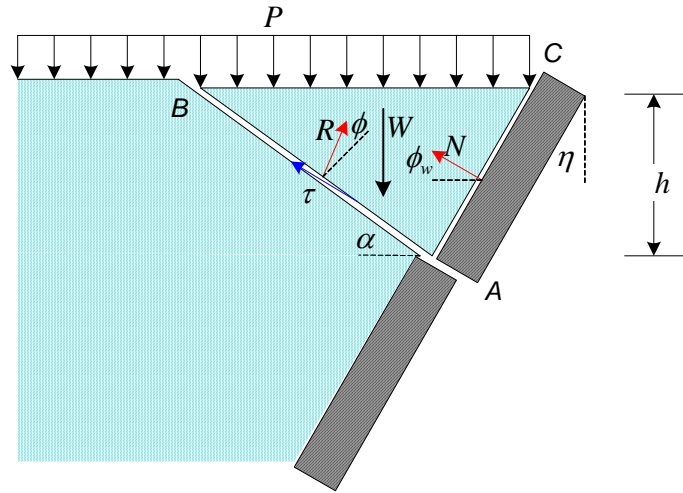
Figure 2.16 Failure of a well due to a normal applied load.

The force N passes through a minimum and maximum, which will depend on the function $f(\alpha)$ in Equation (2.24). As the normal force on the wall is the integral of the normal stress with respect to depth. Shear stress is given by:

$$\sigma = \frac{dN}{dh}\cos\phi \tag{2.25}$$

$$\tau = \sigma\tan\phi \tag{2.26}$$

The force N on an inclined wall has been given by the following complex trigonometrical relationship (Nedderman, 1992):

$$N = \frac{\lambda h^2}{2}\frac{\cos^2(\eta-\phi)}{\cos^2\eta\cos(\eta-\phi_w)\left[1+\sqrt{\frac{\sin(\phi+\phi_w)\sin\phi}{\cos(\eta+\phi_w)\cos\eta}}\right]^2} \tag{2.27}$$

where, η is the angle that the wall makes with a vertical line and λ is the material density. For soil an iterative process is used to find the force on the wall and the angle α of the sliding surface, respectively. Bagasse is inherently more complex than soil, even though researchers have used similar critical state models to describe its deformation characteristics (Adam, 1997; Plaza, 2002). It is considered that the fibrous nature of bagasse would make the Coulomb wedge analysis method impractical.

2.4.7 Reaction forces in grooved elements subjected to compressive load

When a material is compressed into a grooved surface it can cause reacting forces of a magnitude greater than the external force applied. This elemental principle is employed for some machine elements such as the wedge. Wedges are employed to intensify forces, transmit power or motion. Figure 2.17 shows a schematic of the reacting forces produced by a wedged element. The load F applied to the wedge generates normal forces N, and frictional forces f, at each flank of its interface. The reacting forces act in opposite direction to the motion of the wedge.
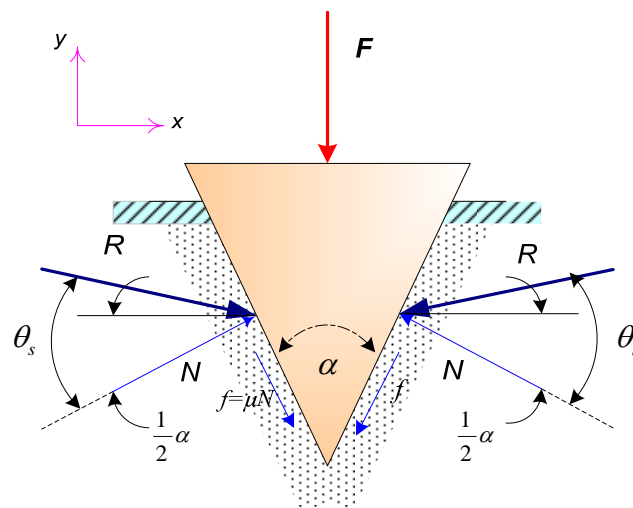
Figure 2.17 *Free-body diagram of the wedge under a vertical force* F.

At equilibrium:

$$2N\sin\frac{\alpha}{2} + 2\mu_s N\cos\frac{\alpha}{2} - F = 0$$

From the above relationship the normal force is deduced as a function of the load, groove angle and the friction coefficient as:

$$N = \frac{F}{2\left(\sin\dfrac{\alpha}{2} + \mu_k \cos\dfrac{\alpha}{2}\right)}$$

(2.28)

Equation 2.28 indicates that in the absence of any vertical load the wedge remains in place with a minimum friction coefficient equal to

$$\mu_s = \tan\frac{\alpha}{2}$$

(2.29)

From Equation 2.28, if the angle of a wedge is varied over the range from zero to 180° the normal force generated shows a downward trend, as the angle of the wedge is increased. For very small angle, the normal force takes very high values with respect to the compressive force applied, as the friction coefficient at the interface is decreased. This normal force is equal to the compressive load when the grooved surface is flat, and is independent of the friction coefficient as shown in Figure 2.18. This principle corroborates the use of wedges to split, lift or hold materials pushed into grooves surfaces. On the other hand, Figure 2.18 also shows that the ratio N/F presents the same downward trend at different friction coefficient values when the angle increases. The ratio of magnification of normal forces to compressive force N/F, seems to be affected by the friction coefficient for groove angles less than 60°.
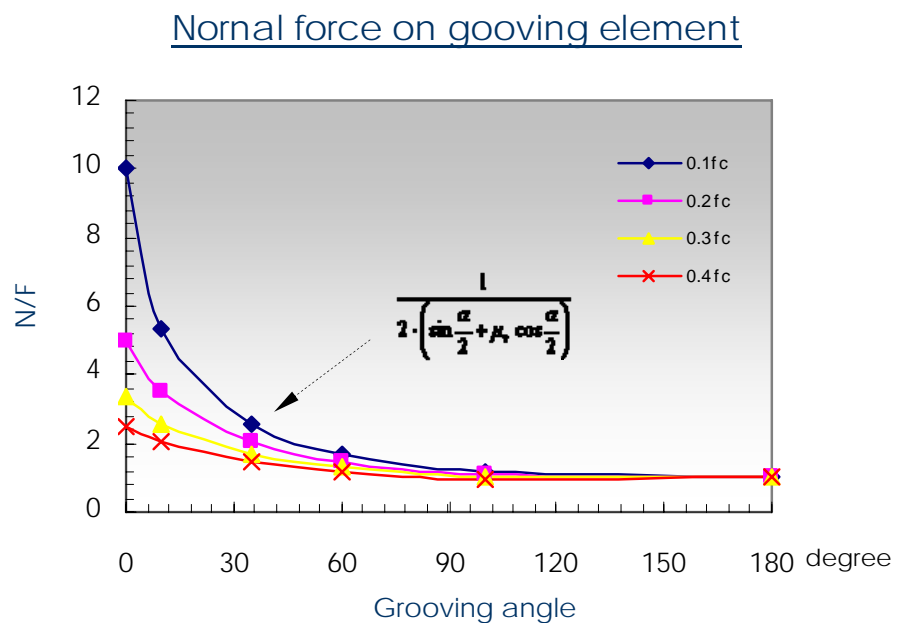
Figure 2.18 Ratio normal to compressive force versus angle and friction coefficient.

The above analysis could permit an understanding of the reactive forces which could be occurring in the interface between bagasse and a groove surface. In practice, it is common to observe bagasse being wedged into grooves, when circumferential groove angles between 35° and 45° are used. If this occurs, it may be argued that one of the causes of this strong wedge attached to the groove is the high reactive normal force produced at that groove angle.

2.4.8 The friction coefficient value on a grooved surface

A typical grooved surface used for extracting liquid contained in prepared cane or bagasse is shown in Figure 2.19. This groove is comprised of two inclined faces and a flat apex. Equation 2.28 suggests that the normal force experienced by the flank of the groove, as a result of a compressive load, varies as a function of the angle of the groove. It indicates that normal force may be different on both the flanks and the tip. As frictional forces do not depend on the area of contact (Williams, 1994), it is expected that frictional force changes along the profile of the groove. Tangential frictional forces are forces which directly affect mill feeding and influence the evolution of stress within the bagasse mat, which might lead to shear failure. On the contrary, radial frictional forces oppose bagasse penetration into the mat.
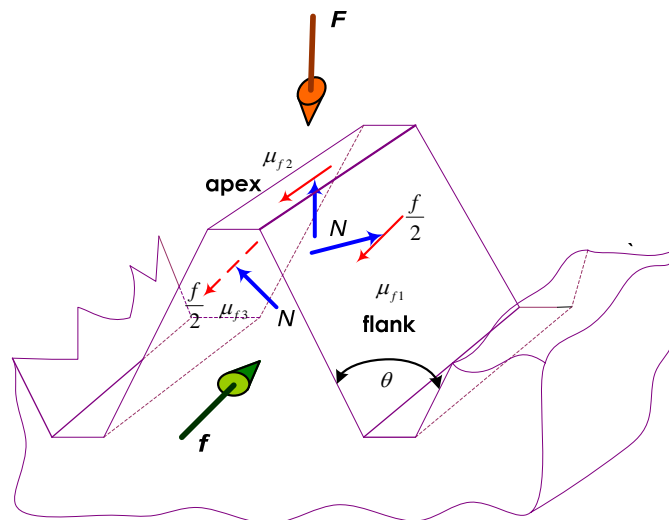
Figure 2.19 *Distribution of frictional forces on a grooved surface.*

Therefore, the average friction coefficient at the interface between the grooved surface and the bagasse is:

$$\mu_{av} = \frac{\mu_{f1} + \mu_{f2} + \mu_{f3}}{3}$$ **(2.30)**

From the Equation (2.15) it is known that

$$\mu = \frac{f}{N}$$ **(2.31)**

where,

μ is the friction coefficient value

f is the tangential force applied to the tooth, and

N is the normal force.

It is assumed that by symmetry each flank is affected by one half of the load F applied to the tooth and one half of the tangential force, f.
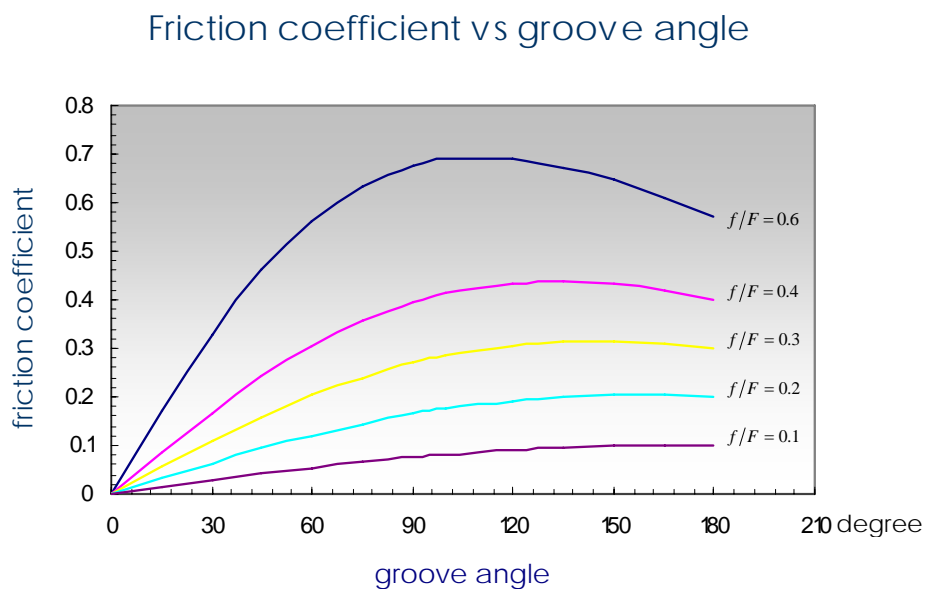
Figure 2.20 Relationship friction coefficient and groove angle as a function of shear and normal force.

Replacing the value of N from Equation (2.28) in Equation (2.31), the friction coefficient for a groove flank is:

$$\mu_{f_i} = \frac{\dfrac{f}{F}\sin\dfrac{\theta}{2}}{1-\dfrac{f}{F}\cos\dfrac{\theta}{2}} \qquad \textbf{(2.32)}$$

When the friction coefficient from Equation 2.32 is plotted, as a function of the groove angle and the ratio f/N, it can be argued that there is a maximum friction coefficient for a determined groove angle at a certain ratio f/N, as shown in Figure 2.20. It also indicates that obtuse angles contribute to an increase in the friction coefficient. The rise of friction coefficient values is due to both an increment of the ratio f/N. The groove angles do not take into account the shear strength of the material, which is related to the failure of a material.

2.5 The texture of the contact surface between bagasse and a grooved platen

The surface of a body exhibits error irregularity in form and shape. The peak to valley heights of the roughness component of a texture may range from roughly $0.05\,\mu$m, for fine lapped and up to $50\,\mu$m for a rough machined surface, with peak spacing from $0.5\,\mu$m to 5 mm (Neale, 1995). The total profile of the components of a surface shows a combination of waviness (undulation with a relatively long wavelength) and roughness (variations with much shorter wavelength).

Total profile

Waviness
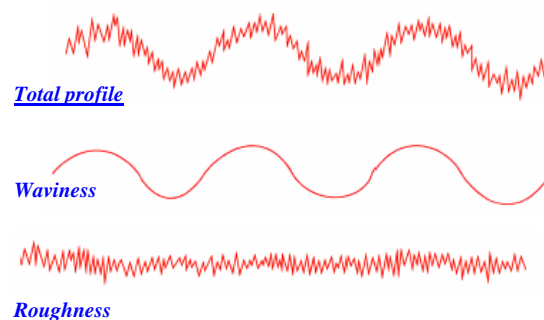
Roughness

Figure 2.21 *Components of the contact surface: roughness and waviness making the total profile.(Anon., 2001).*

Waviness and roughness are superimposed on the geometric shape or form of the component surface, as shown in Figure 2.21. Roughness of a surface can affect many aspects of its behaviour when two bodies are in contact; hence, it is assessed and measured. For example, it is necessary to describe surface texture numerically for communication purposes, especially in drawings. A numerical evaluation of some aspect of the texture is often referred as a 'parameter'. The parameters which define asperities such as height, spacing, slope, crest curvatures and the varied distribution of roughness and waviness, respectively, cannot completely describe the surface. Surfaces having quite different profiles can be numerically equal with respect to such a parameter while being unequal with respect to others. It has been recognised that no single parameter can adequately describe surface geometry (Williams, 1994). It has been postulated that roughness may be expressed as a function of heights normal to the mean plane of the surface together with its spatial distribution, or wavelength, within the surface (Neale, 1995). The two simplest, and still most widely used roughness parameters are the average roughness value, R_a, and root mean square (RMS). The first parameter is expressed by Equation 2.33 and is the internationally recognised.

$$R_a = \frac{1}{L} \int_0^L |y(x)| dx \qquad (2.33)$$

or

$$R_a = \frac{1}{n} \sum_{i=1}^{n} |y_i| = \frac{|y_1| + |y_2| + |y_3| \ldots + |y_n|}{n} \qquad (2.34)$$

where y is the height of the surface measured above the mean level, that is, the line which goes through the area of the material so that the upper area is equal to the areas of the bottom voids; x is the coordinate in the surface; L the measurement length; and n is the number of sample points at equal lengths, as shown in Figure 2.22. One of the disadvantages about using R_a is that it can fail to distinguish between a relatively gently undulating surface and one with one with the highest profile. The roughness average does not provide any information on the shape or size of the surface feature.
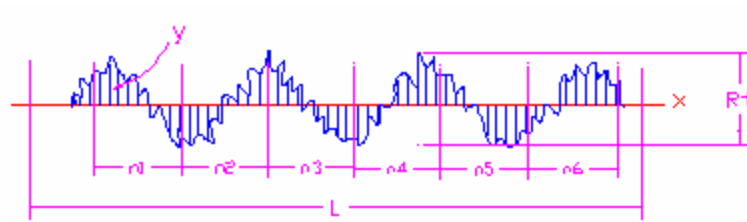
Figure 2.22 *Forms to measure a superficial Irregularity: Average roughness*

$$R_a = \frac{1}{L}\int_0^L |y(x)|dx, \text{ root mean square (rms): } R_q = \sqrt{\frac{1}{L}\int_0^L z^2 dx}.$$

For instance, Figure 2.23 shows four profiles with different shapes, but the same R_a value. The RMS roughness parameter R_q overcomes partly this difficulty. It is defined by Equation (2.35).

$$R_q = \sqrt{\frac{1}{L}\int_0^L z^2 dx} \tag{2.35}$$

or

$$R_q = \frac{1}{n}\sqrt{\sum_{i=1}^n y_i^2} = \sqrt{\frac{y_1^2 + y_2^2 + y_3^2 \ldots + y_n^2}{n}} \tag{2.36}$$
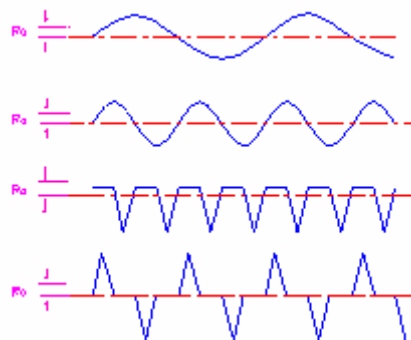
Figure 2.23 *Surface profiles with different shapes, but similar average roughness (Anon., 2001).*

2.5.1 Quantification of hard-facing roughness on a grooved surface

It was mentioned earlier, that the roughness of a roller surface is particularly important for improved throughput. Roller surfaces are often covered with hard facing asperities or nodules in order to cause more grip for prepared cane or bagasse. There are different ways of placing asperities on the roller surface. However, there is no scientifically proven method for measuring the texture of the roller surface.

$$R_a = \frac{\sum_{0}^{i} y_{(i,j)} - y_{b(i,j)}}{i} = \frac{height - height_{base-line}}{i_{po\,int\,s}}$$
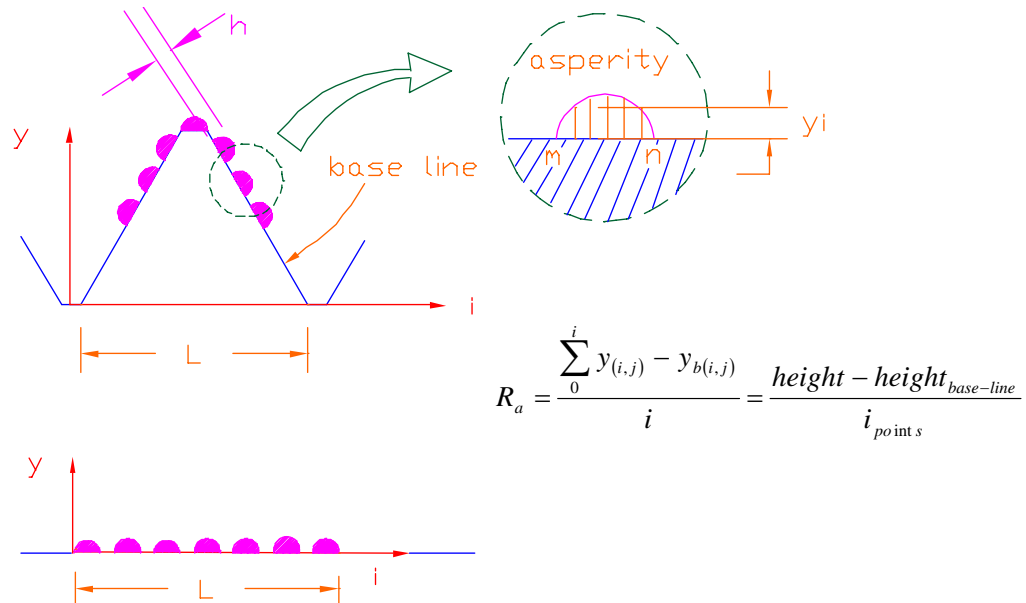
Figure 2.24 *Average roughness,* R_a*, for a grooved surface covered with asperities.*

Three scales of roughness are accepted universally: optical roughness (it occurs at scales $< 1\,\mu m$), micro roughness (at scales between $1\,\mu m$ and $100\,\mu m$) and macro roughness (at scales between 0.1*mm* to 1 *mm*). The type of asperity laid down on sugar mill rollers is typically 1 to 12 mm in diameter (clearly greater than the range of values that defined as macro-roughness). Indeed, they might be better defined as globules (or super-roughness). Figure 2.24 shows a method which could be used to find the average super-roughness. The asperity is discretised into heights and distributed as a series of points on the surface profile. This surface profile can be taken over lines for a quantitative analysis. The average roughness of the super roughness, asperities or nodules can be determined by means of Equation (2.34).

2.6 Dimensional analysis for friction between bagasse and a rolling surface

Any state or process known in mechanics is determined by a set of variables which can take numerical values. Often a problem cannot be formulated mathematically because of the complexity of the physical phenomenon. In such cases the essential physical characteristics of the problem may be investigated experimentally. In addition, dimensional analysis may be used to explore non-dimensional groups. The elements for the dimensional analysis of problems are: the selection of the factors defining the physical quantity of interest, and an adequate knowledge of the significant variables (Zlokarnick, 1991). The factors can be geometric, material (physical properties), or some process-related variable. The properties of matter and the elementary physical laws, which play a substantial role in controlling phenomena, are determined by a number of dimensional or nondimensional parameters, variables or constants. These dimensional and non-dimensional quantities are required to find a numerical value of all unknowns, when a problem has to be formulated mathematically. Using this principle, the analysis of interface friction demands the identification of all relevant variables into non-dimensional groups. From Figure 2.10, the grip of prepared cane or bagasse by the roller starts from the location where the horizontal component F_x of the friction force F is greater than, or at least equal to, the horizontal component N_x of the normal force caused by the compressive load of the roller. In the region A–B no compressive load F is required to be exerted to allow the prepared cane to be fed into the roller, so the friction coefficient can be considered as independent of the pressure applied at that point. Under this condition the friction coefficient will only depend on the geometry and texture of the roller surface. Both the groove angle of the rollers, θ, and groove height, H, are important parameters which affect bagasse penetration and contact area. The roughness on the surface can be assessed as a function of the average height of the asperity, h. Other important parameters acting during the gripping and compressive process are roller speed, v_t, and effective stress, σ. It is assumed that liquid flows from a region of high pressure to one of low pressure. The effect of drained liquid at the interface can be considered to form a potential thin film which acts as a lubricant, exerting a deformation rate (strain rate), $\dot{e}$. The response of the fibre to get aligned in a direction perpendicular to the compressive load, and the tangential forces opposing

spatial displacement cause shear stresses, τ, not only at the interface, but between fibrovascular bundles.

The relevant variables constituting a physical model for the friction mechanism are listed as follows:

a. the friction coefficient, μ = nondimensional, dependent variable

b. the initial contact angle, α_i = nondimensional, a parameter

c. the effective pressure, $p = M^0 F^1 L^{-2} T^0$, a parameter

d. the shear stress, $\tau = M^0 F^1 L^{-2} T^0$, a parameter

e. the compaction level, $\gamma = M^3 F^0 L^3 T^0$, a parameter

f. the height of bagasse penetration, $H = M^0 F^0 L^1 T^0$, independent variable

g. the roughness height, $h = M^0 F^0 L^1 T^0$, independent variable

h. the groove angle, θ, nondimensional, an independent variable.

i. the velocity of the roller, $v_t = M^0 F^0 L^1 T^{-1}$, a parameter

j. the feed force, $F_m = M^0 F^1 L^o T^0$, a parameter

k. the shear strain of liquid film, $\dot{e}$ = nondimensional, an independent variable

l. the density of the fibrous material, $\rho = M^1 F^0 L^{-3} T^0$, a parameter.

The notation $x = M^a F^b L^c T^d$ stands for the dimensions mass, force, length and time. Parameters are variables which are constant during a particular event ($\alpha_i, \gamma, p, v_t, \sigma, \tau, \rho, \dot{e}, F_m$ and v_t in this list).

The mathematical model developed by Coulomb indicates that shear stress on the slip plane will be μ times the normal stress, namely:

$$\tau = c + \mu\sigma \tag{2.37}$$

where, c stands for a constant and defines the properties of the material and geometric arrangements of the bodies in contact. Hence,

$$\mu = c + \frac{\tau}{\sigma} \tag{2.38}$$

Even though, it is not possible to define the mathematical model which relates the friction coefficient, μ, with the independent variables, the complete physical model used to define the relation may be expressed as:

$$\mu = \psi\left(\alpha_i, \tau, p, \gamma, s_t, F, H, h, \theta, \rho, \dot{e}\right) \qquad (2.39)$$

where ψ stands for an unknown function. The function (2.39) can be written as:

$$\psi\left(\mu, \alpha_i, \tau, p, \gamma, s_t, F, H, h, \rho, \dot{e}\right) = 1 \qquad (2.40)$$

In order to identify both physical and dimensional irrelevancy, a dimensional set may be constructed based on Equation (2.40). Dimensional analysis techniques are based on the principle of transformation between dimensional systems (or units), and dimensional homogeneity. Therefore, there exists a numerical factor for the dimensional quantity Q in dimensional system *1,* which is also equivalent in dimensional system *2*. The problem can be solved as:

$$Q \cdot d_1^{e_1} \cdot d_2^{e_2} \cdot \quad . \quad . \quad d_n^{e_n} = x \cdot D_1^{e_1} \cdot D_2^{e_2} . \quad . \quad . \quad D_n^{e_n} \qquad (2.41)$$

where $d_1, d_2,... =$ dimension in system *1*

$D_1, D_2,... =$ dimension in system *2*

$e_1, e_2,... =$ exponents of dimensions in both systems

n $=$ number of dimension in each system, and

x $=$ a numerical system.

An arbitrary change of units for a dimensional variable V_1, can be written as

$$V_1' = d_1^{e_1} \cdot d_2^{e_2} \cdot \quad . \quad . \quad d_n^{e_n} \cdot V_i, \qquad (2.42)$$

For a physical model ψ, with i dimensional variables and $n = 3$ dimensions in the system,

$$\psi\left(V_1, V_2, ..., V_i\right) = \psi\left(d_1^{e_{11}} d_2^{e_{21}} d_3^{e_{31}} V_1, d_1^{e_{12}} d_2^{e_{22}} d_3^{e_{32}} V_2, ..., d_1^{e_{1i}} d_2^{e_{2i}} d_3^{e_{3i}} V_i\right) \tag{2.43}$$

For a relationship among N_v variables $V_1, V_2, ...$ and N_d dimensions $d_1, d_2...$, the task in determining these particular combinations (groups) of variables raised to certain powers (unknowns) which pose a preselected (looked for) dimensional composition, is:

$$\left[V_1^{e_1} \cdot V_2^{e_2} \cdot \quad . \quad . \quad V_i^{e_i}\right] = d_1^{q_1} \cdot d_2^{q_2} \cdot \quad . \quad . \quad d_n^{q_n} \tag{2.44}$$

where, e_i is an exponent for dimensions and q_n for variables, respectively. The following relation can be composed for N_v variables and N_d dimensions, according to Equation (2.44). Table 2.1 shows the list of relevant variables. The dimensional set is exhibited in Figure 2.25, which is the result of four sub-matrices is used to find the products of variables or phi (π_s). From this set, fourteen variables, four dimensions, and ten products of variables can be found.

$$
\begin{aligned}
k_{11}e_1 + k_{12}e_2 + . \quad . \quad . \quad + k_{1n}e_i &= q_1 \\
k_{21}e_1 + k_{22}e_2 + . \quad . \quad . \quad + k_{2n}e_i &= q_2 \\
. \quad . \quad \quad . \quad \quad . \quad \quad . \quad \quad & \\
. \quad . \quad \quad . \quad \quad . \quad \quad . \quad \quad & \\
k_{i1}e_1 + k_{i2}e_2 + . \quad . \quad . \quad + k_{in}e_i &= q_n
\end{aligned}
\tag{2.45}
$$

Or in vector form

$$
\begin{bmatrix}
k_{11} k_{12} & . & . & k_{1n} \\
k_{21} k_{22} & . & . & k_{2n} \\
. & . & . & . \\
. & . & . & . \\
k_{i1} k_{i2} & . & . & k_{in}
\end{bmatrix}
\cdot
\begin{bmatrix}
e_1 \\
e_2 \\
. \\
. \\
e_n
\end{bmatrix}
=
\begin{bmatrix}
q_1 \\
q_2 \\
. \\
. \\
q_n
\end{bmatrix}
\tag{2.46}
$$

Table 2.1 *Relation of relevant variables involved at the interface friction between bagasse and roller*

Variable	Symbol	Dimension	Remarks
Friction coefficient	μ	*1*	
Shear stress	τ	*N/m²*	
Initial contact angle	α_i	*1*	
Bagasse penetration height	*H*	*M*	*Constant*
Asperity height	*h*	*M*	
Groove angle	θ	*1*	
Feed force	*F*	*N*	
Bagasse compaction	γ	*Kg/m³*	
Normal stress	*p*	*N/m²*	
Bagasse shear modulus	*G*	*N/m²*	
Liquid film strain rate	$\dot{e}$	*1/s*	*Liquid phase*
Peripheral speed	v_t	*m/s*	*Movement bagasse*
Bagasse density	ρ	*kg/m³*	*Solid phase*
Gravitational acceleration	*g*	*m/s²*	

From Table 2.1, fourteen variables have been assumed to influence the interface friction. As four dimensions are involved, then the dimensionless set provides ten dimensionless variables, thus:

$$\pi_1 = \mu; \quad \pi_2 = \frac{\tau}{p}; \quad \pi_3 = \alpha_i; \quad \pi_4 = \frac{H \cdot g}{v_t^2}; \quad \pi_5 = \frac{h \cdot g}{v_t^2}; \qquad \textbf{(2.47)}$$

$$\pi_6 = \theta; \quad \pi_7 = \frac{F \cdot \dot{e} \cdot g^2}{p \cdot v_t^4}; \quad \pi_8 = \frac{\gamma}{\rho}; \quad \pi_9 = \frac{G}{p}; \quad \pi_{10} = \frac{\dot{e} \cdot v_t}{g}$$

from which

$$\pi_1 = \psi\left(\pi_1, \pi_2, \pi_3, \pi_4, \pi_5, \pi_6, \pi_7, \pi_8, \pi_9, \pi_{10}\right) \qquad \textbf{(2.48)}$$

where, ψ is some function yet to be determined. The function ψ as an algebraic relation is assumed to be:

$$\pi_1 = k \cdot \pi_2^{n_2} \cdot \pi_3^{n_3} \cdot \pi_4^{n_4} \cdot \pi_5^{n_5} \cdot \pi_6^{n_6} \cdot \pi_7^{n_7} \cdot \pi_8^{n_8} \cdot \pi_9^{n_9} \cdot \pi_{10}^{n_{10}} \qquad \textbf{(2.49)}$$

where, k and $n_2, ..., n_9$ are unknown constants to be determined.

	μ	τ	α_i	H	h	θ	F	γ	G	$\dot{e}$	p	v_t	ρ	g
M	0	0	0	0	0	0	0	1	0	0	0	0	1	0
F	0	1	0	0	0	0	1	0	1	0	1	0	0	0
L	0	-2	0	1	1	0	0	-3	-2	0	-2	1	-3	1
T	0	0	0	0	0	0	0	0	0	0	0	-1	0	-2
π_1	1	0	0	0	0	0	0	0	0	0	0	0	0	0
π_2	0	1	0	0	0	0	0	0	0	0	-1	0	0	0
π_3	0	0	1	0	0	0	0	0	0	0	0	0	0	0
π_4	0	0	0	1	0	0	0	0	0	0	0	-2	0	1
π_5	0	0	0	0	1	0	0	0	0	0	0	-2	0	1
π_6	0	0	0	0	0	1	0	0	0	0	0	0	0	0
π_7	0	0	0	0	0	0	1	0	0	0	1	-4	0	2
π_8	0	0	0	0	0	0	0	1	0	0	0	0	-1	0
π_9	0	0	0	0	0	0	0	0	1	0	-1	0	0	0
π_{10}	0	0	0	0	0	0	0	0	0	1	0	1	0	-1

Figure 2.25 *Dimensional set matrix for friction coefficient composed of ten dimensionless variables*

Three ways are available to determine these constants: experiment, analysis or heuristic reasoning. Applying an heuristic reasoning approach to Equation (2.49)

$$\mu = k \cdot \left(\frac{\tau}{p}\right)^{n_2} \cdot (\alpha_i)^{n_3} \cdot \left(\frac{H \cdot g}{v_t^2}\right)^{n_4} \cdot \left(\frac{h \cdot g}{v_t^2}\right)^{n_5} \cdot (\theta)^{n_6} \cdot \left(\frac{F \cdot g^2}{p \cdot v_t^4}\right)^{n_7} \cdot \left(\frac{\gamma}{\rho}\right)^{n_8} \cdot \left(\frac{G}{p}\right)^{n_9} \cdot \left(\frac{\dot{e} \cdot v_t}{g}\right)^{n_{10}} \quad (2.50)$$

It is obvious from the above relations that the exponents n_2, n_3, n_6, n_8, n_9 and n_{10}, should not be between 0 and 1; otherwise μ would be ill-defined. If the height, h, of the asperity is increased, then μ will increase because of greater penetration into the bagasse; therefore more force will be required to displace fibres into the bagasse. With respect to tangential speed, any increment of the tangential velocity will cause a fall in the friction coefficient value, which makes sense. Hence, n_5 should be zero. For the case of the dimensionless product, π_7, if the feed force, F, is increased and the shear stress, p, remains constant then the friction coefficient would be infinite. Therefore, the exponent n_7 can be ignored. As far as, the dimensionless product, π_{10}, is concerned, this

coefficient relates to the shear strain rate of liquid acting as film between bagasse and motion of the material of the interface. The liquid contained in the bagasse can be considered as a low viscosity fluid, whose deformation is proportional to the shear stress. Any increment of this value implies an increment of frictional stress due to reduction of the film, causing the bodies to approach one another. This film is assumed to move at the same tangential velocity. Therefore, the exponent n_{10}, is also equivalent to zero. Hence:

$$\pi_1 = k \cdot \left(\pi_2 \cdot \pi_3 \cdot \pi_4 \cdot \pi_5 \cdot \pi_6 \cdot \pi_8 \cdot \pi_9 \cdot \pi_{10} \right) \tag{2.51}$$

If it is assumed that p is reduced to zero, then the friction coefficient becomes zero; because no frictional force is produced. In assuming no bagasse penetration ($H=0$) means the bagasse only contacts the apex of teeth, and consequently the friction coefficient value equals zero, However, this does not occur in reality, because there is a minimum friction coefficient at the nip angle. Therefore, Equation (2.51) is untenable under that assumption. That is, the friction model does not represent a geometric progression, but an arithmetic progression. Equation (2.38), which is the actual relation, indicates that the friction coefficient depends not only on frictional stresses generated by the compressive normal load, but also on the material properties and boundaries conditions of the bodies in contact. The constant *"c"* in Equation (2.38) may be assumed as factors inherent to bagasse and the interface friction. Equation (2.51) may be given as

$$\pi_1 = \left(\pi_3 + \pi_4 \cdot \pi_5 \cdot \pi_6 \cdot \pi_8 \cdot \pi_{10} \right) + \pi_2 \cdot \pi_9 \tag{2.52}$$

If the dimensionless product, π_9, which relates the maximum shear stress is expressed as a function of both true and apparent areas of contact, then

$$\frac{G}{p} = \frac{\tau/\gamma_{bss}}{N/A_a} = \frac{N/A_t}{\gamma_{bss} \cdot N/A_a} = \frac{1}{\gamma_{bss}} \cdot \frac{A_a}{A_t}, \qquad A_t < A_a \tag{2.53}$$

where,

A_t is the true area of contact where shear stress is acting on the fibrous material

A_a is the apparent area which the compressive load of asperities is exerting on the bagasse, and

γ_{bss} is the shear strain of the material.
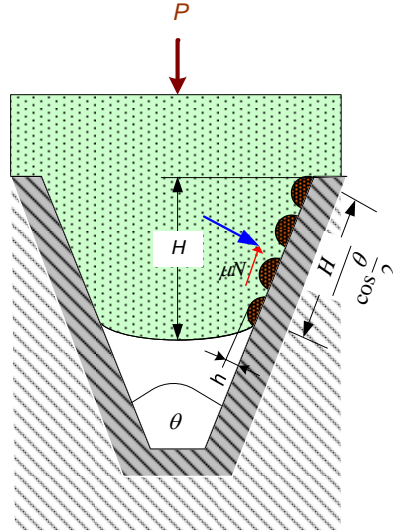
Figure 2.26 *Contact of roughened area as a function of bagasse penetration.*

From Figure 2.26

$$A_a = \frac{H}{\cos\dfrac{\theta}{2}} \cdot \frac{\alpha \cdot \pi \cdot D}{360} \tag{2.54}$$

$$A_t = n \cdot \pi \cdot h^2 \cdot \left(\frac{\alpha \cdot \pi \cdot D}{360} \right) \tag{2.55}$$

where, n is the number of asperities per unit area, and R the mean radio of the roller. The ratio of Equation (2.55) and (2.54) gives

$$\frac{A_t}{A_a} = \frac{n \cdot \pi \cdot h^2 \cdot \cos\theta/2}{H} = const \cdot \left(\frac{\pi_5^2 \cdot \pi_6}{\pi_4} \right)$$

From Equation (2.49), the relation for μ becomes:

$$\pi_1 = \pi_3 + k_1 \frac{\pi_5^2 \cdot \pi_6 \cdot \pi_{10}}{\pi_4 \cdot \pi_8} + k_2 \cdot \frac{\pi_2}{\pi_9} \tag{2.56}$$

$$\mu = \left(\alpha_i + k_1 \cdot \frac{\rho}{\gamma} \cdot \frac{h^2 \cdot \cos\dfrac{\theta}{2}}{H \cdot v_t} \cdot \dot{e} \right) + k_2 \cdot \gamma_{bss} \qquad \textbf{(2.57)}$$

Equation (2.57) suggests that the friction coefficient not only depends on the shear strain of the material, but also depends on the topography of the surface, the groove angle, compaction of the material, viscosity of liquid contained in the material, and peripheral speed of the roller. Height penetration can be assumed as a constant, considering that material is filled in the grooved surface. The variables such as velocity, compaction and normal pressure cause reduction of the friction coefficient; while the other ones contribute to raise it. At the initial condition of operation, the friction coefficient has as value α_i. Compaction, γ, seems to be the most prevalent factor influencing the friction coefficient and exhibits a negative trend with increasing compaction. The following correlation may exist for the friction coefficient in a rolling environment

$$\mu = \psi\left(\gamma, \theta, h, p, v_t, \dot{e}, \gamma_{bss} \right). \qquad \textbf{(2.58)}$$

Summary

This chapter has reviewed the fundamental mechanisms influencing friction in a conventional sliding and more complex rolling environment. A dimensional analysis of pertinent variables has been developed and is included in this chapter for completeness, even though the results of the analysis are not used in the rest of this thesis. It is anticipated that the results may be of use to other researchers who want to continue in this general area.

Chapter three deals with the revision of the literature review of the exponential investigations into the interface friction and the empirical model developed until 2003.

3

LITERATURE REVIEW ON EXPERIMENTAL INVESTIGATIONS

Abstract: This Chapter reviews pertinent empirical models used for predicting friction as a function of milling variables. The models date back almost 50 years and include variables such as pressure, rubbing speed, moisture content and the fineness of the prepared cane. In this Chapter we extend the investigation to include other variables: compaction, groove angle and surface roughness.

3.1 Introduction

Over the last 50 years, several experimental investigations have been conducted into the interface friction between prepared cane and bagasse in contact with platens and a two-roll mill (Bullock, 1957; Murry, 1960; Cullen, 1965; Adam, 1997; Plaza F. and Kent G., 1997). Bullock (1957) was one of the first researchers to conduct experimental investigations into interface friction. Bullock's results led to the claim that the friction coefficient is affected by five variables: the normal pressure applied to the mat, degree of preparation of cane, rubbing speed, topology of the roller surface and dryness of fibre. Bullock's extensive experimental investigations allowed him to develop an empirical model for the friction coefficient as a function of the peripheral speed of the roller, i.e.

$$\mu = 0.43 - 0.008\upsilon \qquad\qquad (3.1)$$

where

μ is the friction coefficient, and

υ is the peripheral speed of the roller, $m/\min^{-1}$.

Bullock's experiments were undertaken using an experimental two-roll mill. The friction coefficient determined by Bullock was termed an "apparent coefficient" to indicate the coefficient calculated from the normal force applied to the bagasse which depends on the actual area of contact of the fibre with the roll. This definition is contrary to the basic concept of friction coefficient where the coefficient is independent of the contact surface. Of the five variables suggested by Bullock as affecting the friction coefficient, only the normal pressure and the condition of the rubbing surface support the influence the friction coefficient (Cullen, 1967; Plaza, 2004). The remaining variables did not appear to affect the friction coefficient. Bullock's experiments were carried out at low pressure (20-90 psig). Murry (1960) reviewed the variables investigated by Bullock and extended Bullock's research over a wider range of material preparations. He also suggested the experiments be conducted under controlled conditions in a uniaxial test cell. Cullen (1965), extended Bullock's and Murry's research, by using a shear box apparatus to determine the behaviour of the bagasse compacted under a compressive load. He used normal pressure up to 19.3 MPa. In

addition, he studied the effect of groove angle, surface conditions and material preparation.

In contrast to Bullock's tests, Cullen experimented with the following conditions: pressure from 400 lb/in^2 to 2800 lb/in^2 at four levels; rubbing speed at 1.76 and 8.22 ft/min; density of the cane preparation at 47.9 lb/cu.ft (750 rpm/15 s*) and 39.2 lb/cu.ft (500 rpm/20 s.); and the groove angle at three different levels: 45°, 55° and 180°, respectively. Cullen found that the friction coefficient between bagasse and a smooth or grooved platen decreased rapidly when the normal pressure was increased. This observation led Cullen to postulate that the bagasse is internally sheared by the tangential forces. His conclusion about the effect of the other variables (rubbing speed, groove angles and cane preparation) were inconclusive. Cullen did not develop any empirical model to relate the factors he investigated to the friction coefficient.

Adam (1997) reviewed all previous bagasse friction experiments and developed an improved empirical model, namely,

$$\mu = 1.00 - 8.65x10^{-2} \log_e(\sigma_n) - 2.21x10^{-3} S_r - 1.27x10^{-3} G_\alpha \qquad \textbf{(3.2)}$$
$$+8.01x10^{-5} \log_e(\sigma_n)G_\alpha + 2.74x10^{-4} \log_e(\sigma_n)S_r$$

where μ is the friction coefficient,

σ_n is the normal pressure on the interface

S_r is the relative rubbing speed between the surface, mm^{-1} , and

G_α is the included angle of the grooving(degree), with $G_\alpha = 180^o$ for flat

surface.

The following observations need to be made about the Adam model:

1. Adam's model is only applicable for a limited range of groove angles (34° and 55°) and for smooth flanks.
2. When the model is scrutinized under an increment of rubbing speed, holding the others variables constant, the response of the predicted increment of friction is contrary to Bullock's and Cullen's results.

---

* The preparation resulting from cane prepared in a Waddell (1963) hammer mill operated at 750 rpm for a period of 15 s.

3. Normal pressure has a strong influence on the friction coefficient with the friction decreasing markedly with pressure (Figure 3.1).

4. The effect of the groove angle shows an interesting trend with the friction coefficient (Figure 3.2). The friction coefficient appears to have a less marked effect as normal pressure is increased, indicating a likely interaction between rubbing speed and pressure. The response of the friction coefficient under the effect of the rubbing speed plotted in Figure 3.3 reflects a negative effect to the friction coefficient at pressure up to 2 MPa. However, for pressure beyond 2 MPa the effect of the rubbing speed is not well defined.
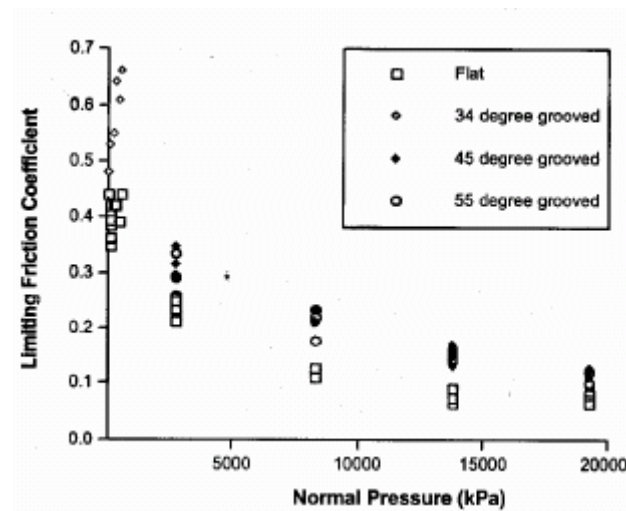
Figure 3.1 *Limiting friction coefficient for different normal pressures*
for fresh prepared cane (Adam 2004).
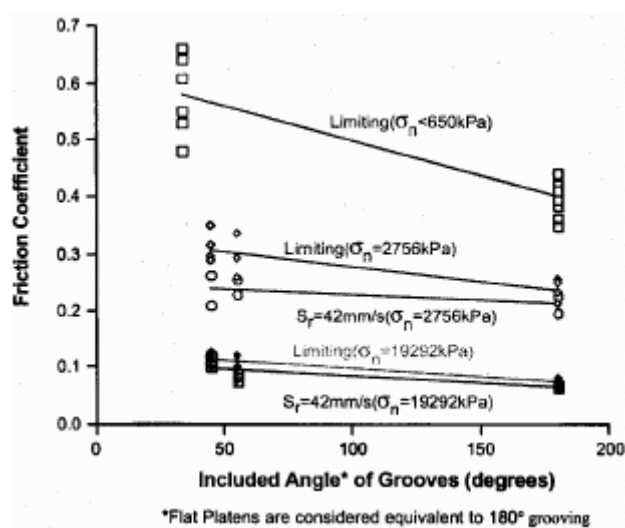
Figure 3.2 *Friction coefficients versus groove angle for various speeds*
at low and high normal pressure (Adam, 2004).
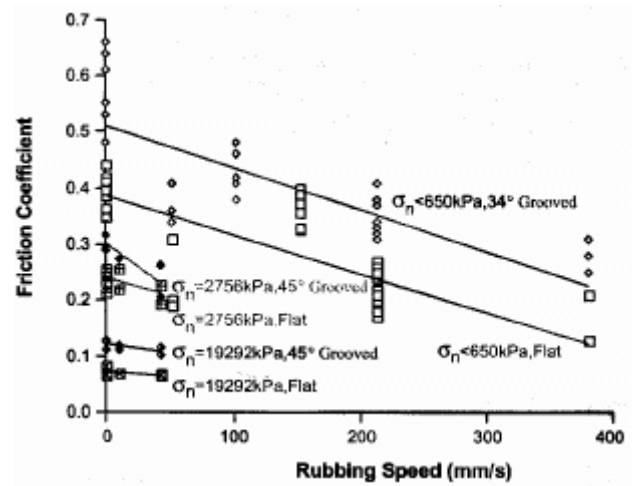
Figure 3.3 *Friction coefficients versus rubbing speed for flat and grooved*

surfaces at low and high speed (Adam, 2004).

Adam and Loughran (2004) also reported the mechanisms of penetration of the bagasse and the frictional forces generated on the flank of the grooved surface (similar to the term wedge in mechanical element), as shown in Figure 3.4, Adam and Loughran (2004) developed an equation for the normal force as a function of pertinent variables, to demonstrate how a grooved surface influences the grip of the mat, i.e.:

$$N = \left[\frac{\cos(G_\alpha/2) + \tan(G_\alpha/2)\sin(G_\alpha/2)}{\mu + \tan(G_\alpha/2)} \right] F_y \qquad (3.3)$$

where

$N =$ the normal force,

$\mu =$ the friction coefficient,

$\alpha =$ the groove angle,

$F_y =$ the compressive load, and

According to Adam's analysis, a grooved surface has the potential to increase the local friction coefficient in proportion to the reactive normal force.
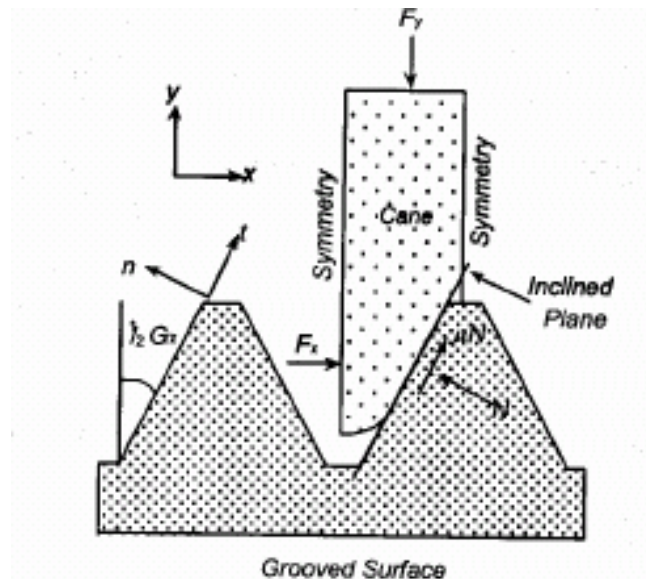
Figure 3.4 *Forces acting on an element of material in a roller groove (Adam, 2004).*

Although this model does not permit the prediction of the friction coefficient in a direction perpendicular to the cross-sectional area of a grooved surface. For flat surfaces (180° groove angle), this model suggests the important role of the angle of a grooved surface may play at the contact surface.

Following Cullen's procedures Plaza (1994) undertook an experimental investigation into the effect of the friction coefficient. In contrast to prior methods, he employed roughened platens covered with small asperities (equivalent to sandpaper). In addition, to test roughness as a factor, Plaza also tested the normal pressure and groove angle (90°, and 180°). The samples used during his experiments were prepared cane and bagasse from final mill. Plaza used the ratio of shear coefficient to friction coefficient to determine the effect of the pressure and roughness on the friction coefficient. Plaza found that the friction coefficient decreased with applied pressure and he postulated that bagasse fails by shear (supporting Cullen's results). Plaza also concluded that roughness does not affect the friction coefficient. Neither the size nor the shape of an asperity influenced the friction. Plaza's results are somewhat limited due to groove angles and roughness dimensions.

Following Bullock (1957), Brunelly (1994) found an empirical coefficient to relate the friction coefficient to the groove angle:

$$\mu' = \mu \frac{1}{\sin \dfrac{\alpha}{2}} \qquad\qquad (3.4)$$

where, μ is the empirical parameter given in Equation (3.1) and α is the groove angle. Brunelly did not justify this statement theoretically, but he reported that the groove angle influences the friction coefficient in an inverse manner. He also believed that the application of asperities on the teeth improve the friction coefficient due to a potential increment of the angle of the flank of the teeth. Brunelly believe that a 60° groove angle would be the maximum angle to achieve maximum feeding.

Summary

Over the last fifty years, several experimental investigation have been undertaken in order to solve problems involving throughput and extraction performance. Both throughput and extraction performance are strongly influenced by the friction between the grooved circumferential rolls and the bagasse mat. This Chapter reports on the strengths and weaknesses of existing empirical models. A particular weakness in all models to date is their inability to account for surface roughness and a wide distribution of groove angles. These weaknesses are addressed in Chapters 4 and 5.

4

RESEARCH METHODOLOGY

Abstract: *The materials and method employed during the experiments are described in this chapter. It also provides details for reproducing the results. The materials, as well as the instrumentation and apparatus required for the tests are illustrated. Also outlined in this chapter are the conditions of the investigation in which the tests were conducted. The method and procedure used to measure shear stress are explained. Finally, the experimental design is developed and the computational analysis is described.*

4.1 Description of the sample

Samples of bagasse were collected from the final milling unit of CSR Macknade Sugar Mill in November 2004. As this investigation was focused on observing the response of the friction coefficient, the inputs for the study were geometry (including roughness), speed of compression (and possibly shear speed), blanket thickness, final compaction, and bagasse preparation. Outputs were friction coefficients, reaction force traces, and visual observations of the local deformation in the vicinity of the tips of teeth and flanks. The average values of the main parameters of the collected bagasse during the tests are shown in Table 4.1.

Table 4.1 *Average values of constituent parameters of bagasse used during the tests.*

Parameters	Average Value(%)
Dry fibre	45.00
Soluble solids	2.80
Moisture	52.20

Cane variety is a parameter which has a potential marked effect on the mechanical properties of the material. In order to avoid potential effects in the observed responses, the total mass of bagasse required for this investigation was sourced at the one time. The effect of the extraneous matter on the responses was not taken into account.

4.1.1 Weight and number of samples

The mass of bagasse required for every test was calculated depending on the selected compaction levels. Parameters such as: the fibre, work opening and area of the test cell (a shear box was used to measure the shear forces) were considered constant. Appendix A shows the calculation method used to determine the mass of bagasse as a function of the compaction level. Factors which influenced the procedure to determine the number

of samples required were expected variance, margin of error, standard deviation and level of precision. These parameters were obtained by reviewing the results of Cullen. Applying these parameters to the present investigation is valid according to Arvanitis (1997). He claims that when the parameters of a population are unknown, it is acceptable to follow the procedure used by previous researchers. The parameters of the present investigation found at 95 % precision indicated that the number of tests to be run were in the order of 100 (Appendix B). However, due to limited resources and time the number of test was limited to 72 using appropriate factorial design techniques.

4.1.2 Collection of samples

Fresh bagasse was taken directly from the exit of the final crushing unit at Macknade Sugar Mill. It was brought to the facilities of James Cook University (JCU) on the same day. The bagasse was lodged in 7 kg amounts in sealed bins and kept in a cold room at a temperature of 10°C. This prevented evaporation of water from the bagasse, so that the fibre content in bagasse was quite close to that exiting the milling unit.

Every day bagasse was taken from the bin and spread on a galvanised tray sheltered from sun. It was mixed and sampled according to Method 5 of the Laboratory Manual for Australian Sugar Mills (Anon., 2001). Prior to routine tests, about half a kilogram of bagasse was taken for fibre content analysis. The average of two analyses was recorded. This analysis was done everyday to take into account loss of weight by evaporation.

4.2 Experimental apparatus and instrumentation

4.2.1 The shear box

The main apparatus used in this experiment was a specially designed and constructed shear box or test cell (Figure 4.1 below). The apparatus consisted of a rectangular metal box composed of two grooved platens, and two lateral plates. The platens were designed so that one of them could move in both a vertical and horizontal direction. The platen with horizontal displacement rested on a heavy linear bearing. This linear bearing enabled the platen to move with a negligible friction coefficient equal to 0.002-0.003 (Anon., 2004). The shear box employed for experiments is depicted in Figure 4.1 and its

design is shown in Appendix C. The design of the test cell was based on the highest compaction level to be tested, the type of grooved angle of the platens and the maximum horizontal displacement of the platen (Appendix A). The box had a plan area of 78 x 97.5 mm and the allowable travel was 310 mm.
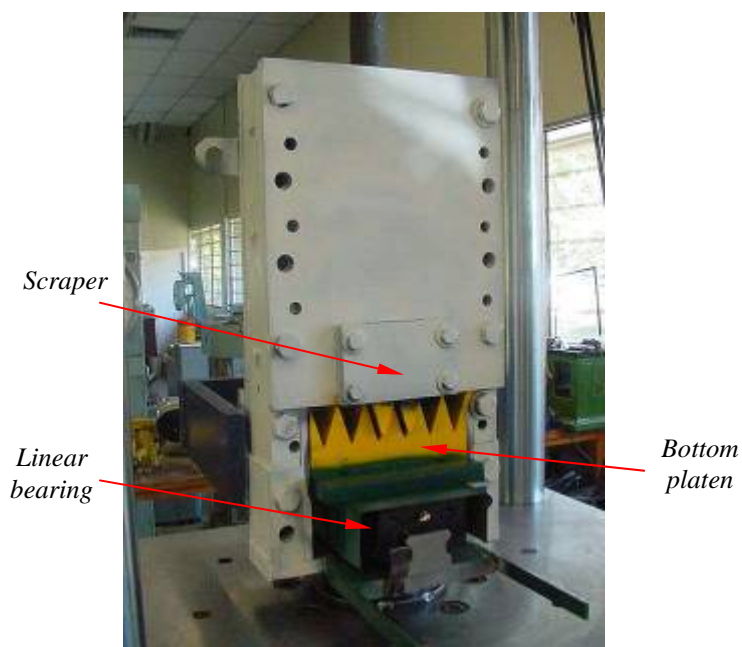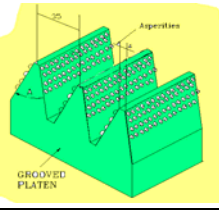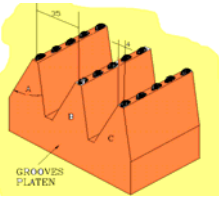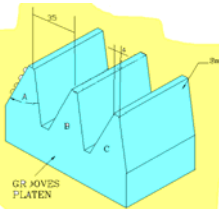
Figure 4.1 *Shear box used for the experiment to determine shear forces.*

4.2.2 The platens

The platens were made of mild steel and can be assumed to be rigid in comparison to the bagasse. Each platen had a minimum of one full tooth and two halves. This arrangement allowed the platens to have enough area to generate frictional forces. The main characteristics of the platens are shown in Table 4.2 and Appendix D. Three pairs of grooved steel platens, classified into three groups were used in the experiment: a) smooth; b) 2-2.5 mm average globules; and c) 4-5 mm average nodules. The last two pair of roughness was made by electric arcing along the flanks of the groove. Three lines of asperities were randomly attached along the flank of the tooth. The reason for experimenting with 2-2.5 mm asperities is because this diameter of roughness is commonly used in the majority of Australian sugar mills. In contrast 4.5 mm welding nodules of hard-facing is routinely used in Brazilian sugar mills (Kent, 2000).

Table 4.2 *Main characteristics of the platens used during the tests.*

Type	Quantity	Angle	Roughness	Criteria
GROOVED PLATEN	2	35° 60° 100° 180°	*2-2.5 mm asperities*	*Australian practice*
GROOVES PLATEN	2	35° 60° 100° 180°	*4-4.5 mm nodule 25 mm apart*	*Brazilian practice*
GROOVES PLATEN	2	35° 60° 100° 180°	*Smooth*	*To compare to roughened platens*

In the experiment, 4.5 mm average nodules were spaced 25 mm apart. The grooves of each group had 38mm pitch and a tip of 4mm width; these parameters were considered constant in order to measure only the effect of the groove angle. The first group of platens had the following characteristics: 35° angle, the second group had 60° angle, the third group had 100° angle, and the fourth group was considered having an angle of 180°. The linear bearing which was used to support the load and cause resistance forces between the bottom platen and bagasse had a static load capacity of 400 kN. The friction coefficient in the linear bearing was assumed to be zero.

An Instron 6600 Controller served as a data acquisition and capture unit. To weigh the sample of bagasse, a precision scale, Mettler PC24, was used. The asperities located on the flank and tips of teeth were big enough to be measured by a vernier. To record the potential shear plane of the bagasse and adherence of the fibre around the profile of the teeth a digital camera was used. The different types of instrumentation used and the measurements involved during the experiments are shown in Table 4.3.

Table 4.3 *Variables measurements and instrumentation applied*

Parameter	Instrumentation used	Unit
Forces	Load cell	kN
Displacement	Potentiometer	mm
Fibre/bagasse	S.R.I. Can Fibre Machine	g/g
Roughness	Vernier	mm
Weight	Precision Scale	g

The fibre analyser which permitted the direct determination of the fibre in bagasse is shown in Figure 4.2

Figure 4.2 *Fibre machine, apparatus for determining the fibre content in bagasse (after Loughran et., al. 1988).*

The MTS machine located in the structural testing laboratory at JCU was employed to apply the compression loads (Fig. 4.3). It has a capacity of 1000 kN and a stroke of 140 mm. Its ram was set up to travel at a speed of 0.01 m/s.

Figure 4.3 *MTS machine for uniaxial compression tests.*

To apply a shear force to the specimen of bagasse, a horizontal hydraulic ram was employed. This horizontal ram was positioned to the back side of the shear box so that it allowed the bottom platen to be pushed away. The frame which supported the horizontal ram was bolted to the main frame of the test cell in order to avoid movement of the cell in the direction of the applied shear force. The hydraulic cylinder-pump has a capacity of 20 ton and 8.25-inch stroke. A schematic representation of the facility used for the experiments is depicted in Figure 4.4.

4.3 Description of the experiment

4.3.1 The variables

This experimental investigation was carried out to determine the factors affecting the interface friction between bagasse and grooved steel platens. The response or dependent variable was the friction coefficient. The outcome of the response variable was quantitative.
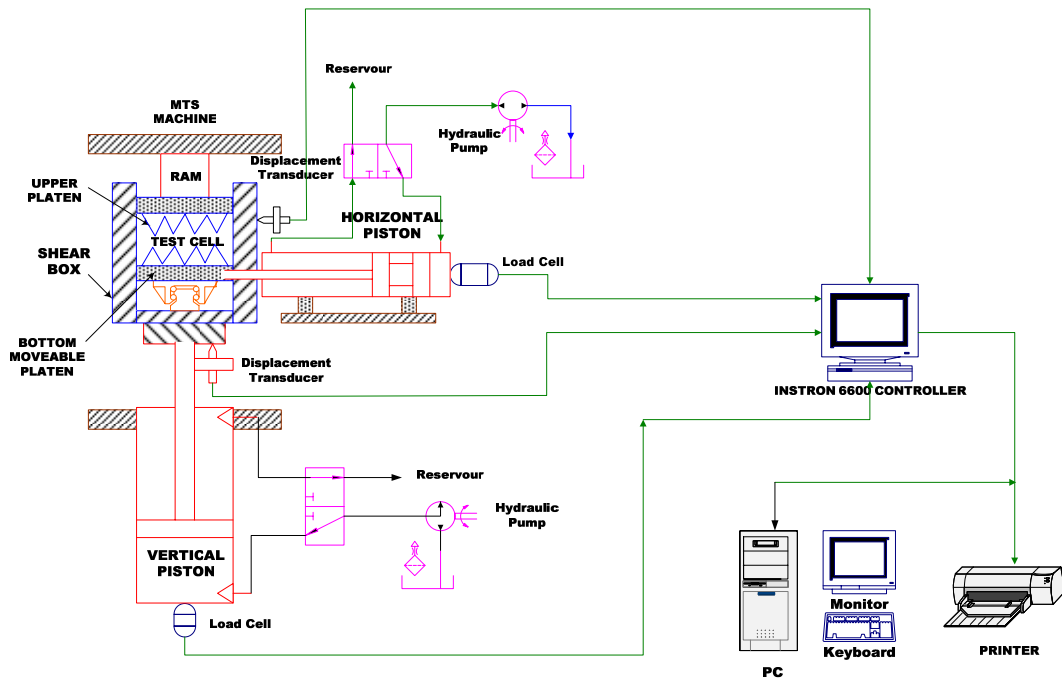
Figure 4.4 *Diagram of equipments and instrumentation for experimental tests.*

The controllable independent variables that contributed to the variable response were roughness, groove angle and bagasse compaction level. The levels selected and the units of each independent variable are shown in Table 4.4. In order to express the limits of the roughness in quantitative magnitudes, the smooth level has been assumed to have a roughness equivalent to zero. This assumption is based on the fact that the other two roughness levels are relatively big with respect to a smooth surface. Variables other than the above mentioned ones were assumed to remain constant and appear as random error in the prediction.

Table4.4 *Levels selected for each variable and its measurement units*

Independent Variables	Unit	Level
Roughness, R	mm	0 *, 2.25 asperities and 4.5 nodules on tip as an average height
Groove Angle, G	Degree	35, 60,100,180
Bagasse Compaction , C	kg/m^3	400, 700, 1000

(*) :The smooth surface was assumed to have an average roughness ,Ra, equal to zero.

The different selected levels from the three factors were combined in order to obtain values of the response variable. As the levels of the each factor were chosen in advance, the resulting model was considered fixed.

4.3.2 The experimental procedure

The cell test was positioned in the MTS machine and the instrumentation set up for recording vertical and horizontal loads. Work opening, the mass of bagasse, the compressive load and shear load were measured to calculate the friction coefficient. These measurements were recorded with the limit errors shown in Table 4.5.

Table 4.5 Measurement errors of main parameters to measure shear forces

Parameter	Units	Measurement Errors
Work opening	mm	± 1.0
Compressive load	kN	± 0.01
Shear load	kN	± 0.5
Mass	g	± 0.01

Bagasse was taken out of cold storage, placed in a plastic bag, and mixed following the procedure stated in Anon. (2001). Next, a sub-sample of material was taken and weighted with a precision scale in quantities shown in Table 4.6. An average of six tests a day was conducted. Before charging the test cell, an analysis of fibre content was carried out by using the can fibre machine. A test consisted of charging the test cell from the top, positioning the test cell in the MTS, precompressing through axial travel of the top-head, fixing the top head, loading the sample uniaxially to achieve the desired compaction, shearing the sample horizontally.

The compressive load was held for two and a half minutes as follow: 1) One-half minute to drain out the liquid contained in the specimen, in order to minimise any potential porous water pressure in the material; 2) One minute to push the bottom platen and cause shear failure; 3) One minute to check the work opening and find the effective compaction. The maximum stroke covered by the push force was 14 to 15 mm.

Table 4.6 *Mass of bagasse used for the tests as a function of compaction at different groove angles.*

Groove (degree)	Set opening (mm)	Deep Groove (mm)	Work Opening (mm)	Cell Area (m²)	Total Volume (m³)	Average Fibre Bagasse (%)	Mass of Bagasse (kg)		
							C = 1000 Kg/m³	C = 700 Kg/m³	C = 400 Kg/m³
35	40	51	91	0.007605	0.000652	45	1.44	1.01	0.58
60	40	28	68	0.007605	0.000495	45	1.10	0.77	0.44
100	40	13.5	53.5	0.007605	0.000396	45	0.88	0.59	0.35
180	40	0	40	0.007605	0.000304	45	0.68	0.47	0.27

The horizontal shear force was set up so that the bottom platen could travel at an average velocity of 0.009 m/s. In order to avoid shear failure in the compressed sample when the shear force was applied, a groove scraper was installed in the test cell (Figure 4.1). The clearance between the scraper and the platen was 1mm. It is possible that some local failure could occur in the interface friction between bagasse and the grooved platen; however the teeth showed clean surfaces at the end of the push test. This procedure was applied to each test performed. The compressive load was recorded by the Instron controller, while the tangential force applied to the platen was calculated from readings taken from the pressure gauge. Pressure readings were converted into load readings using an Arber Universal testing apparatus. The quantification of the shear force was made possible by removing the scraper and allowing the bagasse to undergo shear failure. The friction coefficient was calculated making use of Equation 4.1. The quotient of the horizontal force and the normal load was recorded as coefficient of friction. The normal force was determined by Equation (2.40). The friction coefficient determined was static. Kinetic friction was not recorded due to the lack of suitable instrumentation. However, in situ observations showed that the shearing force was in the order of 15% less than the maximum tangential force applied to the sample

$$\mu = \frac{F_c}{F_t} \qquad (4.1)$$

where

F_c = normal load, kN; and

F_t = tangential load, kN.

At the end of each test, the compacted sample was discarded. Each new test was performed with fresh bagasse. The tests were performed at a temperature of 23 $^{\circ}$C. Analysis of fibre in bagasse was done daily. The order of the test followed during the experiment is shown in Table 4.7. The type of groove roughness, the groove angle and the compaction level of the material were taken as independent variables, X_n. No proof of the alignment of the fibres and deformation of the bagasse in the proximity of two rough teeth was obtained. However, observations of the fibre adhered to the roughened flanks were taken (Appendix E).

4.3.3 Experimental design

The following experimental design was selected to obtain data, which can provide objective results and valid conclusions with minimum expenditure of time and resources. The model which describes the number of experimental conditions is

$$N_s = k_1 \cdot k_2 \cdot ... \cdot k_n \qquad \textbf{(4.2)}$$

where

N_s = number of responses or tests in the experiment

k = number of levels of a factor, and

n = total number of factors in the experiment.

The number of tests or combinations required is:

$$3C \times 4G \times 3R = 36 \; combinations$$

Therefore, there are 36 experimental conditions needed to measure the potential effect of the three independent variables on the friction coefficient between bagasse and steel grooved platens.

4.3.4 Analytical model describing the experiment

The design of the mathematical model was given by Equation (4.3). This model describes the response variable as a function of the measured factors and the unmeasured parameters in the problem. The model permitted the interpretation of the dependence that the response variable had on each factor during the experiment

$$y = f(X, E) \tag{4.3}$$

where

$X =$ is the independent variable or factors $x_1, x_2 \ldots, x_p$

$E =$ is the parameter that influences the outcome of the problem but is not
identifiable or controllable, and

$y =$ is the objective outcome or the dependent variable in the problem.

The model used was

$$y_{ijkm} = c + \tau_{ijk} + \varphi_{m(ijk)} \tag{4.4}$$

where

$c =$ the true mean or common effect on y in all cells of the experiment

$\tau =$ the true effect of the ith level of factor on the response y

$\xi =$ the true effect of the unmeasured parameters in all cells, and

$y =$ the true response in the ith cell.

4.3.5 The design of the experimental model

A number of replications are sometimes necessary in order to understand how much variation exists between experimental tests. Analysis of variance (ANOVA) allows the replications to see whether these differences are real or due to the noise in a system. The number of times that the functional model is replicated is based on the total of number of degree of freedom for every factor analysed. For example, a sum of degree of freedom less than 6 may give a response requiring more replications. This empirical rule

indicated that the minimum number of replicates should have been three. However, this would mean running 108 tests which was not feasible. As a result this experiment was restrained to only two replicates. The number of tests for the experiment was calculated by Equation (4.5)

$$N = nN_f \qquad\qquad \textbf{(4.5)}$$

where, N is the number of tests in the experiment and n is the number of replicates

$$N = 2r \times (3C \times 4G \times 3R) = 72 \ \text{tests}$$

The 72 tests were randomised in order to ensure that each sample or treatment in the experiment had an equal chance of being assigned to each combination. According to the number of independent variables selected the following mathematical model was defined

$$y_{ijkm} = \bar{y} + R_i + C_j + RC_{ij} + G_k + RG_{ik} + CG_{jk} + RCG_{ijk} \qquad\qquad \textbf{(4.6)}$$

with

$i = 1,2,3 \qquad j = 1,2,3 \qquad k = 1,2,3,4 \qquad m = 1,2,;$

where

$\tau_{ijkm} = R_i + C_j + G_k + RC_{ij} + RG_{ik} + CC_{jk} + RCG_{ijk;}$

and

$\varphi_{m(ijkn)} = NID(0, \sigma_e^2), \ random \ error$

where, R_i denotes the effect of the ith level of factor R, G_{ijk} denotes the interaction effect of the i_{th} level of R and the j_{th} level of C, and m is the number of observations or replications. The error term $\varphi_{m(ijkm)},$ is usually considered to be a normally and independently distributed (*NID*) random effect with mean value of zero and the same variance for all treatments (levels).

4.3.6 Boundary conditions and restrictions for the experiments

In some experiments a completely randomised order of experimentation is used in order to average out the effects of the variables which cannot be controlled. Such averaging does not remove those effects completely; they still increase the variation of factors (variables) tested in the observed data. In the particular case of this experiment it was possible to randomise completely or even randomise within a block. This was due to two restrictions to the model: the manipulation and change of the platens in the shear box, and the variation of the sample mass which took time. Preliminary tests indicated that the time required to complete a test was typically 1-2 hours. A change of treatment or combination required from half an hour to one hour. Due to these long periods of time, an average of five to six runs was feasible per day. In order to achieve two replications, by complete replication of the whole experiment, the following arrangement was fixed: it was required to run each replication in either the same day or the following day. This restriction required a blocked design. Within each block; an experiment was run putting a certain mass of bagasse equivalent to a determined level of compaction using the platens with three asperities and four groove angles. After the roughness was selected, all three compactions were tested at that groove angle. Then another groove angle was selected and all three compactions were tested. The others two groove angles remaining were tested in a similar manner. The remaining two types of roughness also followed the same procedure. Both roughness and groove angle were variables with randomisation restrictions within a block. The groove angle formed three subplots. The angles were randomised. Finally, compaction formed three sub-subplots and was tested randomly. This arrangement permitted the use of the experimental design called *split-split plot.* Split-split plot design means that two main effects (compaction and roughness) are confounded with blocks. Groove angle and roughness were confounded because they were of interest in this experiment. The interaction groove-angle-roughness was also considered to be of interest. By throwing three dices, the order of randomisation was made. The samples of bagasse and the boundary conditions of the test cell were assumed not to change significantly, except for possible evaporation in the samples. The order of the tests in every replication for a split-split-plot design is shown in Table 4.7.

Table4.7 *Randomised order of the samples for the split-spilt-plot design for shear*
force tests on steel grooved platens

Block	Roughness,R / Groove,G / Compaction (kg/m³)	Smooth, 0 mm				Asperities, 2.25 mm				Nodules, 4.50 mm			
		35°	60°	100°	180°	35°	60°	100°	180°	35°	60°	100°	180°
1	400	3	16	12	22	65	69	56	49	36	30	39	43
		5	14	7	21	63	70	55	50	31	26	38	48
2	700	2	15	9	19	62	72	57	51	34	25	42	44
		4	18	11	23	66	71	60	53	32	27	37	46
3	1000	1	17	10	24	64	68	58	52	33	28	40	45
		6	13	8	20	61	67	59	54	35	29	41	47

The mathematical model for the split-split plot design is given by Equation (4.7)

$$Y_{ijkmq} = \bar{y} + \underbrace{n_i + C_j + nC_{ij}}_{whole-plot} + \underbrace{R_k + nR_{ik} + CR_{jk} + nCR_{ijk}}_{split-plot} \qquad (4.7)$$

$$\underbrace{+ G_m + nG_{im} + CR_{jm} + nCG_{ijm} + RG_{km} + nRG_{ikm} + CRG_{jkm} + nCRG_{ijkm} + \varepsilon_{q(ijkm)}}_{split-split-plot}$$

where,

   n is the number of replicates,

   $i = 1,2,,\ \ j = 1,2,3,\ \ k = 1,2,3,\ \ m = 1,2,3,4$ and $q = 1$.

4.3.7   Collection of the experimental data

Compression and shear data were recorded and store in the Instron digital controller. This unit interfaces with a personal computer measured load, and position at a sampling rate of 2Hz. The controller uses a Win COM Plus data communications program to share data and results with Windows-based spreadsheet and database programs. The results of the tests were displayed in Excel, which permitted the visualization and recording of the load applied to the samples as a function of time and position. The precompression tests were not recorded because they were not of interest. The exception was when tests at 1000 kg/m^3 and 35° groove angles were conducted. The precompression reached up to 120 mm height.

4.4 Research hypothesis

The object of this investigation is to determine if the three independent variables selected affect the interface friction between bagasse and a grooved steel platen. As this experiment was run to determine if roughness, groove angle and compaction effects are interacting with the interface friction, the following hypothesis was stated:

> ***"no real roughness, no groove angle and no compaction effects are present at the interface friction between bagasse and the grooved platens".***

From the data analysed it is expected to be able to determine that the above hypothesis will be true if and only if $H_o : \Theta_o = 0$. This result implies that the variables studied do not affect the friction coefficient. On the other hand, it will be considered false if the stated hypothesis returns $H_1 : \Theta_1 > 0$ *(Induction).* Accordingly, the hypothesis will be rejected. The value of the significant level used to determine the probability of obtaining a value of the test statistic, was $\alpha = 0.05$. That is, if α is greater than the observed p value, then the stated hypothesis is accepted as a true.

4.5 Statistical technique of evaluation

Analysis of variance (ANOVA) is required to investigate the stated hypothesis. ANOVA bases its analysis on the sum of square of the deviation of the fixed model and the observed values of the dependent variable, y. A good decision making technique for testing the hypothesis is through the *F-ratio*, which relates the mean square of the treatments (main variables or interacted variables) to the mean square of the error. The rejection of the hypothesis is based on

$$P\left[F_{obs} > F_{\alpha}\right] = \alpha \qquad\qquad \textbf{(4.8)}$$

In order to simplify the calculation of the statistical analysis involved, the calculations of ANOVA were done using two commercial statistical software programs: Minitab and Design-Expert.

4.5.1 The empirical model

A possible empirical model to predict the friction coefficient is

$$y = \beta_o + \underbrace{\beta_1 x_1 + \beta_2 x_2 + \beta_3 x_3 + \beta_4 x_1^2 + \beta_5 x_2^2 + \beta_6 x_3^2 + \beta_7 x_3^3}_{Main.effects}$$

$$+ \underbrace{\begin{array}{l} \beta_7 x_1 x_2 + \beta_8 x_1 x_2^2 + \beta_9 x_1 x_3 + \beta_{10} x_1 x_3^2 + \beta_{11} x_1^2 x_2 + \beta_{12} x_1^2 x_3 \\ + \beta_{13} x_2 x_3 + \beta_{14} x_2 x_3^2 + \beta_{15} x_2^2 x_3 \end{array}}_{\substack{Two-ways \\ Interactions}}$$

$$+ \underbrace{\beta_{16} x_1 x_2 x_3 + \beta_{17} x_1 x_2 x_3^2 + \beta_{18} x_1^2 x_2 x_3 + \beta_{19} x_1 x_2^2 x_3}_{\substack{Three-way \\ int\,ercactions}} + \varepsilon$$

(4.9)

where

$y =$ predicted friction coefficient

$x_1 =$ compaction (kg/m^3)

$x_2 =$ roughness (*mm)*

$x_3 =$ groove angle (*degree)*

$\beta_o =$ constant

$\beta_1, \beta_2 ... \beta_{19} =$ coefficients (linear, quadratic and cubic), and

$\varepsilon =$ random error.

Equation (4.9) is complex and it is difficult to determine all coefficients. A more practical model would be quadratic or cubic (Belz, 1973). The order of the model which represents the observed values of the response depends on either the lack of fit or the coefficient of determination, *R-q*. However, if the experiment is not so large to induce much curvature a response of the high-order terms can be neglected and this will not unreasonably distort the response (Mendelhall, 1968). The empirical equation for a quadratic and cubic model is given by equation (4.10) and (4.11) respectively.

$$y = \beta_o + \underbrace{\beta_1 x_1 + \beta_2 x_2 + \beta_3 x_3 + \beta_4 x_1^2 + \beta_5 x_2^2 + \beta_6 x_3^2}_{Main.effects} + \underbrace{\beta_7 x_1 x_2 + \beta_8 x_1 x_3 + \beta_9 x_2 x_3}_{\substack{Two-ways \\ Interactions}}$$ (4.10)

$$y = \beta_o + \underbrace{\beta_1 x_1 + \beta_2 x_2 + \beta_3 x_3 + \beta_4 x_1^2 + \beta_5 x_2^2 + \beta_6 x_3^2}_{Main.effects} + \underbrace{\beta_7 x_1 x_2 + \beta_8 x_1 x_3 + \beta_9 x_2 x_3}_{\substack{Two-ways \\ Interactions}}$$ (4.11)

$$+ \underbrace{\begin{array}{l} \beta_{123} x_1 x_2 x_3 + \beta_{112} x_1^2 x_2 + \beta_{113} x_1^2 x_3 + \beta_{122} x_1 x_2^2 + \beta_{133} x_1 x_3^2 \\ + \beta_{223} x_2^2 x_3 + \beta_{233} x_2 x_3^2 + \beta_{111} x_1^3 + \beta_{222} x_2^3 + \beta_{333} x_3^2 \end{array}}_{\text{three-way interaction}}$$

Analysis of variance for two replication of a $3\times3\times4$ factorial is shown in Table 4.8

Table 4.8 *Analysis of variance for $3\times3\times4$ factorial.*

Source	d. f.	SS	MS
x_1	2	$SS\,x_1$	$SS\,x_1$
x_2	2	$SS\,x_2$	$SS\,x_2/2$
x_3	3	$SS\,x_3$	$SS\,x_3/2$
x_1x_2	4	$SS\,x_1x_2$	$SS\,x_1x_2/3$
x_1x_2	6	$SS\,x_1x_2$	$SS\,x_1x_2/6$
x_2x_3	6	$SS\,x_2x_3$	$SS\,x_2x_3/6$
$x_1x_2x_3$	12	$SS\,x_1x_2x_3$	$SS\,x_1x_2x_3/12$
Replications	*1*	*SSr*	*SSr*
Error	35	SSE	SSE/35
Total	71	$\sum\limits_{i=1}^{72}\left(y_i-\bar{y}\right)$	

4.5.2 The best response curve

It is common practice to graphically represent a variable of interest as a curvilinear function of a single independent variable. However, when the independent variable *y* is a function of two or more variables, $x_1,x_2...,x_k$, it is no longer possible to use a single curve on a two-dimensional graphic representation, but on a $(k+1)$-dimensional space (*k* is the number of independent variables). This method of representing a function is called a response surface. Although it is not viable to visualise surfaces in more than three dimensions, the analogy is functional. In this experimental investigation a good approximation to the response surface is required so as to assist in locating the maximum response (friction coefficient) of the independent variables. A $3\times3\times4$ factorial experiment for fitting a second/third-order model to a response surface requires a great number of experimental points, which makes it a computationally expensive process. An orthogonal composite design is preferred to the 3^k factorial design. This design utilizes a 2^k factorial experiment augmented by points at the axes of the independent variables and at the design centre (Cochran, 1966). There are two designs of the response surface widely adopted: Box-Behnken Design (BBD) and Central Composite Designs (CCD). The selected design to model the interface friction between

bagasse and the grooved platen was the Box-Behnken Design (BBD). This design was selected because it was less expensive to run than Central Composite Designs (CCD) and required few combinations of the factors to estimate the response of the dependent variables compared to the CCD. The mathematical relationship of the response (friction coefficient) on these factors was approximated by the quadratic (second-order) polynomial equation as:

$$y = b_o + \sum_{j=1}^{k} b_j x_j + \sum_{j=1}^{k} b_{jj} x_j^2 + \sum_{i=1}^{k-1}\sum_{j=i+1}^{k} b_{ij} x_i x_j \qquad (4.12)$$

with the response model

$$FC = b_o + b_1 R + b_2 G + b_3 C + b_{12} RG + b_{13} RC + b_{23} GC + b_{11} R^2 + b_{22} G^2 + b_{33} C^2 \qquad (4.13)$$

For a cubic polynomial model:

$$\begin{aligned} FC = {} & b_o + b_1 R + b_2 G + b_3 C + b_{12} RG + b_{13} RC + b_{23} GC + b_{11} R^2 + b_{22} G^2 + b_{33} C^2 \\ & b_{113} RGC + b_{112} R^2 G + b_{113} R^2 C + b_{122} RG^2 + b_{133} RC^2 + b_{233} G^2 C + b_{233} GC^2 \\ & b_{111} R^3 + b_{222} G^3 + b_{333} C^3 \end{aligned} \qquad (4.14)$$

where

FC = predicted friction coefficient
b_o = constant
b_1, b_2 and b_3 =   linear coefficients
b_{12}, b_{13} and b_{23} = cross product coefficients
$b_{123}, b_{112}, b_{113}, b_{122}, b_{133}, b_{223}$ and b_{233} = cross product coefficients
b_{11}, b_{22} and b_{33} = quadratic coefficients, and
b_{111}, b_{222} and b_{333} = cubic coefficients.

The levels of the three independent factors were arranged as follow: roughness (R) ranging from 0 mm to 4.5 mm average roughness, groove angle (G) varying from 35° to 180° and compaction, (C) which varied from $400\,kg/m^3$ to $1000\,kg/m^3$. To satisfy the code units (-1, 0, +1) the following formula was used (Box, 1978):

$$a = \frac{x - \bar{x}}{\Delta x} \qquad (4.15)$$

where
  $a = $ coded value
  $x = $ natural value,
  $\bar{x} = $ natural value in the centre of the domain,
  $\Delta x = $ increment of x corresponding to one unit of a

Table 4.9 shows the boundaries of the experimental field and the levels selected for every independent variable represented in code and natural units.

Table 4.9 *Code units* and l*evel of the variables selected for the experimental design.*

Experimental Factors			
Code Units	Average Roughness R_a (mm)	Groove angle (degree)	Compaction (kg/m³)
-1	0.00 mm smooth	35	400
0	2.25 mm globules	60	700
+1	4.50 mm nodules	100	1000

The level required to satisfy the centre of the domain of the design in respect to the factor groove angle should have been 107.5^o according to Equation (4.14). However, 100° was the angle employed for being of routine use. Table 4.10 shows codes used for each factor at double replicates.

Table 4.10 *The Box-Behnken design for the three variables at two replicates*

Test(N_o)	Roughness (*mm*)	Groove angle (º)	Compaction(*kg/mm³*)
1	-1	-1	0
2	1	-1	0
3	-1	1	0
4	1	1	0
5	-1	0	-1
6	1	0	-1
7	-1	0	1
8	1	0	1
9	0	-1	-1
10	0	1	-1
11	0	-1	1
12	0	1	1
13	0	0	0
14	0	0	0
15	0	0	0
16	0	0	0
17	0	0	0
18	0	0	0
19	0	0	0
20	0	0	0
21	-1	-1	0
22	1	-1	0
23	-1	1	0
24	1	1	0
25	-1	0	-1
26	1	0	-1
27	-1	0	1
28	1	0	1
29	0	-1	-1
30	0	1	-1
31	0	-1	1
32	0	1	1
33	0	0	0
34	0	0	0
35	0	0	0
36	0	0	0
37	0	0	0
38	0	0	0
39	0	0	0
40	0	0	0

Summary

In the methodology chapter above the selection of the sample, apparatus and the experimental design used to investigate the interface friction between bagasse and a steel grooved platen was described. Emphasis is given to the factorial experiment design selected. This factorial experiment design constituted an important part of the investigation process in achieving, valid conclusions and objective results. It determined the order of the experimentation, the method of randomisation (split-split-plot design), and the mathematical model for the experiment. In addition, the factorial experiment design established the hypothesis for the relationship between friction coefficient and the three independent variables (no real roughness, no groove angle and no compaction affects are presented in the friction coefficient between bagasse and the steel groove angle). The procedure to accept or reject the stated hypothesis and the results observed was described.

In the next chapter the responses of the friction coefficient under the affect of the three independent variables are shown.

5

RESULTS

Abstract *This chapter presents the effect of three independent variables: roughness; groove angles; and compaction on both the friction coefficient value and dewatering of bagasse. A statistical analysis of the results is reported in order to validate the original hypothesis which states that the roughness, groove angle and compaction do not influence on the friction coefficient. The results are presented graphically to show how the friction coefficient responds to each of the factors tested.*

5.1 Response of friction coefficient to roughness, groove angle and compaction

The friction coefficient responses for each of the 36 duplicated experiments are shown in Table 5.1.The observed results reflect that the dependent variable responded in a well-defined manner at every level tested and every combination among variables. Similarly, the replicated tests showed that the responses were not similar to each treatment. However, they showed the same trend at every level tested. This behaviour demonstrated that the responses were reliable, and the experimental design was proper. The results show that the friction coefficient is influenced by compaction, groove angle and roughness. The response with compaction is negative and marked while the response with groove angle and roughness is positive and less marked. Roughness caused less increment on the friction coefficient than groove angle. Figure 5.1 exhibits three line graphs of the average friction coefficient versus the independent variables as main effects. The average of the 72 computed tests indicated that the friction coefficient value was 0.323. Figure 5.1 can be explained as follow. Each point in Graph (a), (b) and (c), respectively, is the response mean of the mean for each factor level of two factors holding the other factor as a constant. The dotted line is the overall mean in the three graphs. This overall mean is the average of three response means for each factor level combined with two factors. For example in Graph (a), a friction coefficient value of 0.313 results from the mean of each level of compaction and groove angle, respectively, holding roughness at 0.00 mm height. Roughness at 0.00 mm height is –0.010 from the overall mean, while roughness at 2.25 mm height is 0.041 from the overall mean. Therefore, the means for roughness at 0.00 mm and roughness at 2.25 mm differ from the overall mean.

Graph (a), in Figure 5.1, shows how the coefficient varies from smooth surface to 4.5mm height roughness (nodules). When the surface is smooth the coefficient value is 0.313. The coefficient reached a peak value of 0.364 when roughness was 2.25 mm. The graph also shows that increments in height greater than 2.25 mm result in a drop in the magnitude of the coefficient (0.293 when roughness was 4.5 mm height).

Graph (b) displays the variation of the friction coefficient with respect to the angle of a grooved surface. The friction coefficient increases rapidly from 0.188 to 0.416 when the angle is varied from 35° to 180°. Graph (b) also shows that from 60° on, the coefficient increased steadily over the average friction coefficient value.

Table 5.1 *Friction coefficient results between bagasse and grooved steel platens*

		Average roughness											
		0 mm (smooth)				2.25 mm (asperity)				4.5 mm (nodules)			
		Groove angle (degree)				Groove angle (degree)				Groove angle, (degree)			
Replication	Compaction, Kg/m³	35	60	100	180	35	60	100	180	35	60	100	180
I	400	0.341	0.290	0.320	1.392	0.244	0.984	0.976	0.761	0.206	0.375	0.847	0.609
	700	0.147	0.252	0.301	0.143	0.199	0.246	0.278	0.229	0.240	0.260	0.268	0.157
	1000	0.085	0.203	0.149	0.121	0.157	0.157	0.186	0.146	0.157	0.149	0.156	0.145
II	400	0.180	0.523	0.195	1.523	0.234	0.536	1.207	0.673	0.218	0.397	0.758	0.630
	700	0.151	0.235	0.218	0.188	0.195	0.264	0.266	0.180	0.209	0.258	0.245	0.162
	1000	0.119	0.141	0.162	0.132	0.153	0.165	0.150	0.155	0.153	0.149	0.142	0.145
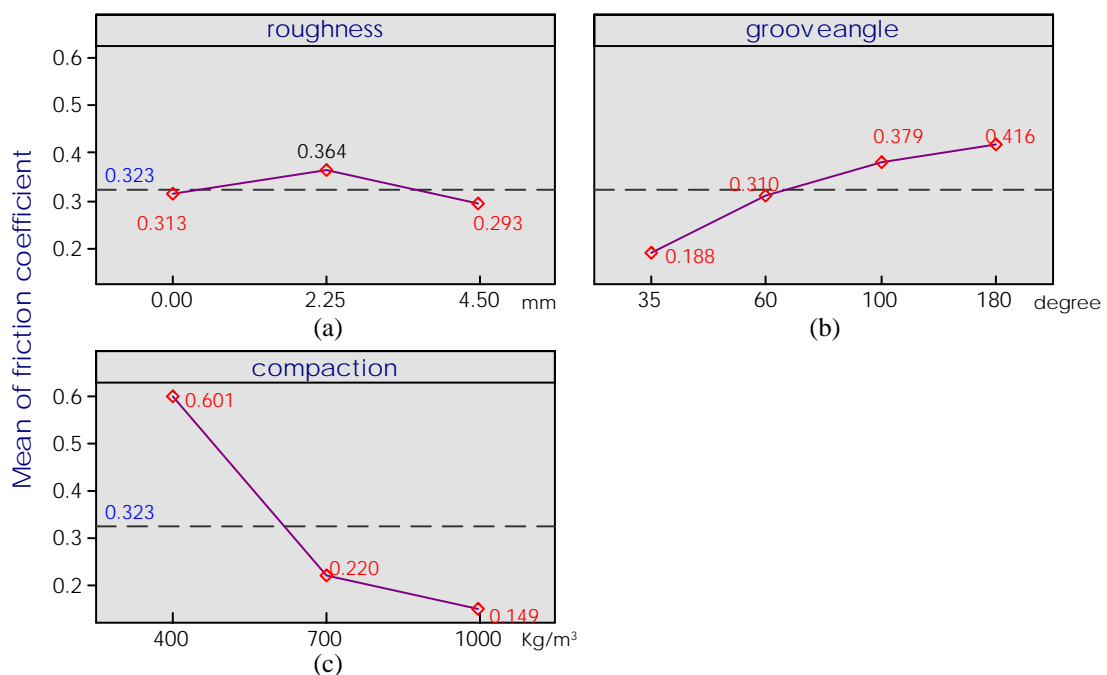
Figure 5.1 *The effect of roughness, groove angle and compaction on the mean value of the friction coefficient.*

Graph (c) in Figure 5.1 shows the effect of the compaction on the friction coefficient. The coefficient exhibits its maximum value of 0.601 when the bagasse is compacted at $400\,kg/m^3$. As compaction is increased the coefficient starts to decrease markedly with a minimum average value of 0.149 at the maximum compaction of $1000\,kg/m^3$. Examining graph (c) the friction coefficient drops sharply from 0.601 to 0.202 when the compaction

rises from 400 to $700\,kg/m^3$. The response of the coefficient is less marked between 700 and $1000\,kg/m^3$. Examining Table 5.1, the most remarkable aspect of the observed results is that the effect of one factor on the response did not remain the same for every level tested. In similar way, the responses are different when two or three factors are combined. This implies that there is an interaction between terms. For example, the friction coefficient resulting from a combination of roughness and groove angle is different for the smooth and roughened platens, at groove angles greater than 100° (at the same compaction). This result suggests that there is an interaction between roughness and groove angle. Therefore, the effect of the groove angle on the friction coefficient depends on the roughness. The interaction effects between the friction coefficient and the independent variables are graphically depicted in Figure 5.2(a) to (f).

Graph (a) shows the average values of the friction coefficient versus roughness, both interacting with groove angle and compaction. Analysing graph (a) the friction coefficient shows variation due to main and interaction effects between groove angle and roughness. While an increase in the value of the friction coefficient depends on an increment of both angle and roughness, the coefficient only increases if there is interaction for smooth surfaces with groove angle greater than 100°; otherwise, the coefficient decreases when the angle is between 100° and 180°. The coefficient reaches its maximum value when the angle is greater than 100 and the height of the asperity increases from smooth to 2.25mm.

The response of the friction coefficient versus groove angle, interaction with compaction and roughness is exhibited in graphic (c) and (d) in Figure 5.2. Graph (c) which depicts the same response of the coefficient as graph (a) indicates that the coefficient remains constant as roughness increases when the angle is 180° (flat surface). According to graph (d) the coefficient declines not only with compaction and increase in groove angle but also when these two independent variables are interacting. Graph (f), which is the same response as graph (d), shows that the interaction compaction-angle effect is significant when compaction rises from 400 kg/m^3 to 700 kg/m^3 as the angle increases. This interaction seems not to be significant between 700 kg/m^3 and 1000 kg/m^3, indicating that friction coefficient only depends on compaction, particularly at 1000 kg/m^3. The interaction between compaction and roughness indicates that this combination has an effect on the friction coefficient. Graphs (e) and (f) indicate that roughness and compaction can only exert a main effect and interaction (between the above two factors) on friction coefficient when the bagasse compacted is 400 kg/m^3 and the height of the roughness is increasing.

For compaction greater than 400 kg/m^3, there is no significant effect of roughness (0.00 mm to
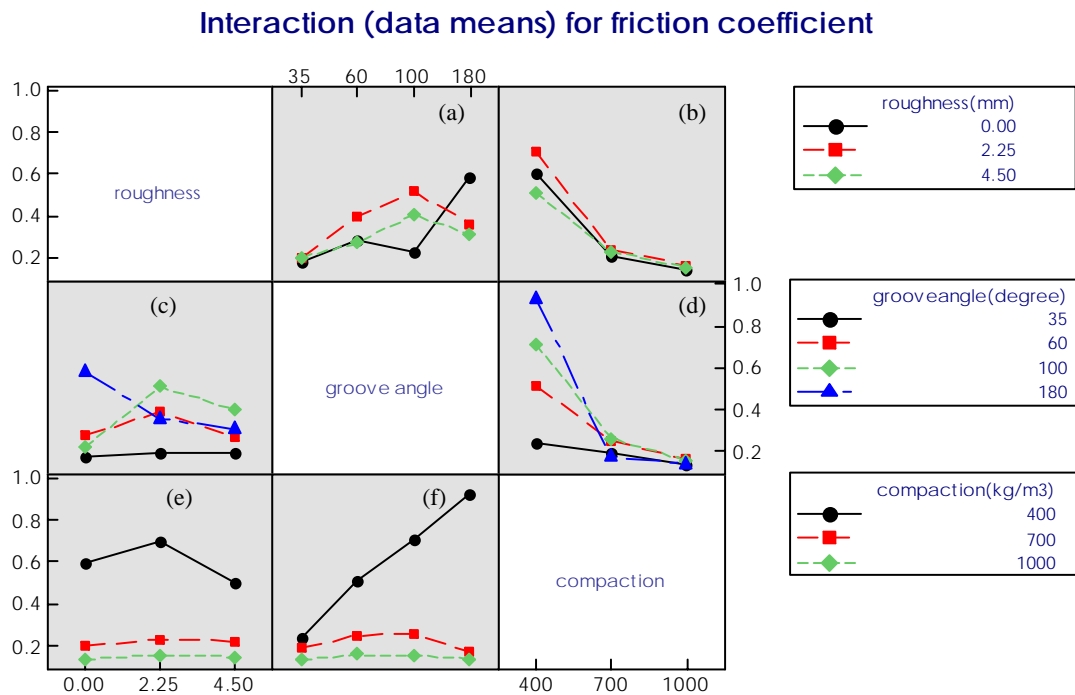
Figure 5.2 *Plots of the mean friction coefficient value for roughness, groove angle, and compaction, at three-way interactions.*

4.50 mm). Graph (b) shows responses, corresponding to every level of roughness and compaction, suggesting no effect of the interaction of the factors roughness and compaction on the friction coefficient. Figures 5.1 and 5.2 suggest that the coefficient depends on roughness, groove angle and compaction. However, this does not permit the rejection or acceptance of the stated hypothesis. Table 5.2 shows an analysis of variance (ANOVA) for friction coefficient with respect to roughness, groove angle and compaction. The ANOVA indicates that the probability (p-value) of every variable both as a main and interacting effect on the coefficient is less than the probability associated with the stated hypothesis (p-value = 0.05). This is; there is no roughness effect, no groove angle effect, and no compaction effect. Furthermore, there is no interaction between roughness and groove angle, roughness and compaction, and groove angle and compaction, and no three-way. For instance, roughness is shown to be significant for any p-value ≤ 0.007. Groove angle and compaction are significant for any reasonable value of α. The ANOVA indicates also that the interaction between the independent variables was significant at any value of α. Therefore, the stated hypothesis was rejected, indicating that roughness,

groove angle, and compaction are factors which affect significantly the friction coefficient. Table 5.3 exhibits a comparison of level across every factor tested. The Tukey's method was used to determine which level caused a greater friction coefficient. A negative difference of means signifies that the reference level is greater; while a positive difference of means signifies that the level is less marked. Examining the roughness factor, asperities at 2.25 *mm* average caused a greater friction coefficient value compared to the other two types of roughness tested. Its p-value (< 0.05) indicated it was significant. A smooth surface was not significant with respect to 4.5 mm average roughness. This response evidenced that a roughened surface produces a greater friction coefficient value than a smooth surface. The average difference in friction coefficient between smooth surfaces and roughened surfaces was estimated at 16%.

Table 5.2 *Analysis of variance for friction coefficient under roughness, groove angle compaction factors.*

Source	DF	SS	MS	F	P-value	H_o
Roughness	2	0.06458	0.03229	5.75	0.007	*rejected*
Groove angle	3	0.54281	0.18094	32.21	0.000	*rejected*
Compaction	2	2.83065	1.41533	251.94	0.000	*rejected*
Roughness * Groove angle	6	0.50795	0.08466	15.07	0.000	*rejected*
Roughness * Compaction	4	0.09565	0.02391	4.26	0.006	*rejected*
Groove angle * Compaction	6	1.06539	0.17757	31.61	0.000	*rejected*
Roughness * Groove angle * Compaction	12	1.08252	0.09021	16.06	0.000	*rejected*
Error	36	0.20224	0.00562			
Total	71	6.39180				

In comparing with groove angle caused the greater friction it was noted that a 180° groove angle (flat surface) contributed most. A flat surface caused a 21.3% greater friction than a grooved (35 degree) surface with all other variables being kept constant. Groove angles other than 35° were significant for any value of α. The difference between a 100° and a flat surface was not significant, confirming that angles over 100° did not show substantial differences and they may cause the same response. According to Table 5.3, for compaction every level marked a difference in the coefficient value, and each comparison of level was significant at any level of α. The friction coefficient decreases up to 300% when the material was compacted from 400 kg/m^3 to 1000 kg/m^3.

5.2   The friction coefficient model

The empirical modelling technique Response Surface Methodology (RSM) was used to determine the relation between friction coefficient and the three variables (roughness, groove angle and compaction). According to the experimental Box-Behnken design, forty tests were required to use the RSM (Hicks, 1999). Only twelve tests were tested of the forty tests undertaken, the remainder was taken from the achieved results to determine the friction coefficient response.

Table 5.3 *Comparisons among levels within each factor tested which caused a greater friction coefficient.*

Factors	Value means	Difference of means	SS of difference	T-Value	p-Value
ROUGHNESS					
0.00 subtracted from:					
2.25	0.364	0.05125	0.02164	2.3687	0.0700
4.50	0.239	-0.01983	0.02164	-0.9167	1.0000
2.25 subtracted from:					
4.50	0.239	-0.07108	0.02164	-3.285	0.0068
GROOVE ANGLE					
35° respect to:					
60	0.310	0.1220	0.02498	4.883	0.0001
100	0.379	0.1909	0.02498	7.640	0.0000
180	0.416	0.2279	0.02498	9.124	0.0000
60° respect to:					
100	0.379	0.06889	0.02498	2.757	0.0431
180	0.416	0.10594	0.02498	4.241	0.0008
100° respect to:					
180	0.416	0.03706	0.02498	1.483	0.4579
COMPACTION					
400 respect to:					
700	0.220	-0.3803	0.02164	-17.58	0.0000
1000	0.149	-0.4518	0.02164	-20.88	0.0000
700 respect to:					
1000	0.149	-0.07142	0.02164	-3.301	0.0060

The RSM demanded the testing of each factor at three levels: low, middle, and high; as shown in Table 4.9. The results are exhibited in Table 5.4. The tests were conducted at two replications. Table 5.5 shows the ANOVA for friction coefficient under the effect of the three factors based on RMS. This ANOVA was for a cubic model. The ANOVA indicated

that the probability of the factors as main effects, two-way and three-way interactions was less than the probability at a significance level p-value ($\alpha = 5\%$).

Table 5.4 *Experimental and predicted value for the friction coefficient*

Run No	Roughness (mm)	Grooved angle (degree)	Compaction (kg/m³)	Friction Coefficient		Error in model value (%)
				Observed experimental value	Predicted[a] value	
1	0.00	35	700	0.147	0.154	5.55
2	4.50	35	700	0.240	0.214	-12.15
3	0.00	180	700	0.143	0.174	-17.82
4	4.50	180	700	0.157	0.154	-1.95
5	0.00	100	400	0.320	0.256	-25.00
6	4.50	100	400	0.847	0.796	-6.41
7	0.00	100	1000	0.149	0.164	9.15
8	4.50	100	1000	0.156	0.144	-8.33
9	2.25	35	400	0.244	0.234	-4.27
10	2.25	180	400	0.761	0.714	-6.58
11	2.25	35	1000	0.157	0.154	-1.95
12	2.25	180	1000	0.146	0.154	5.19
13	2.25	100	700	0.278	0.280	0.71
14	2.25	100	700	0.323	0.280	-15.36
15	2.25	100	700	0.279	0.280	0.36
16	2.25	100	700	0.318	0.280	-13.57
17	2.25	100	700	0.312	0.280	-11.43
18	2.25	100	700	0.251	0.280	10.36
19	2.25	100	700	0.240	0.280	14.29
20	2.25	100	700	0.241	0.280	13.93
21	0.00	35	700	0.151	0.154	1.95
22	4.50	35	700	0.209	0.214	2.34
23	0.00	180	700	0.188	0.174	-8.05
24	4.50	180	700	0.162	0.154	-5.19
25	0.00	100	400	0.195	0.256	23.83
26	4.50	100	400	0.758	0.796	4.77
27	0.00	100	1000	0.162	0.164	1.22
28	4.50	100	1000	0.142	0.144	1.39
29	2.25	35	400	0.234	0.234	0.00
30	2.25	180	400	0.673	0.714	5.74
31	2.25	35	1000	0.153	0.154	0.65
32	2.25	180	1000	0.155	0.154	0.65
33	2.25	100	700	0.266	0.280	5.00
34	2.25	100	700	0.300	0.280	-7.14
35	2.25	100	700	0.276	0.280	1.43
36	2.25	100	700	0.273	0.280	2.50
37	2.25	100	700	0.273	0.280	2.50
38	2.25	100	700	0.228	0.280	18.57
39	2.25	100	700	0.270	0.280	3.57
40	2.25	100	700	0.268	0.280	4.29

[a]*The predicted value is found according to empirical model using Equation (5.2)*

The empirical equation obtained by RMS for a model of quadratic polynomial order in terms of coded factors, relating the friction coefficient with roughness, groove angle and compaction is given in Equation 5.1.

$$FC_{pred} = 0.28 + 0.076r + 0.053g - 0.18c - 0.04r^2 - 0.066g^2 + 0.10c^2 - 0.02rg - 0.14rc - 0.12gc$$ **(5.1)**

$$r = \frac{R - 2.25}{2.25}, \qquad g = \frac{G - 107.5}{72.5}, \qquad c = \frac{C - 700}{300}$$

FC_{pred} is the predicted friction coefficient

R is roughness

G is groove angle, and

C is compaction.

The quadratic model showed a p-value (< 0.0001) with a low lack of fit ($\alpha < 0.0001$) and it was rejected for predicting only 66.16% of the observed values.

The cubic model for the friction coefficient related with the three independent factors is

$$FC_{pred} = 0.28 + 0.13r + 0.12g - 0.16c - 0.040r^2 - 0.066g^2 + 0.10c^2 - 0.020rg$$
$$- 0.14rc - 0.124gc - 0.13r^2g - 0.026r^2c - 0.12rg^2$$ **(5.2)**

The coefficient of determination, $R-Sq$, for the cubic model was 98.24 %. The prediction coefficient of determination, *Pred. R-Sq*, was 97.47%. This means that the developed regression model cannot explain 2.53 % of the variation. The results are displayed graphically in Figure 5.3. The error term *s =0.0008* is very low and the lack of fit is 2.79 for an α =0.035 (p-value < 0.05). The model is significant at any level of α. By the same token, the residual plots depicted in Figure 5.3 shows that the frequency of the differences is in a range of ± 0.06. Figure 5.4 shows a comparison between the experimental and predicted calculation values for the friction coefficient.

Table 5.5 *ANOVA for response surface cubic model*

Source	Degree of Freedom	Sum of squares	Mean square	F	p-value
Model	12	1.16	0.097	121.17	< 0.0001 S^b
R	1	0.14	0.140	182.05	< 0.0001
G	1	0.13	0.130	158.04	< 0.0001
C	1	0.13	0.130	158.04	< 0.0001
R^2	1	0.14	0.140	176.21	< 0.0001
G^2	1	0.17	0.140	207.18	< 0.0001
C^2	1	0.22	0.220	273.68	< 0.0001
RG	1	0.13	0.130	163.21	< 0.0001
RC	1	0.28	0.280	348.99	< 0.0001
GC	1	0.24	0.240	304.20	< 0.0001
R^3	0	0.00			
G^3	0	0.00			
C^3	0	0.00			
R^2G	1	0.13	0.130	158.04	< 0.0001
R^2C	1	0.13	0.130	158.04	< 0.0001
RB^2	1	0.13	0.130	158.04	< 0.0001
RC^2	0	0.00			
G^2C	0	0.00			
GC^2	0	0.00			
RGC	0	0.00			
Residual Error	26	0.000796			
- Lack of fit	12	0.001217	2.79	0.0351	< 0.0001 S^b
- Pure error	14	0.000436			
Total	39	1.19			
	Mean = 0.28	R-Sq= 98.94	Predicted R-Sq =0.9743	Adjusted R-Sq = 0.9743	

S^b stands for *significant*

Residual plots for the predicted values of friction coefficients
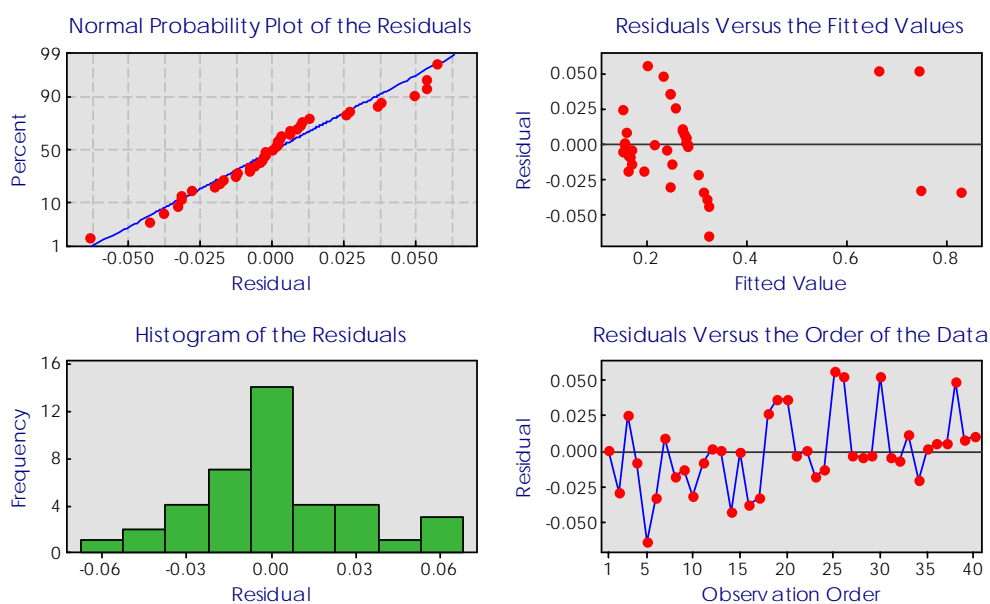
Figure 5.3 *Residual plots for the friction coefficient observations*

The observed values are close to the parity line, at both low and high friction coefficient values, suggesting that the developed empirical model yields friction coefficients values in good agreement with the experimental values.
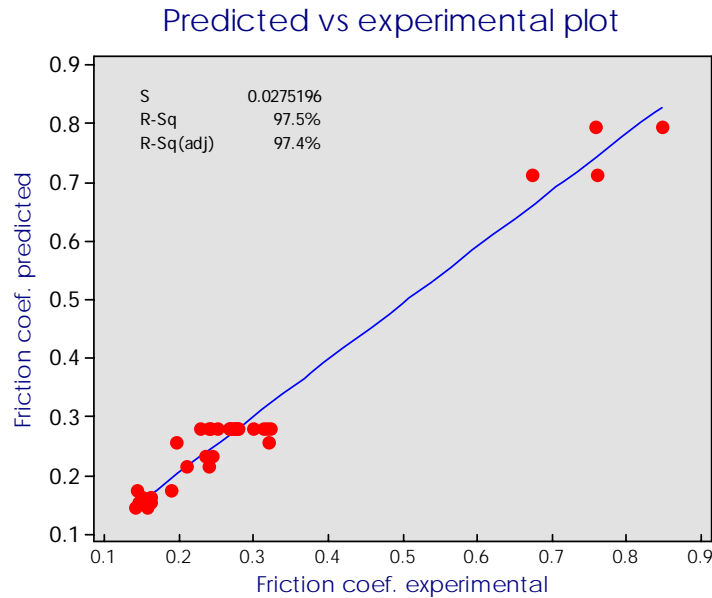
Figure 5.4 *Comparison between the predictive and experimental values*
for the friction coefficient.

5.3   Optimisation of the friction coefficient

The search for a local optimum of the friction coefficient constituted one of the justifications in this investigation (see pp.9). In order to determine the optimum combination among roughness, groove angle and compaction, and consequently the prediction of the best response, contour plots for surfaces of third degree with respect to these three variables have been developed in this thesis. The optimum value can be found by taking the first derivative of Equation (5.2), with respect to key variables:

$$\frac{\partial FC}{\partial r} = 0 \ , \qquad \frac{\partial FC}{\partial g} = 0, \qquad \frac{\partial FC}{\partial c} = 0$$

which gives:

$$r' = b_1, \ g' = b_2, \ c' = b_3 \ \text{and} \ FC' = X_0$$

The canonical form can be written as

$$Y = Y' + x'Ax$$

where

$$x = \begin{pmatrix} x_1 - x_1' \\ x_2 - x_2' \\ \cdot \cdot \cdot \\ x_n - x_n' \end{pmatrix}, \quad A = \begin{pmatrix} b_{11} & \frac{1}{2}b_{12} & \cdot & \cdot & \cdot & \frac{1}{2}b_{1n} \\ & b_{22} & \cdot & \cdot & \cdot & \frac{1}{2}b_{2n} \\ & & & \cdot & \cdot & \cdot & \cdot \\ & & & & & b_{nn} \end{pmatrix}$$

The characteristic equation is $|A - \lambda I| = 0$. The canonical form for the equation of the response surface is

$$\mu = \lambda_1 X_1^2 + \lambda_2 X_2^2 + \lambda_3 X_3^2 \tag{5.3}$$

where,

$$X_1 = f(G,C), \quad X_2 = f(R,C), \quad X_3 = f(R,G) \tag{5.4}$$

From Equation (5.4), either a three-dimensional surface graph or two-dimensional contour lines can be obtained to locate maximum friction coefficient values and determine the variation of the response in the dependence on the factors tested. An example of the calculation is developed in Appendix A. Figures 5.5 through to 5.22 show graphics of surface plots and contour plots, respectively, for friction coefficient affected by the compaction-groove angle, compaction-roughness, and roughness-groove angle relations. The response is assessed at three levels for each variable; low (smooth-35°-400 kg/m^3), medium (2.25 mm-100°-700 kg/m^3) and high (4.5 mm-180°-1000 kg.m^3). Examining the response at low level (smooth platens) as shown Figures 5.5 and 5.6, the combination of a flat surface and low compaction 400 kg/m^3 caused the highest friction coefficient values. The following engineering observations can be drawn from the empirical responses displayed in Figures 5.5 through to 5.22:

1. Examining the variables at their low levels of treatment combinations (smooth-35°-400 kg/m^3). From Figure 5.5 to 5.10.
    a. For a smooth surface, the friction coefficient responds negatively with increasing compaction and groove angle. For this combination, the highest friction coefficient is obtained when the groove angle increases at a

compaction level of 400 kg/m^3, or the compaction increases when the groove angle is 35°. See Figures 5.5 and 5.6.

b. For a 35° groove angle, there is no change in the friction coefficient when compaction and roughness are increased. The coefficient only responds if either roughness is increased when the compaction is at 400 kg/m^3, or the compaction is increased under a smooth surface. See Figures 5.7 and 5.8.

c. From Figures 5.9 to 5.10. At 400 kg/m^3 the friction coefficient value increases rapidly when groove angle and compaction increases.

2. Examining the variables at their middle levels of treatment combinations (2.25mm-100°-700 kg/m^3). From Figure 5.11 to 5.16:

a. At a 2.25 mm constant roughness, the coefficient responds negatively as compaction and groove angle increase. The friction coefficient value increases as the groove angles increase when compaction is at 400 kg. At high compaction, the coefficient responds with the highest values only for groove angles between 100° and 130°. See Figures 5.11 and 5.12.

b. When 100° groove angle is maintained constant, the friction coefficient responds in a similar manner to (a). This is; the friction coefficient responds negatively as compaction and roughness are raised. See Figure 5.13 and 5.14.

c. From Figures 5.15 to 5.16. At 700 kg/m^3 constant compaction, the surface plot for the friction coefficient responds positively. This suggests that there is a maximum value for the coefficient. The maximum coefficient occurs with the combination 100° and 4.50 mm. and average roughness. Groove angles greater than 100° cause a decrease in the coefficient at any roughness value.

3. Examining the variables which are at their high levels of treatment combinations (4.50 mm-flat-1000 kg/m^3), from Figures 5.17 to 5.22:

a. If roughness at 4.50 is kept constant, the friction coefficient value responds positively at high compaction, with a downward trend at groove angles greater than 100°. The highest coefficient is obtained with increasing compaction and groove angles between 80° and 130°.

b. With flat surfaces as an invariant, the response for the friction coefficient is favourable as compaction is increased at any roughness values. For roughness values between1.13 and 3.38 mm, the friction coefficient reaches the highest values at any compaction value. See Figure 5.19 and 5.20.

c. For a 1000 kg/m^3 constant compaction, the friction coefficient surface responds positively for acute groove angles and for smooth surfaces. The coefficient only increases for groove angles less than 100° and roughness less than 2.25 mm.
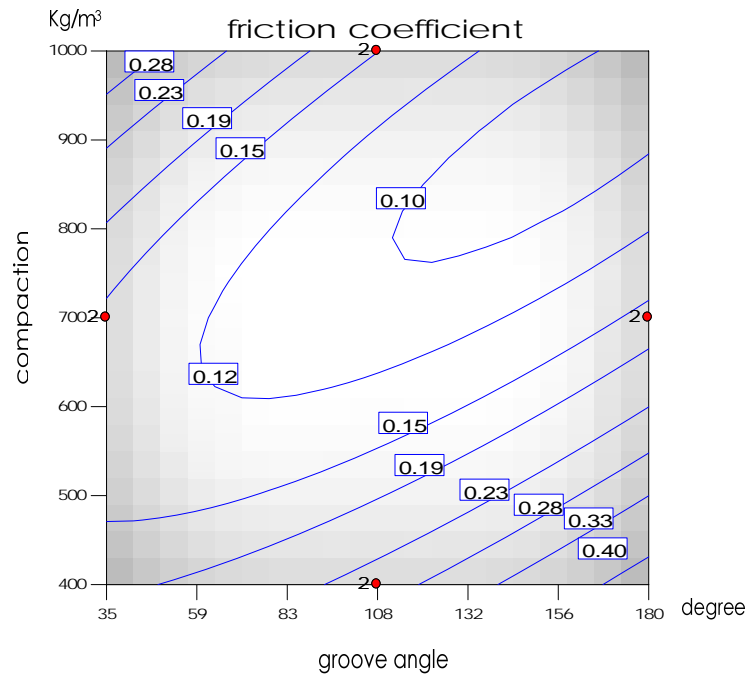
Figure 5.5 *Contour plots for the friction coefficient under a combination of compaction and groove angle with constant roughness at 0.00 mm.*
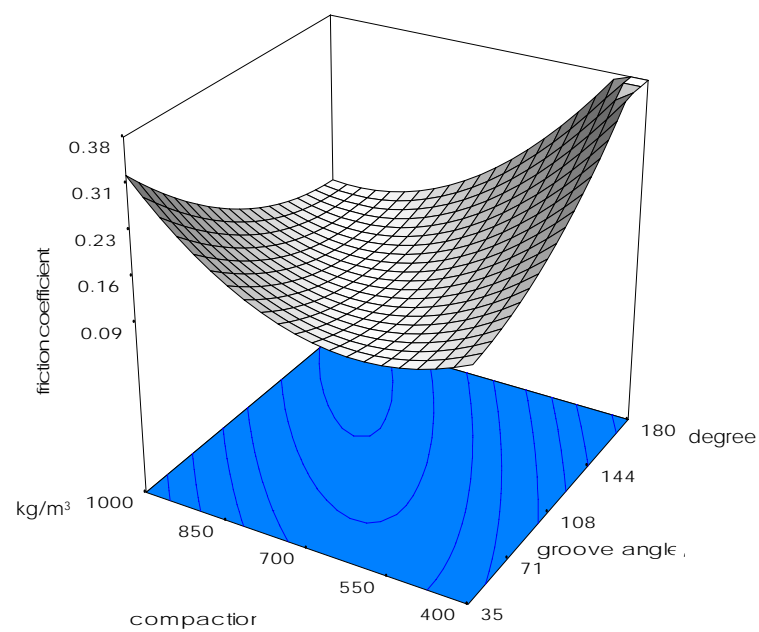
Figure 5.6 *Surface plot for the friction coefficient under combination of compaction and groove angle, with constant roughness at 0.00 mm.*
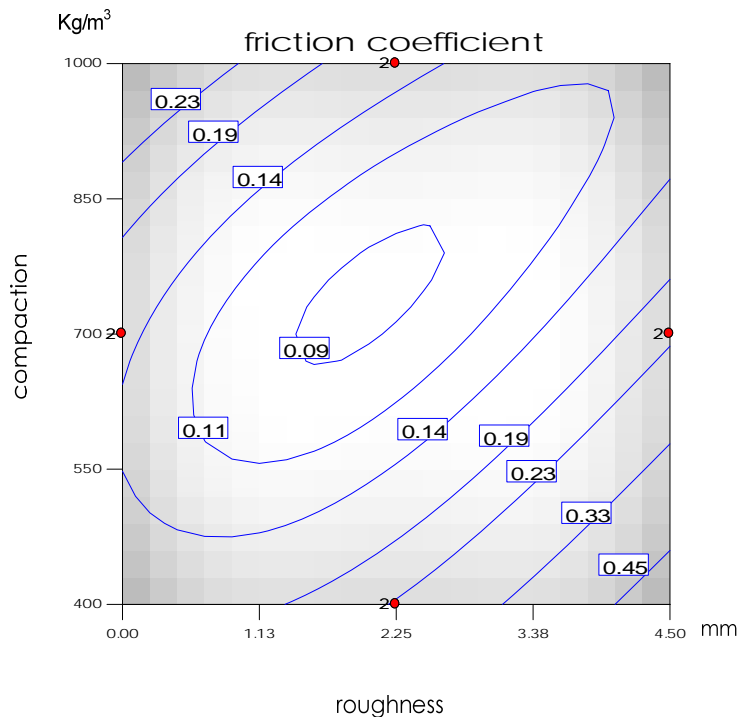
Figure 5.7 *Contour plots for the friction coefficient under a combination of compaction and roughness, holding a35^o groove angle.*
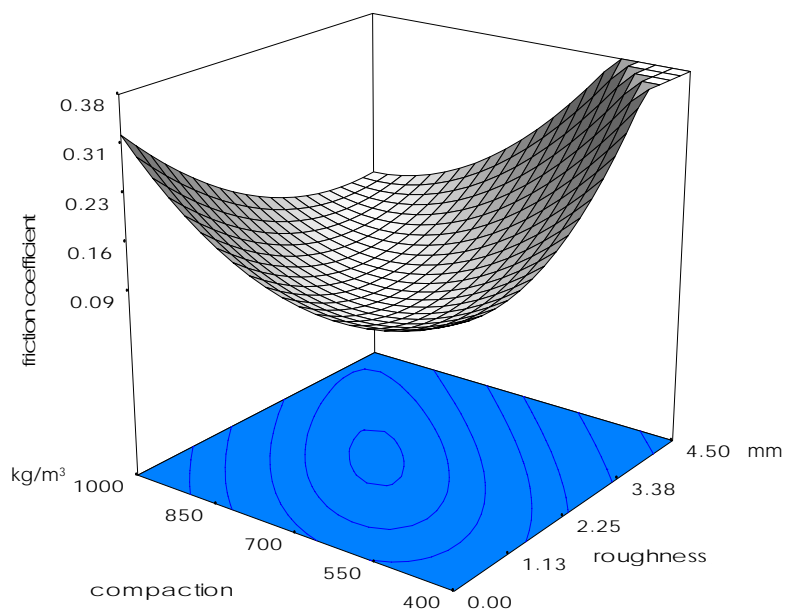
Figure 5.8 S*urface plot for the friction coefficient under a combination of compaction and roughness, holding a 35° groove angle.*
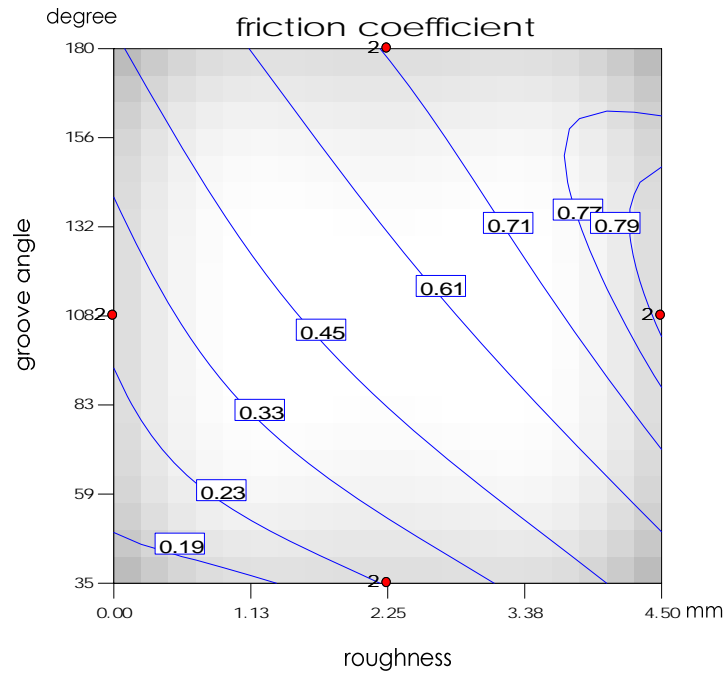
Figure 5.9 *Contour plots for the friction coefficient under a combination of groove angle and roughness, holding compaction at 400 kg/m³.*
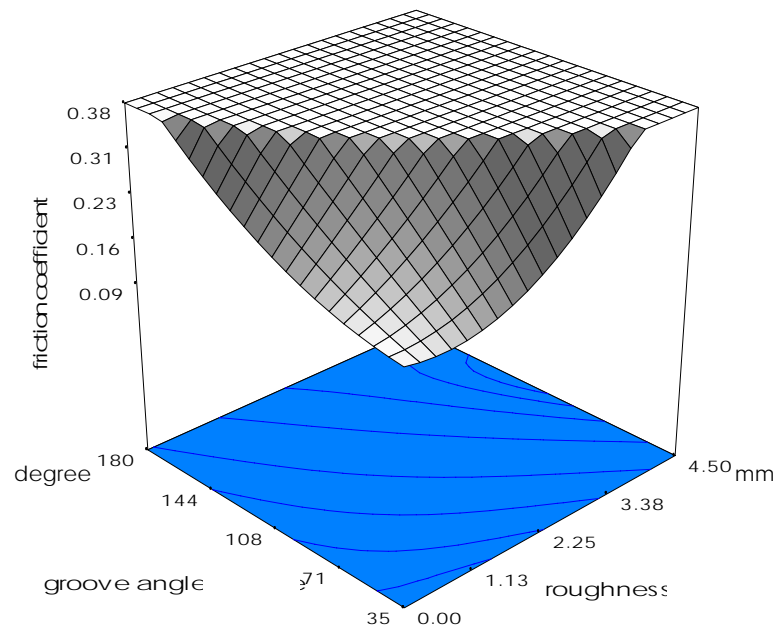
Figure 5.10 *Surface plot for the friction coefficient under a combination of groove angle and roughness, holding compaction at 400 kg/m³.*
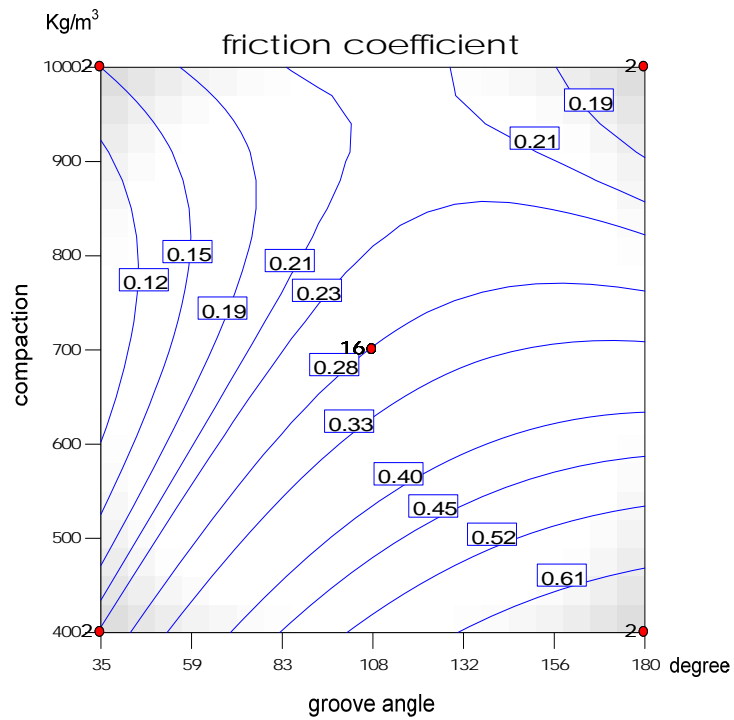
Figure 5.11 *Contour plot for the friction coefficient under the combined effect of groove angle and compaction, holding roughness held at 2.25mm.*
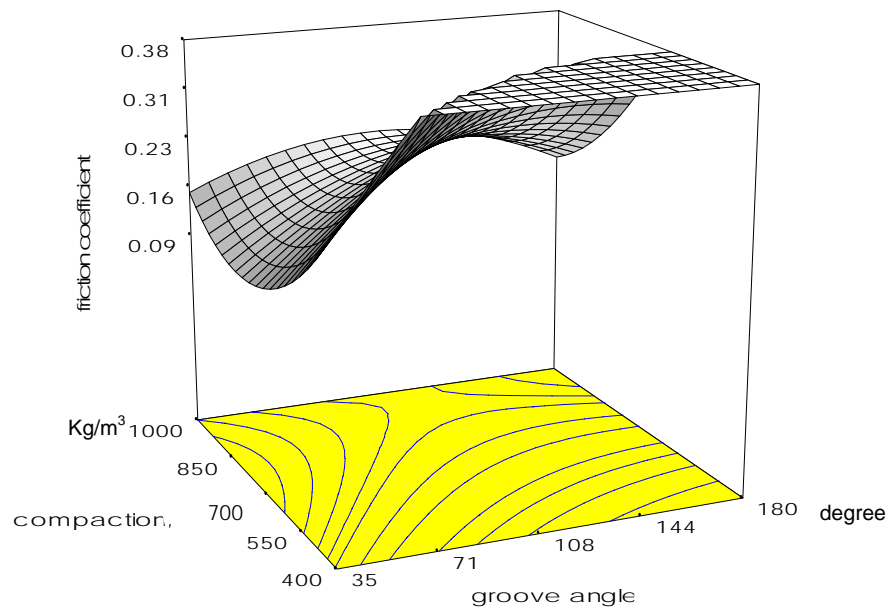
Figure 5.12 *Surface plot for the friction coefficient responses under the factors* groove angle and compaction, holding roughness at 2.25 mm.
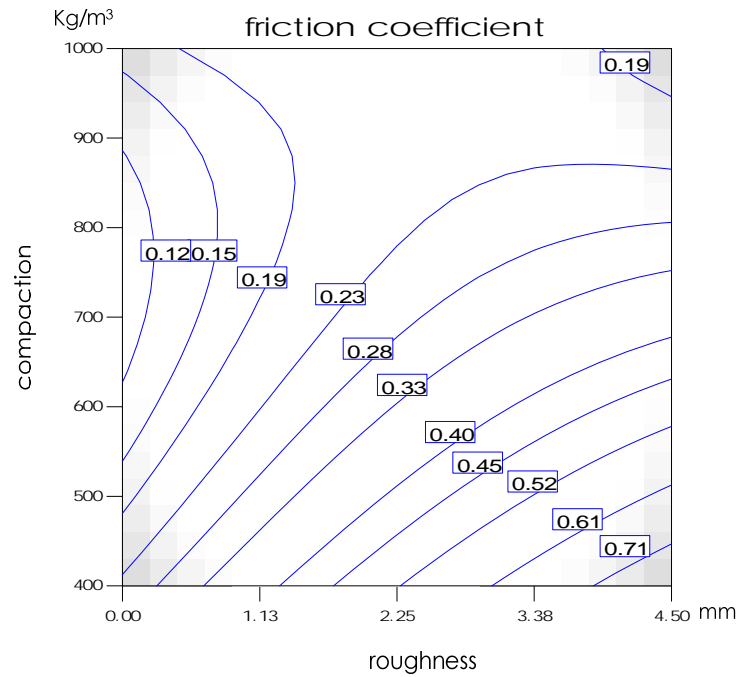
Figure 5.13 *Contour plots for the friction coefficient under the combined effect of roughness and compaction, holding a 100ᵒ groove angle*
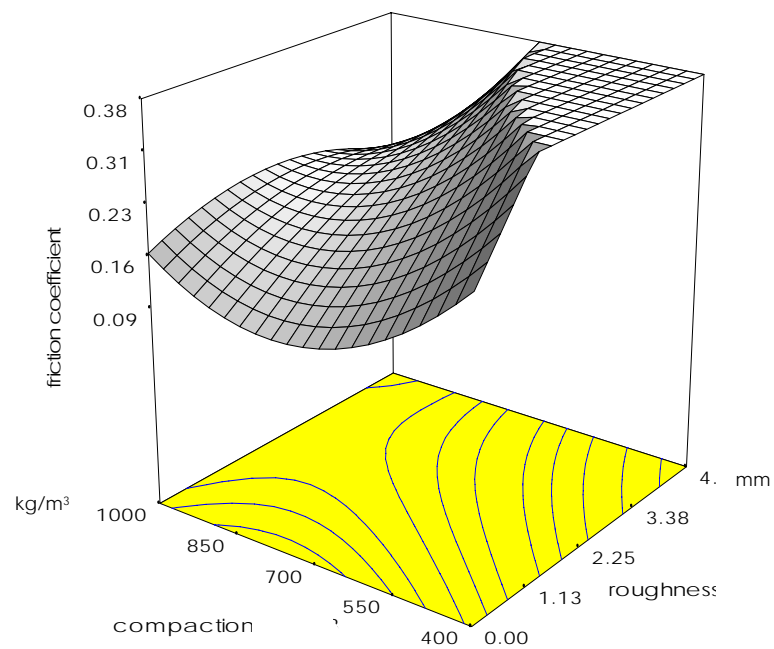
Figure 5.14 *Surface plot for the friction coefficient responses under the factors of roughness and compaction, holding a 100ᵒ groove angle.*
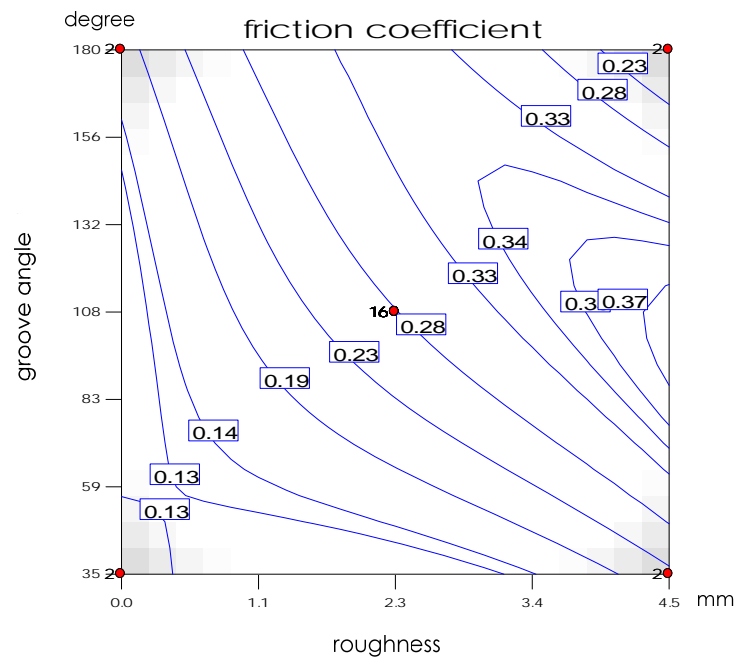
Figure 5.15 *Contour plots for the friction coefficient under the combined effect*
of groove angle-compaction, holding compaction at 700 kg/m³.
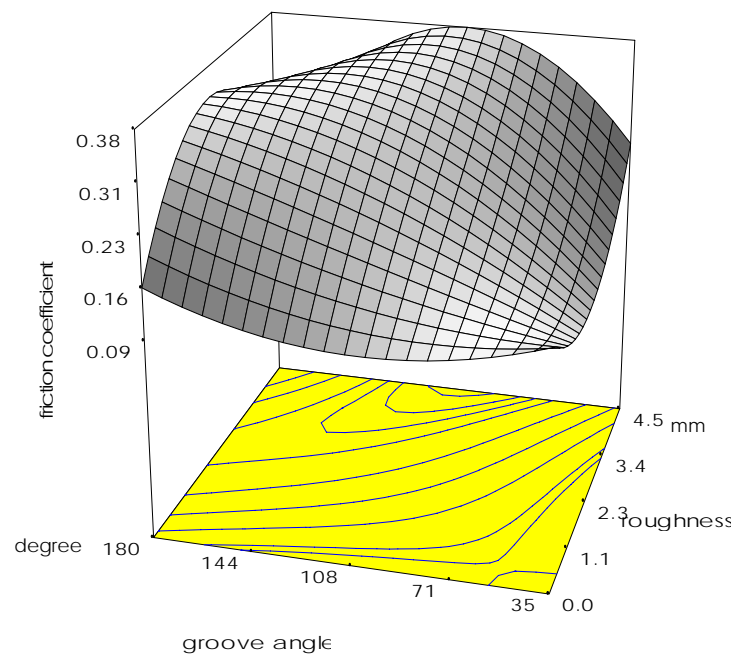
Figure 5.16 *Surface plot for the friction coefficient responses under the*
factors of roughness and groove angle, holding compaction at 700kg/m³
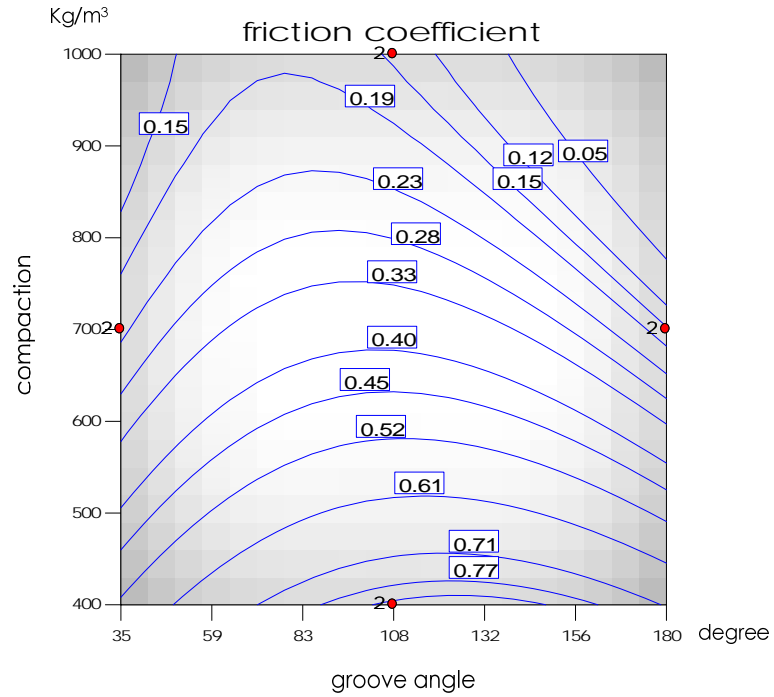
Figure 5.17 *Contour plots for the friction coefficient value versus compaction groove, holding average roughness at 4.50 mm.*
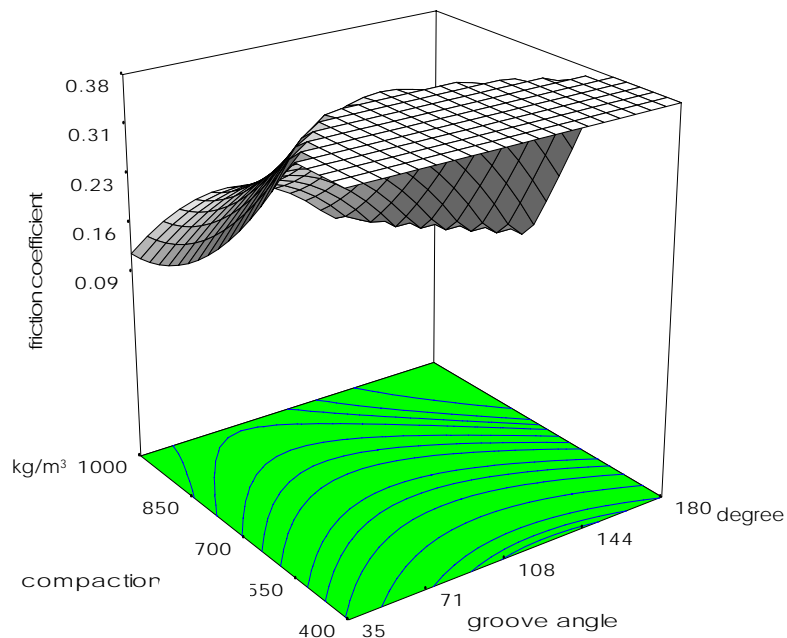
Figure 5.18 *Surface plot for the friction coefficient response versus compaction and groove angle, holding average roughness at 4.50mm.*
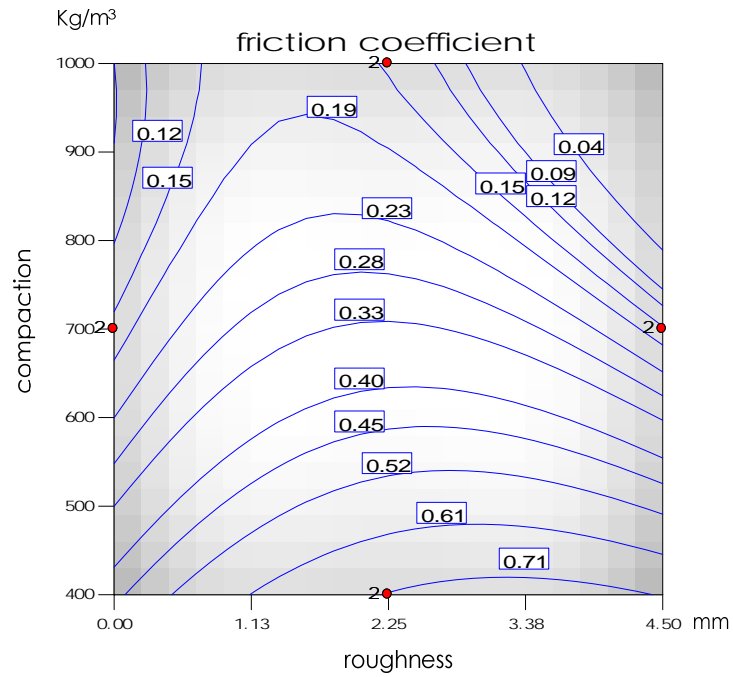
Figure 5.19 *Contour plots for the friction coefficient value under the combined effect of roughness and compaction, holding a 180° groove angle.*
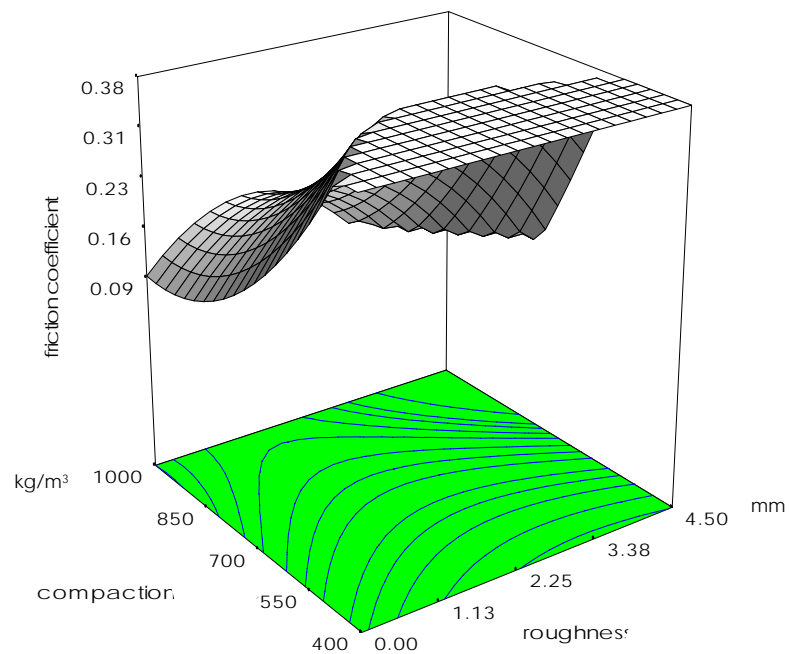
Figure 5.20 *Surface plot for the friction coefficient value under the conditions of roughness and compaction, holding a 180° groove angle.*
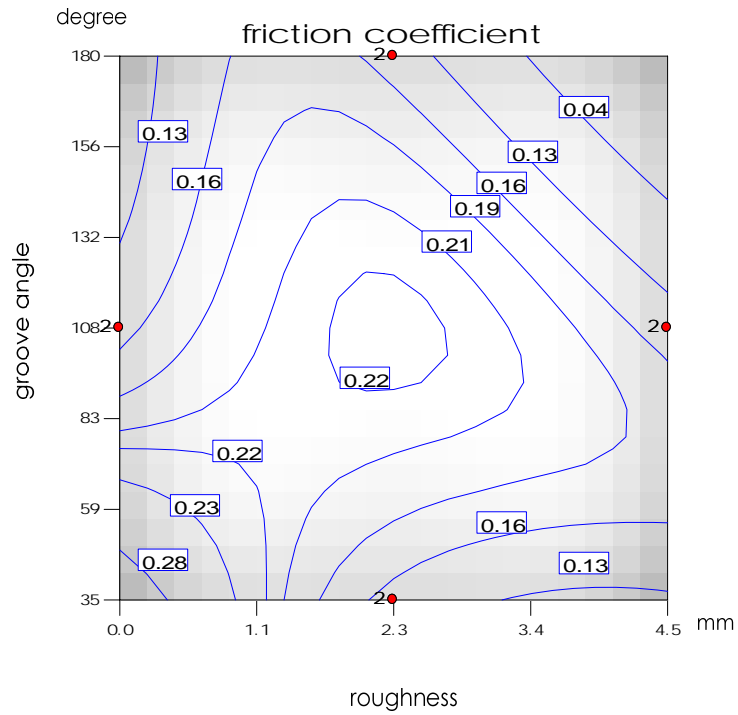
Figure 5.21 *Contour plots for the friction coefficient value under the combined effect of roughness and groove angle, holding compaction at 1000 kg/m^3.*
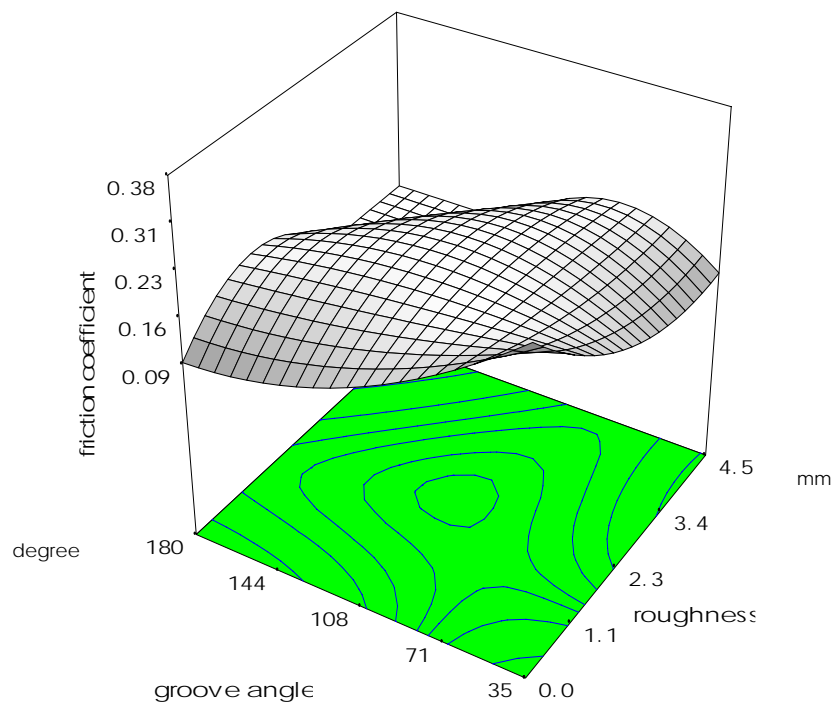
Figure 5.22 *Surface plot for the friction coefficient response versus groove angle and roughness, holding compaction at 1000 kg/m^3.*

5.4 Bagasse shear failure analysis

Due to the decrease in value of the friction coefficient when bagasse was subjected to high compaction values, a series of tests were conducted to determine whether or not it was limited by the shear strength of the bagasse. The shear coefficient and friction coefficient were tested at three compaction levels: 400 kg/m^3, 700 kg/m^3 and 1000 kg/m^3. Furthermore, the shear coefficient was compared to the friction coefficient across two angles and two textures: 2.25 mm average roughness and 60° groove angle (FCA60); 2.25 mm average roughness at 180° (FCA180); and 0.00 mm at 180° (FCS180).

The results for shear coefficient and friction coefficient are plotted in Figure 5.23. Both shear coefficient and friction coefficient show a decreasing trend with compaction (with the shear coefficient being less marked). At high compaction both responses align suggesting that the tests for friction coefficient were accompanied by possible failure of the material, at a plane other than the interface. Another further observation related to the shear and friction coefficient is that when compaction is between 700 kg/m^3 and 1000 kg/m^3, the combination of roughness and groove angle does not seem the influence to friction coefficient. On the other hand, in the range between 400 kg/m^3 and 700 kg/m^3, the coefficient shows a marked change.
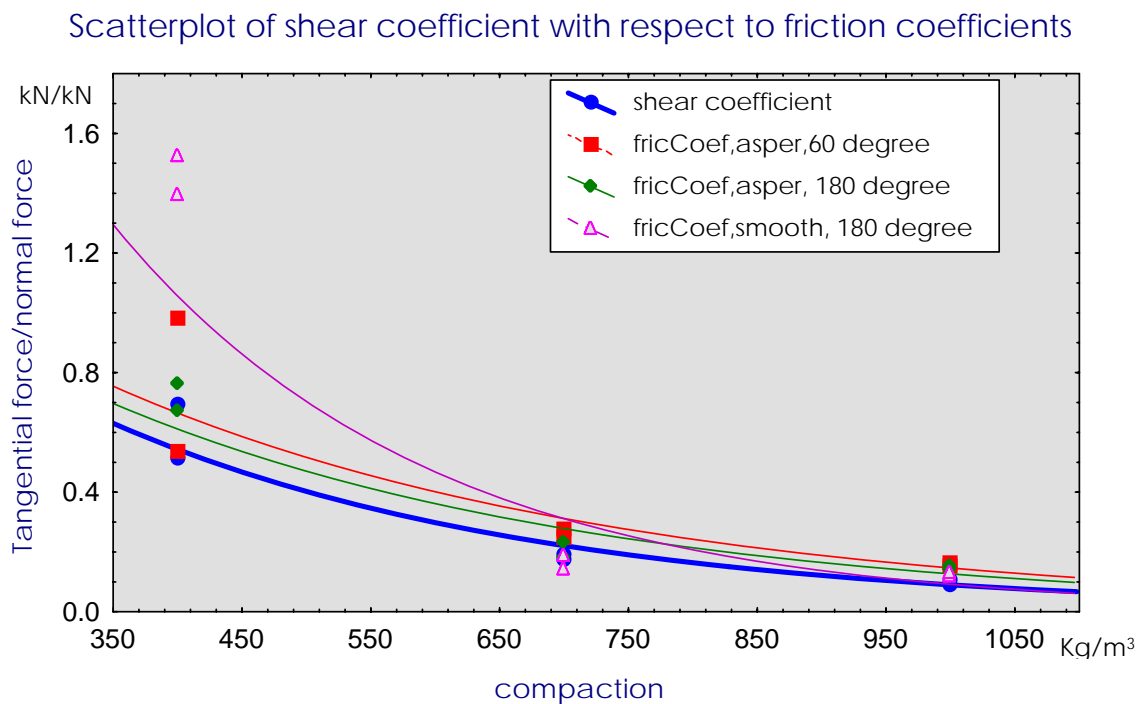
Figure 5.23 *Shear and friction coefficient as a function of the compaction at different groove angles and roughness of surface.*

Figure 5.24 displays the responses for the shear coefficient and the friction coefficient as a function of the normal pressure applied to the samples. The friction coefficient shows a downwards trend as the normal pressure increases but there is less variability across groove angles and roughness. Close inspection of this figure indicates that the difference between the friction coefficient and shear coefficient responses is small, suggesting that normal pressure is a weak parameter to show the behaviour of the friction coefficient with respect to the shear coefficient, because what it really is showing is the internal friction coefficient of the bagasse. Similar behaviour of bagasse subjected to compression and shear failure has been reported by Cullen (1965) and Plaza (1994).
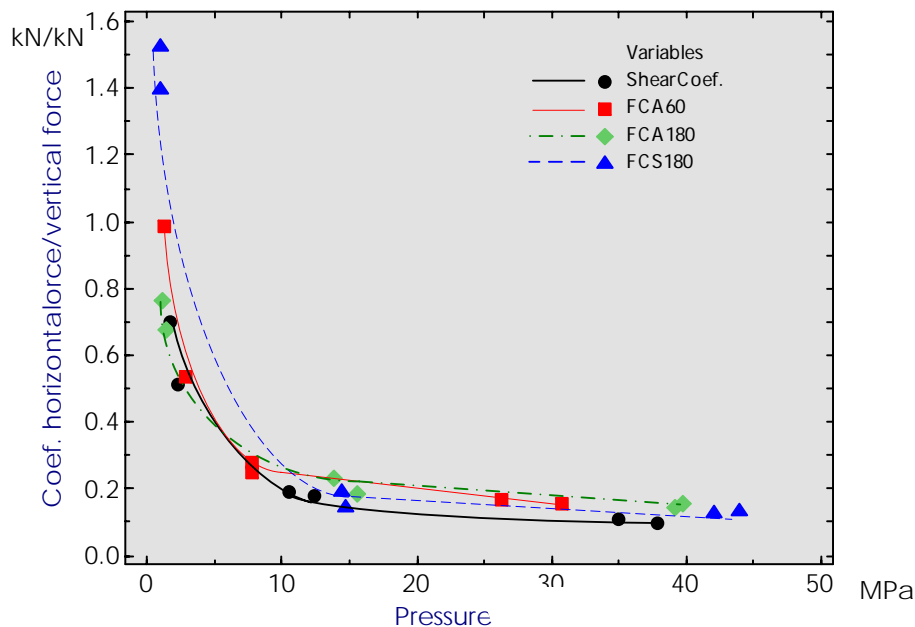
Figure 5.24 *Shear and friction coefficient versus normal force at different groove angles and roughness .*

Figure 5.24 also shows that for pressure greater than 15 MPa both shear coefficient and friction coefficient are not affected by the pressure, suggesting that the material is failing due to the maximum tangential force required to cause a shear coefficient at 15 MPa. Table 5.6 shows the results of the shear coefficient for three of compaction levels. The analysis of variance indicates that the shear coefficient of bagasse is affected by compaction. The p-value for compaction was less than p-value = 0.05 (Table 5.7).

Table 5.6 *Data for the shear coefficient at three compaction levels.*

Replicate	Compaction (kg/m³)		
	400	**700**	**1000**
I	0.513	0.190	0.107
II	0.697	0.175	0.092

Table 5.7 *Analysis of variance for the shear coefficient.*

Source	Degree of Freedom	Sum of squares	Mean square	F	P-value
Compaction	2	0.29395	0.14698	25.71	0.013
Error	3	0.01715	0.00572		
Total	5	0.31110			

s = 0.0756153   R-Sq = 94.49%

Figure 5.25(a) and 5.25(b) show photographs of the samples of bagasse subjected to shearing in order to determine both the friction coefficient and the shear coefficient. The pictured scraper allowed the sample to be sheared internally. The tests to determine the shear coefficient were conducted without using the scraper.

Figure 5.25 *Shear and friction coefficient measurements: (a) shear test without scraper; (b) friction coefficient test using scraper to avoid internal shear failure.*

5.5 The influence of liquid in bagasse on the interface friction and shear coefficient values

The average mass of liquid in the tested samples of bagasse prior to compression was 52%. Extraction of liquid occurred when the samples were subjected to a compaction greater than 700 kg/m^3. Shear stress applied to any material depends on the maximum shear strength that the material can sustain (Williams, 1994). It was of interest to determine if the residual liquid in the sample of bagasse influenced its strength. The shear coefficient was tested under the effect of bagasse moisture content at two levels: 11% and 52 % (fresh bagasse), and three levels of compaction: 400, 700 and 1000 kg/m^3. Twelve tests, with two replications, were required: six tests with fresh bagasse (52% moisture) and six tests with dried bagasse (11% moisture), respectively. Table 5.8 shows the responses for shear coefficient versus compaction and bagasse moisture. Figure 5.26 shows the response of shear coefficient to compaction and moisture content.

The effect of moisture content on shear coefficient over a compaction range 400-1000 kg/m3 is marked. At low compaction the shear coefficient for moist bagasse is higher than for dried bagasse. However, the trend is reversed at high compaction. These results suggest a likely influence of the liquid on the shear coefficient. However, the ANOVA for the observed results, as shown in Table 5.9, reveals that the probability associated with the variable moisture (p-value = 0.633) was much greater than the significant level p-value = 0.05. This indicates that the liquid content in the sample was not a variable which affected on the shear coefficient, suggesting that other factors were involved.

Table 5.8 *Data for the shear coefficient under the combined effect of compaction and moisture.*

Replicate	Compaction (Kg/m³)	Bagasse/moisture (%)	
		11.00	52.00
I	400	0.418	0.513
	700	0.233	0.190
	1000	0.204	0.107
II	400	0.380	0.697
	700	0.200	0.175
	1000	0.180	0.092
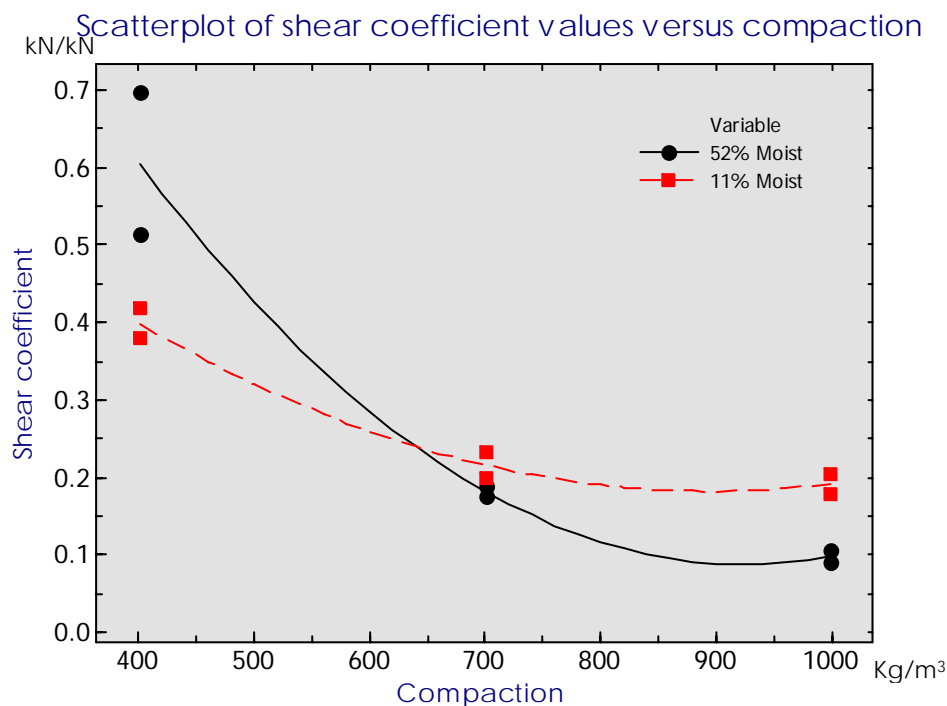
Figure 5.26 *Comparison of shear coefficient at two different levels of bagasse moisture*
as a function of compaction.

Table 5.9 *Analysis of variance for the shear coefficient versus compaction and moisture.*

Source	Type factor	Degree of Freedom	Sum of squares	Mean square	F	P-value
Compaction	fixed	2	0.295135	0.147567	17.18	0.001
Moisture	random	1	0.002117	0.002117	0.25	0.633
Error		8	0.068717	0.008590		
Total		11	0.365969			
	s = 0.09268	R-Sq = 81.22%				

5.6 Liquid content in bagasse versus friction coefficient

Bullock (1958) and Murry (1967) postulated that the friction coefficient depends on the dryness of the bagasse. In order to determine whether or not the liquid contained in the samples affected the friction coefficient between bagasse and a steel grooved platen, several tests were carried out using a grooved platen roughened at 2.25 mm average height, bagasse moisture at two levels: 11% and 52%, and compaction at three levels: 400, 700 and 1000 kg/m^3. Table 5.10 shows the results of these tests.

Table 5.10 *Results for the friction coefficient, by combining moisture, groove angle and compaction, holding 2.25mm average roughness.*

Moisture/bagasse (%)	Compaction (kg/m³)	Groove angle (degree)			
		35	60	100	180
11.00	400	0.214	0.291	0.405	0.414
	700	0.184	0.282	0.275	0.334
	1000	0.214	0.250	0.268	0.269
52.00	400	0.239	0.760	1.091	0.717
	700	0.197	0.255	0.272	0.204
	1000	0.155	0.160	0.168	0.151

Figure 5.27 and 5.28 show that friction coefficient decreased when the bagasse moisture decreased from 52% to 11%. These graphics also depict that the liquid content in bagasse was interacting with groove angle and compaction values. Examining Table 5.11 on the analysis of variance for friction coefficient values for the three tested variables moisture, groove angle, and compaction shows that the moisture did not exert any influence on the friction coefficient. For moisture the p-value = 0.277, greater than the p-value = 0.05. According to ANOVA the liquid content in bagasse did not represent a significant variable which could cause a difference on the friction coefficient responses.

Table 5.11 *Analysis of variance for the friction coefficient versus moisture, groove angle and compaction.*

Source	Type factor	Degree of Freedom	Sum of squares	Mean square	F	P-value
Moisture	random	1	0.03912	0.03912	1.26	0.277
Groove angle	fixed	3	0.14321	0.0774	1.54	0.241
Compaction	fixed	2	0.45391	0.22695	7.32	0.005
Error		17	0.52669	0.03100		
Total		23	1.16322			

$s = 0.146066$ $\quad$ R-Sq = 54.705
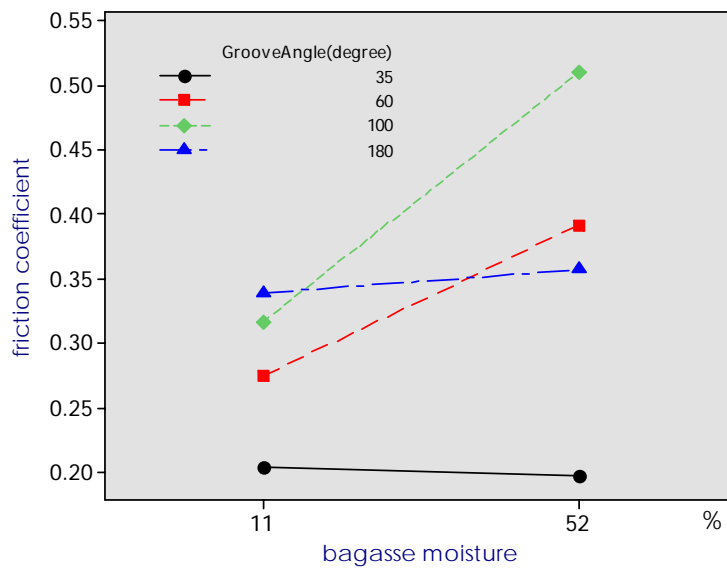
Figure 5.27 Friction coefficient values versus bagasse moisture and groove angle.
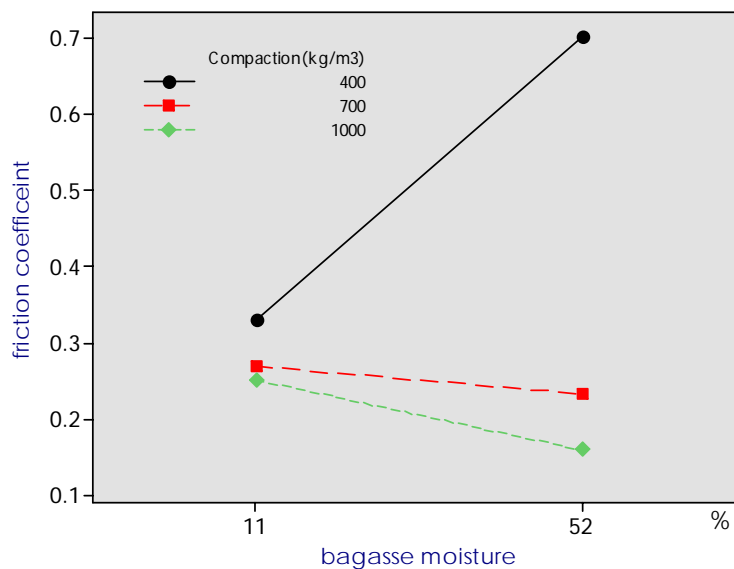
Figure 5.28 Friction coefficient values versus bagasse moisture and compaction.

5.7 The effect of roughness, compaction and groove angle on bagasse dewatering

Dewatering of prepared cane or bagasse has been extensively investigated, in order to improve extraction performance and bagasse surplus (Crawford, 1957; Murry, 1957, Adam 1997; Plaza and Kent, 2000, Kauppila, 2001). These investigations have been focused on

the effect of pressure (Crawford, 1957), roughness (Plaza and Kent, 2000) and groove angle (Bullock, 1957; Murry, 1967; Adam, 1997; Kauppila, 2001). The latter parameter has received considerable attention recently. In the present investigation attention is focused on extending the research findings of Kauppila (2001). A group of 24 tests were carried out to find whether or not roughness and groove angle can affect the dewatering of bagasse when compaction was varied from 400 kg/m^3 to 1000 kg/m^3. The tests employed a procedure (Anon., 1958) to measure the mass of liquid extracted from the bagasse sample, following compression and shear. The removed liquid was calculated as a percentage of the weight of the total liquid contained in bagasse (see Appendix A). Average roughness at two levels (2.25 and 4.50 mm) and groove angles at four levels (35°, 60°, 100°, and 180°) were tested. The observed results for the mass of liquid removed from the samples of bagasse are shown in Table 5.12. A value equivalent to zero meant that no liquid was extracted. No drainage was obtained when the sample was compacted at 400 kg/m^3. The fields where no values appear mean missing observations caused by material not being available or measurement errors. Hence, the results were processed as an unbalanced factorial design ANOVA (Ott, 1984). According to Table 5.12, groove angles between 60 and 100 degree demonstrate maximum effect on moisture.

Table 5.12 *Data for bagasse dewatering as a function of compaction, roughness and groove angle.*

Replicate	Compaction, kg/m³	Roughness							
		Asperities 2,25 (mm)				Nodules 4.5 (mm)			
		35°	60°	100°	180°	35°	60°	100°	180°
I	400	0.00	0.00	0.00	0.00	0.00	0.00	0.00	0.00
	700	10.94	13.66	11.06	7.50	15.31	-	17.80	10.71
	1000	29.24	33.13	31.62	36.76	34.44	-	34.04	31.76
II	400	0.00	0.00	0.00	0.00	0.00	0.00	0.00	0.00
	700	9.68	9.99	20.65	15.26	-	-	19.17	12.14
	1000	27.23	31.68	42.72	24.33	-	-	35.49	33.26

Table 5.13 shows that the effect of groove angle is significant (observed p-value < p-value at 0.05). Further, compaction is significant at any value of α. The effect of roughness is not significant. The observed results (Figure 5.29 through to 5.36) confirm the ANOVA statistics graphically. Roughness is the only factor which did not affect the extraction of liquid. See Figure 5.29(c). Examining Figure 5.29(a), the extraction increased up to a peak value when the angle varied from 35 to 100°, after which the trend is reversed. The extraction exhibited a steady increase when compaction was tested from 400 to 1000

kg/m^3, as shown in Figure 5.29(b). Over the range of roughness 2.2.5-4.5 mm there was no noticeable effect on extraction.

Table 5.13 *The analysis of variance for bagasse dewatering.*

Source	Degree of Freedom	Sum of squares	Mean square	F	P-value
Roughness	1	12.8	12.8	1.34	0.254
Groove angle	3	89.2	29.7	3.13	0.038
Compaction	2	7541.5	3770.8	397.15	0.000
Error	35	332.3	9.5		
Total	41	8164.9			
	s = 3.08133		R-Sq = 95.93		

Interaction effects are depicted in Figure 5.29. Groove angle and compaction as main and interaction effects, respectively, caused the extraction to vary. The drop of the extraction at 60° for the combination roughness-groove angle and at 4.5 mm for the combination roughness-compaction was due to the missing information (shown in Table 5.12). Both groove angle and compaction are shown to be the most significant variables influencing the dewatering of bagasse. From Figures 5.31 and 5.36, the main and interaction effect of the three variables on extraction, is depicted by surface and contour plots respectively. Contour plots permit a better analysis of how the extraction varies as a function of two variables. For instance, Figure 5.32 shows how the extraction was only affected by compaction. The parallel extraction lines indicate that there is no interaction effect with roughness. Examining the effect roughness-groove angle, shown in Figure 5.34, the extraction was only affected by groove angle. The graph also indicates that the extraction was a maximum when the angle was between 100° and 150°.

The increased extraction of liquid from bagasse as roughness varies from 2.25 mm to 4.5 mm, when the groove angle is between 35° and 80°, is explained by the lack of response (Table 5.12). For the compaction and groove angle combination (Figure 5.35 and 5.36), the graphics show that these two variables have a marked interaction effect on extraction. Even though the extraction was increased by compaction, an additional increment of extraction occurs when the angle is between 100° and 120°, suggesting that the combined effect of compaction and groove angle caused a maximum extraction of the liquid content of bagasse.

Main effect plot (data means) for extracted liquid, %
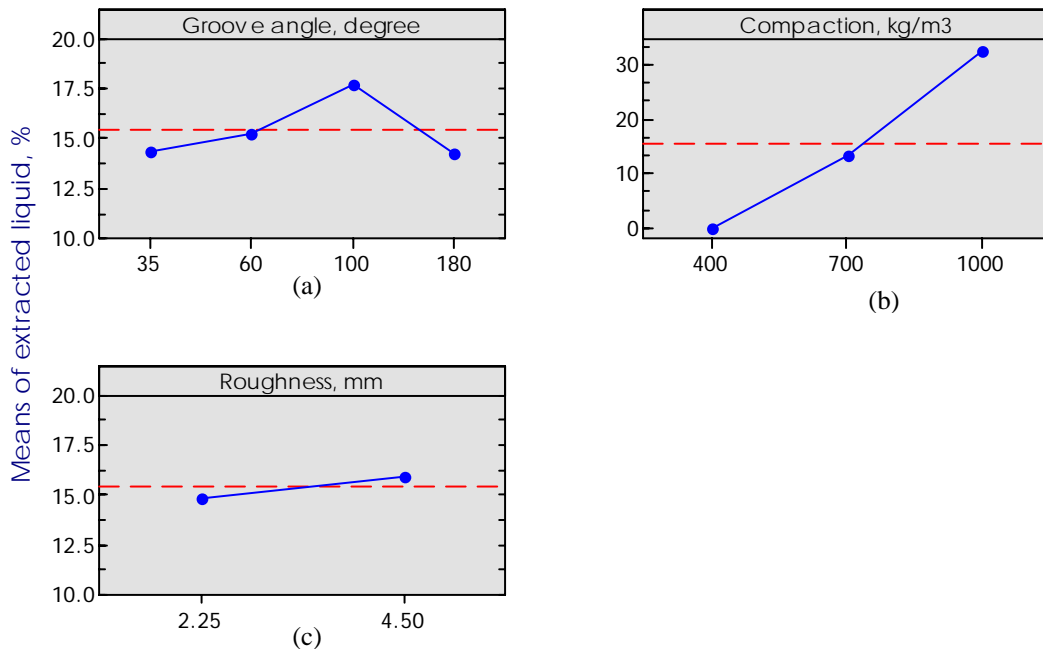
Figure 5.29 *Profile plots for extracted liquid versus roughness, groove angle, and compaction.*

Interaction plot (data means) for extracted liquid from bagasse (%)
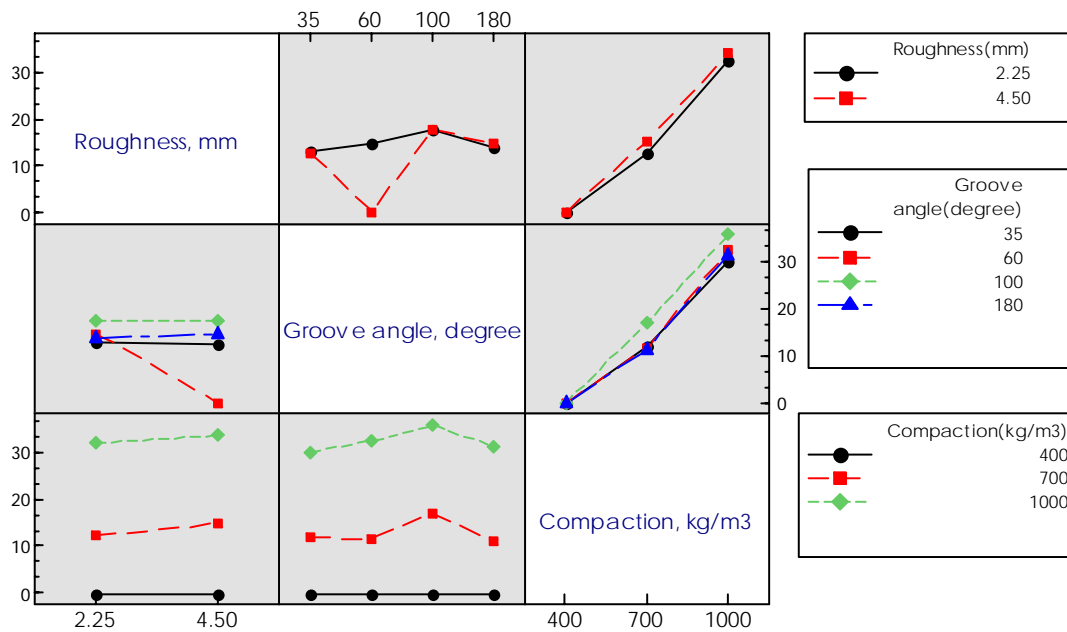
Figure 5.30 *Interaction plots for extracted liquid and roughness, groove angle, and compaction effects.*

Contour plots of extraction (%) vs roughness, compaction
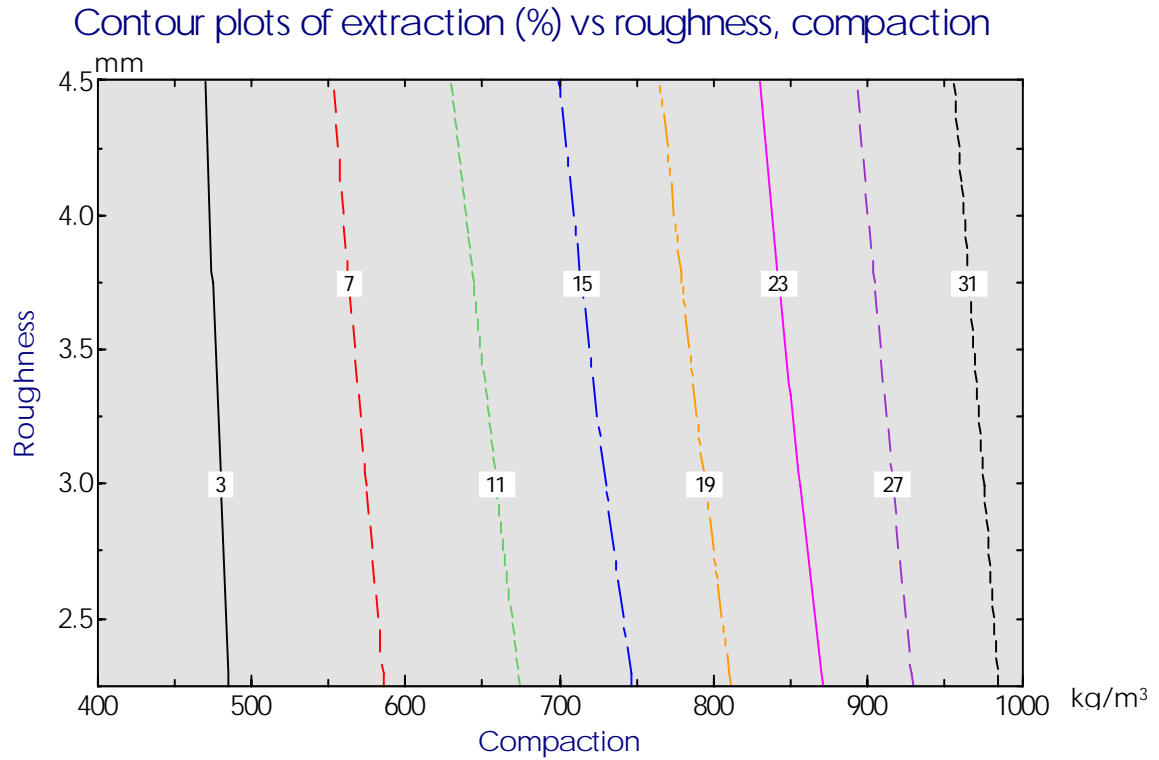
Figure 5.31 *Contour plots of extraction versus roughness and compaction.*

Surface plot of extraction (%) vs roughness, compaction
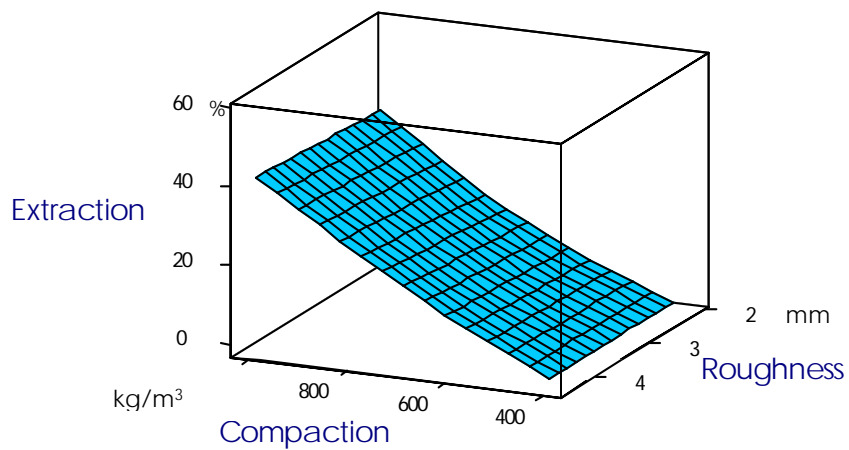
Figure 5.32 *Surface plot for extraction versus compaction and roughness.*
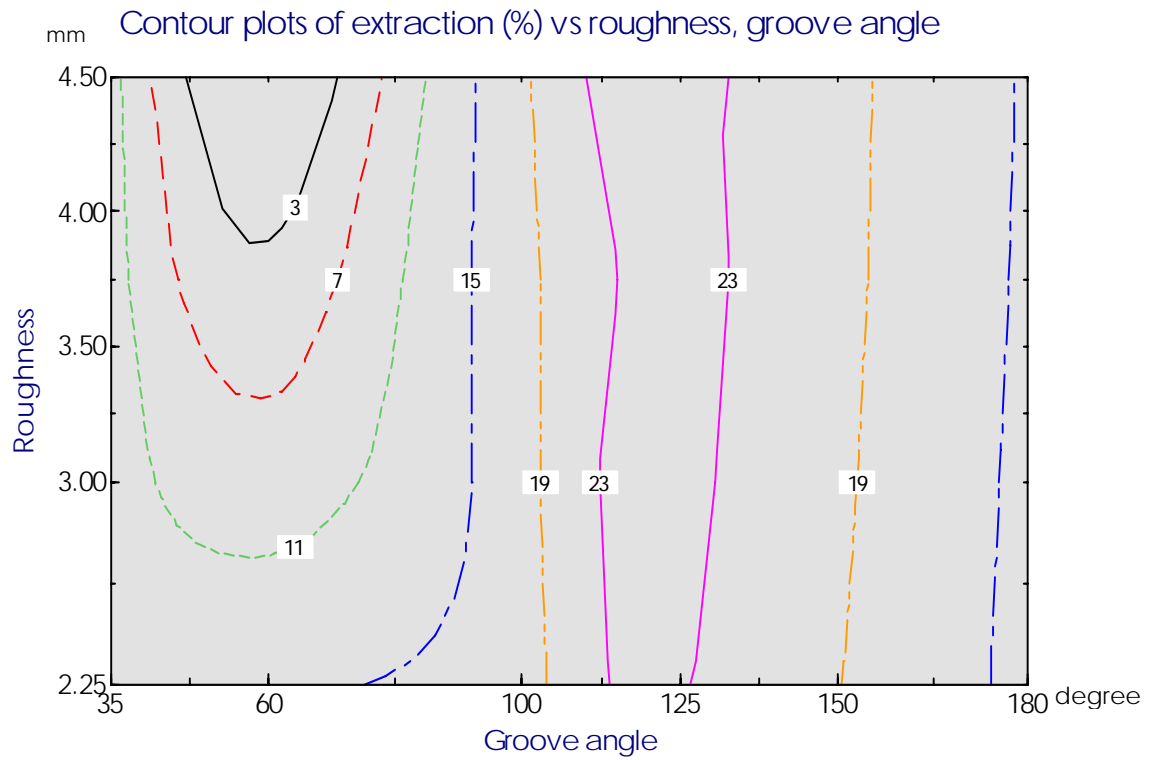
Figure 5.33 *Contour plots of extraction versus roughness and groove angle.*

Figure 5.34 *Surface plots of extraction versus roughness and groove angle.*

Contour plots of extraction (%) vs compaction, groove angle
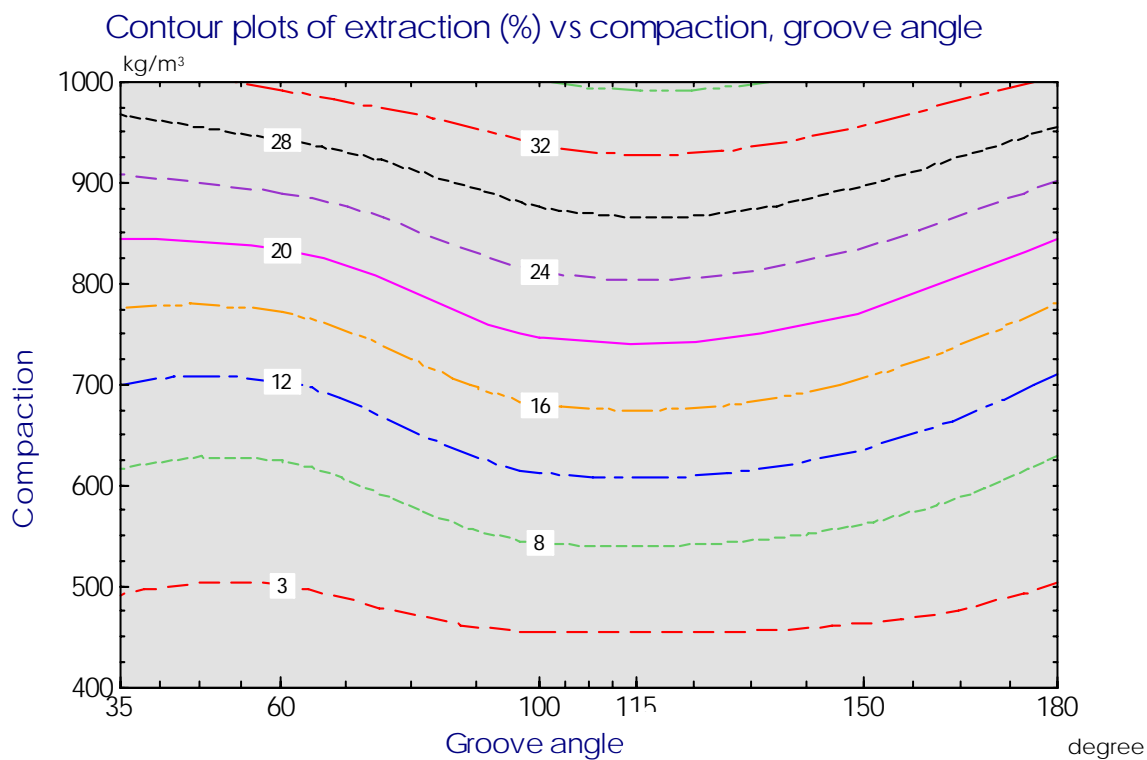
Figure 5.35 *Contour plots of extraction versus compaction and groove angle.*

Surface plot of extraction (%) vs compaction, groove angle
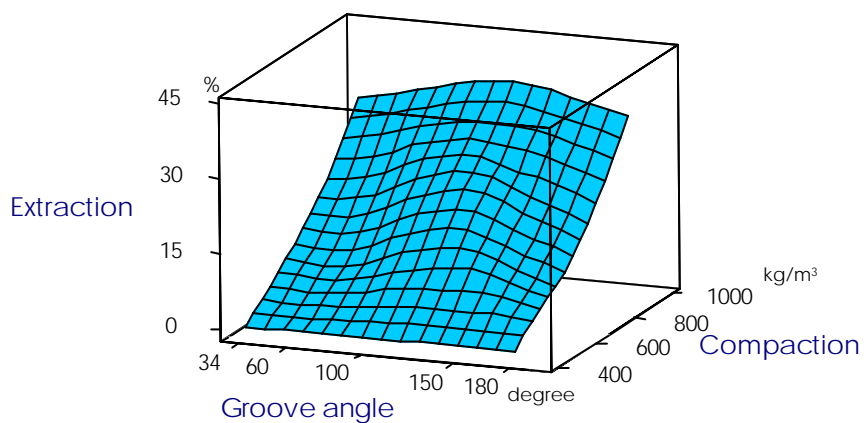
Figure 5.36 *Surface plots of extraction versus compaction and groove angle.*

Summary

This Chapter presents friction and shear results for moist and dry bagasse tested under uniaxial compression. The key variables were compaction, groove angle and roughness. It was observed that groove angle and roughness caused the friction coefficient to increase, while compaction caused a marked negative response. The shear coefficient was shown to be strongly affected by compaction. The dewatering of bagasse was shown to be influenced by compaction and grooved angles, but not roughness. The empirical model developed permitted the prediction of 97% of the observed friction coefficient values.

In the next Chapter, the observed results are discussed in detail

6

DISCUSSION

Abstract: This chapter presents the analysis and interpretation of the results. The probable cause of the negative response of the friction coefficient with compaction is discussed. In addition the positive effect of roughness and groove angles on friction is discussed. Finally, the potential impact of the findings on the dewatering of bagasse is considered.

6.1 The response of the friction coefficient to roughness, groove angle, and compaction

The underpinning hypothesis was that roughness, groove angle and compaction do not influence the friction coefficient when bagasse is compressed between grooved steel platens. The stated hypothesis was rejected because the value of the significant level, α, for each tested variable was greater than the observed p-value, as shown in Table 5.2. All three factors were shown to influence the interface friction. Compaction was the most significant factor which affected the friction coefficient negatively. The friction coefficient fell dramatically for compaction between 400 kg/m^3 to 1000kg/m^3. The same response was noted with the other two factors (Fig 5.2). It appears that the bagasse fibres reach a critical state and shear more easily as compaction is increased (Figure 6.1). Close inspection of a roughened platen (2,25 mm asperities height) following shearing at a compaction of 1000 kg/m^3 (filling ratio = 0.65) demonstrated that no significant ploughing occurred on the contact surface of the sample . The traces left by the asperities were intact, indicating that the failure plane was other than the interface friction, as shown in Figure 6.2. This failure of a porous material subjected to compaction and shear can be further discussed through application of a non-conventional modified Drucker-Prager /Cam (DPC) plasticity model shown in Figure 2.15.

Figure 6.1 *Traces left by asperities on bagasse after contacting a roughened steel flat platen at 1000 kg/m^3 compaction.*

Figure 6.2 *Evidence of the shear failure of bagasse after having been pushed 14 mm.*

At high compaction where the material is subject to high pressure (Figure 5.1(c) and 5.24) and densification (in the cap region), the local stresses on the material will be always on the yield locus. The yield locus at the cap region does not depend on pressure. The material exhibits plastic volumetric flow. It might be possible to develop an extended isotropic DPC model to capture the bagasse response by adjusting β, as a function of hydrostatic stress (Figure 2.15). Note that the figure is drawn with β, varying with hydrostatic stress, in an attempt to capture the observed reduction in critical state with increase in compaction.

From data exhibit on table 5.6, the yield surface should be a function of densification (Figure 6.3). The greater the densification the lower the current yield surface. A typical loading path in the *p-q* plane is illustrated using a dotted line in Figure 2.15. The final stress state "A" on the yield surface represents the point of failure of the material given the current location of a history dependent cap. Figures 6.4 and 6.5 show two cases of failure of bagasse by shear.
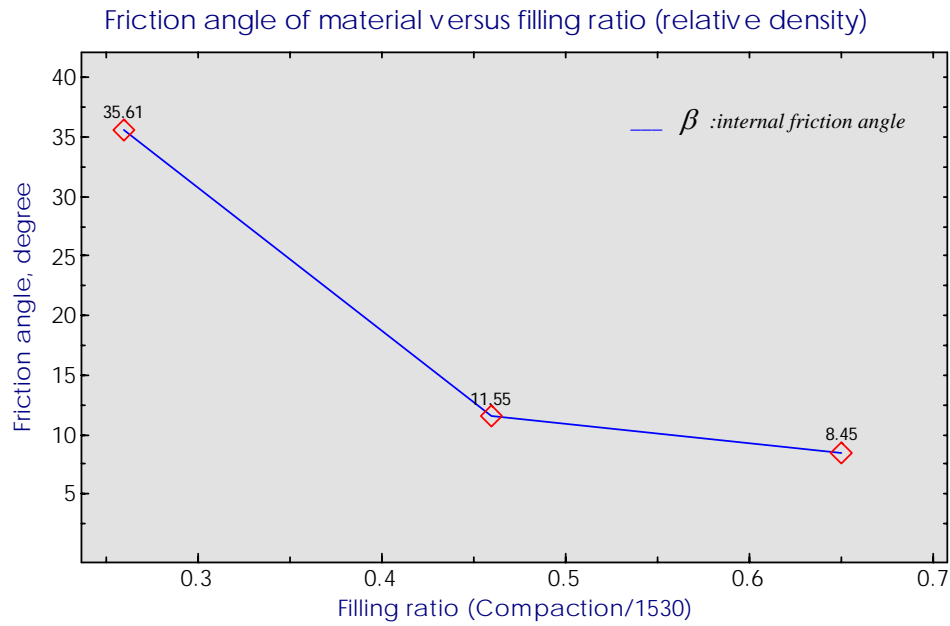
Figure 6.5 *The internal friction coefficient of the bagasse as a function of filling ratio (referred to density fibre = 1530 kg/m³)*

.
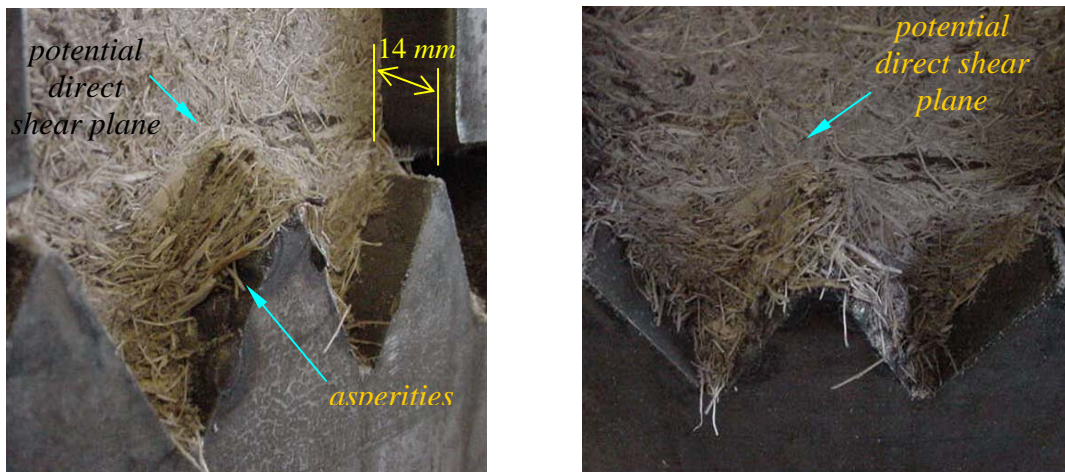
Figure 6.4 *The friction coefficient tests at 1000 kg/m³ compaction, 60° groove angle, and 2.25 mm average roughness. Slippage seems to occur outside the interface.*

Figure 6.5 *The friction coefficient test at 1000 kg/m³ compaction, 180° groove angle, and 2.25 mm average roughness. Potential slippage outside the interface.*

The photographs, in Figure 6.4, show roughened platens with a layer of fibre strongly adhered along the flank of the tooth, suggesting that there was sliding between layers of aligned fibres, (direct shear, Figure 6.6). The same behaviour seemed to occur when a flat roughened surface was tested (Figure 6.5). Bagasse does not slide at the interface when its contact surface is roughened.

σ' = normal stress
τ = shear stress
δ_h = horizontal displacement
δ_v = verical displacement
γ = shear strain
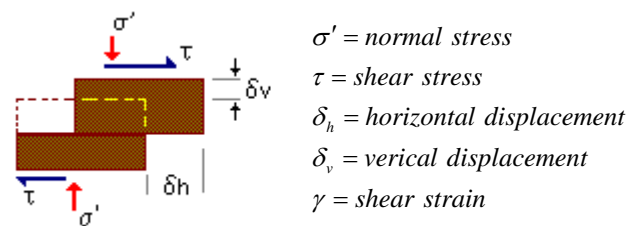
Figure 6.6 *A typical example of material subjected to direct shear (Atkinson, 2002)*

Plaza postulated that a roughened surface causes shear inside the bagasse due to the adherence of a fibre layer at the contact surface. According to the Plaza's postulation an internal friction coefficient of the bagasse (shear coefficient) is generated when a roughened surface is used. The results from this thesis (plotted in Figure 5. 23) do not seem to be in good agreement with Plaza's postulation. It is likely that the disagreement with Plaza´s results is due to Plaza determined the friction coefficient existing between fibres. Theses results could have given low friction coefficient values. There exists a permissible

difference between the shear and friction coefficient when material is compacted up to 700 Kg/m^3, suggesting that the failure of the material may be caused by other factors in addition to the roughness factor. Another discrepancy with the Plaza´s results could be that Plaza used platens of different geometry and roughness. For instance: 5 mm deep of groove angle and 1 mm height asperities. Figure 6.7 shows an idealised schematic representation of the contact between bagasse and a platen. The asperities (j_1 and j_2) have established contact under the applied force. The asperities offer resistance to plastic deformation due to ploughing or interlocking. As load increases, the region between the junction j_1 and j_2 fills with bagasse thus increasing the contact area, with the platen
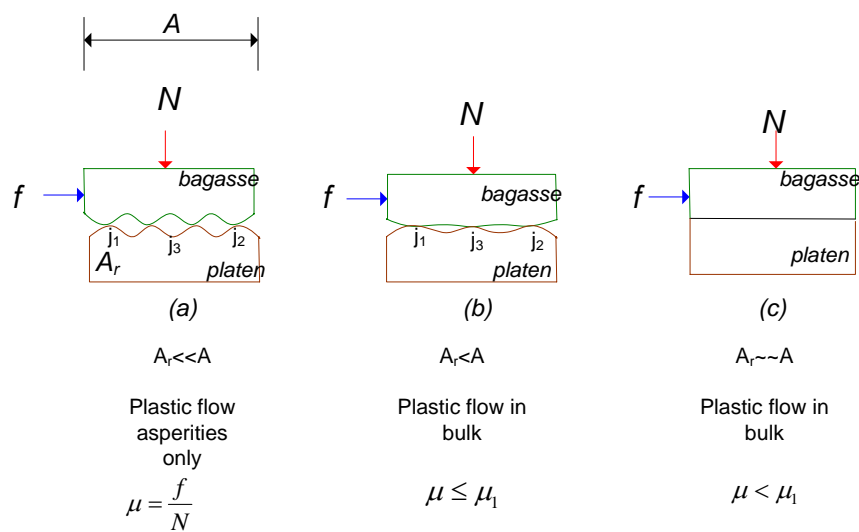
Figure 6.7 *A schematic diagram of friction mechanism: (a) Shear stress rises with the increment of normal pressure. (b) Plastic flow alternated with ploughing. (c) Shear stress remains constant, μ decreases with increasing normal pressure.*

If a sufficient number of junctions have been filled, then plastic flow will be initiated in a sub-layer of the bagasse material. It is not necessary that the area of all the junctions be equal to the apparent area. The strength of the junctions is much greater than that of the bulk material because of their relatively small size. The plasticity condition is given by the bulk effective stress acting on the bagasse, as a softer material, when this fibrous material is subject to uniaxial compressive stress. It follows that the maximum shear stress in the sub-layer will depend on the effective stress. The formed sublayer can only be sustained by the maximum shear strength of the bulk material. Figure 6.8(a) shows a photograph of the aligned appearance of fibre. The shear force now remains constant and μ decreases with increasing normal pressure. It is thus clear from the analysis that the height of the

roughness on the platen will not change the response of the friction coefficient, because of the "apparent" accumulated plasticity undergone, in, and around the sublayer formed within the material.

Groove angle causes more interactive effect on the coefficient than roughness.

(a)   (b)

Figure 6.8 *(a) Aligned appearance of fibres under 1000 kg/m^3 compaction, smooth, 100° groove angle. (b)Randomised appearance of fibres under 400 kg/m^3 compaction, 2.25mm height of asperity, and 35° groove angle.*

According to Figure 2.18, the normal force in a grooved element decreases as the angle of the groove increases. Hence there is a strong likelihood that the effective strength of the bagasse will be exceeded when the groove angle is acute. The positive effect of the groove angle at the interface seems also to change the response of the shear coefficient of bagasse (at low densification). Kauppila (2003) postulated that wider groove angles contribute to reduce frictional sliding and internal shearing. The tangential force which acts in a radial plane is reduced as groove angle increases. The reasoning given above is supported by Kauppila (2003). However, the positive effect of the groove angle on the friction coefficient is contrary to that purported by Adam (2004). He claims that the friction coefficient decreases with increasing groove angle. This discrepancy may be due to the significant scatter in his data.

The increment of the measured friction coefficient due to the size of roughness (16 % with respect to a smooth surface) corroborates the generalised belief by mill engineers that a roughened surface significantly increases the frictional forces at the interface, and

consequently, mill feeding (Kroes, 1999). These findings are opposed to that of Plaza (1994) who claims that the size and shape of roughness is not important for pressure in the range 0.2 to 20 MPa.
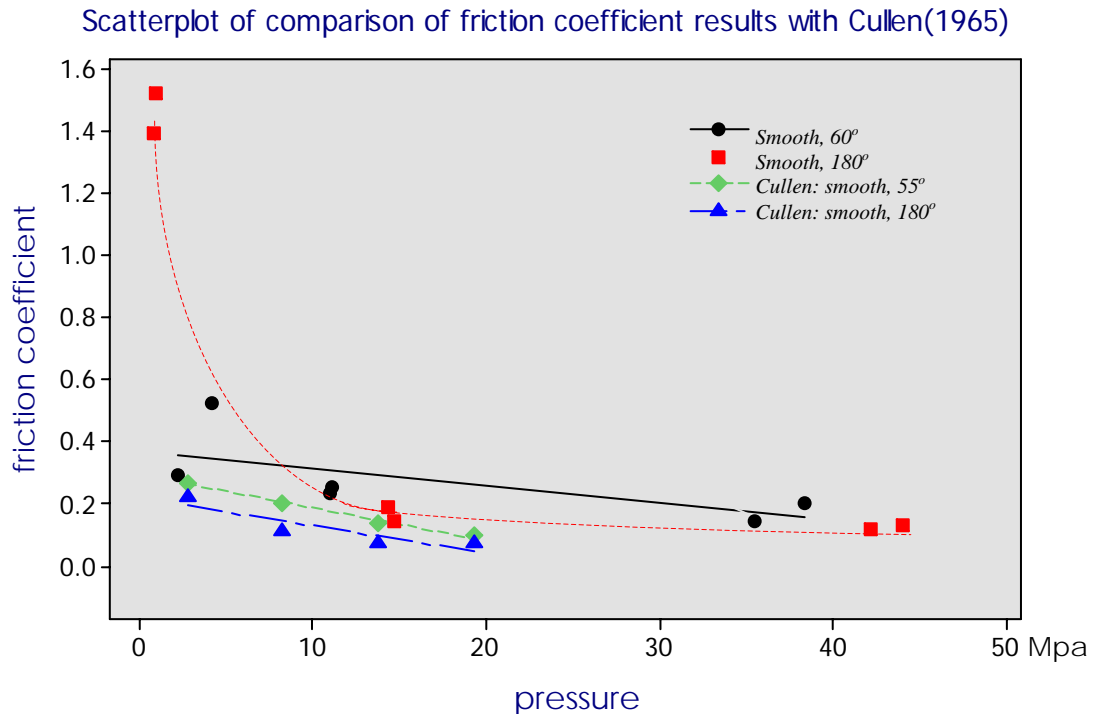
Figure 6.9 *A comparison of friction coefficients with respect to Cullen (1965).*

Examining Figure 5.1, for roughness less than the 2.25 mm, the friction coefficient responds positively (for low and high compaction). The probable causes are: bagasse, which is densified strongly, adhering to the sublayer formed over the asperities (Figure 6.4). This explains the non-significant effect of the roughness for high compaction (Figures 5.2, 5.20, 5.23, and 5.24). The dissimilarity of the observed responses for the friction coefficient for low pressure with smooth surfaces (Figure 6.9), with respect to Cullen (1965) may be due to the design of the platens or the bagasse material. The present tests involved deeper groove angles. However, this difference is small for normal pressure greater than 10 MPa. An important observation in Figure 6.9 is that the coefficient responds with no change for pressure greater than 20 MPa, suggesting that the material is failing at the same maximum shear strength. Figure 6.10 shows comparative line graphics of the ratio shear coefficient/friction coefficient versus normal pressure.
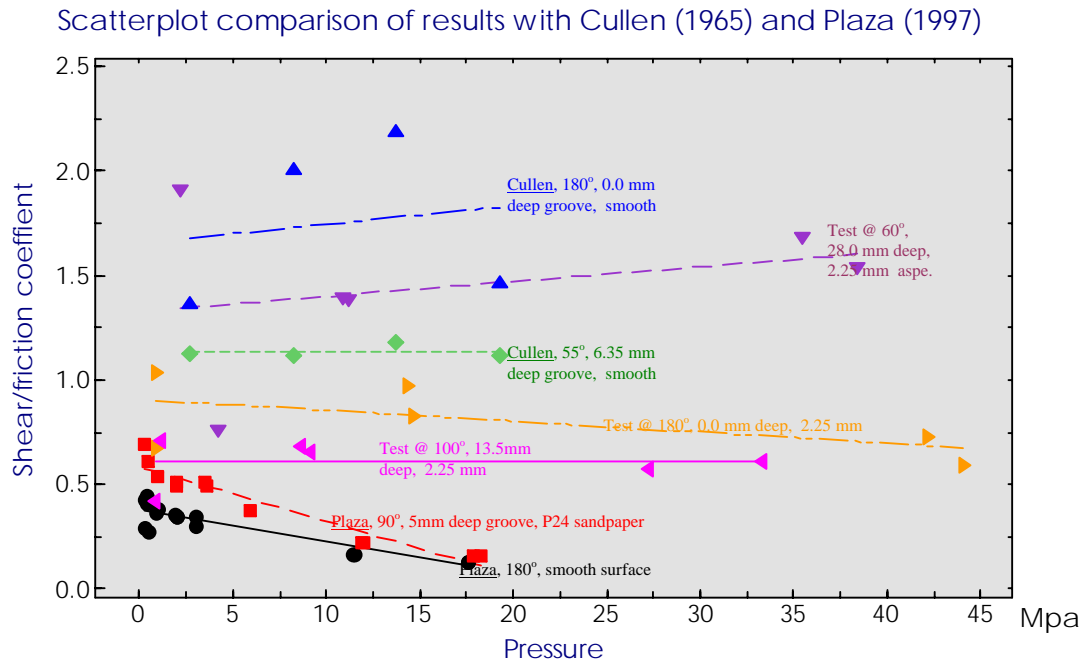
Figure 6.10 *Relation shear/friction coefficient compared to the results of Cullen (1965) and Plaza (1997).*

This ratio represents the maximum frictional force needed to cause internal failure in the material. It is expected that the ratio shear coefficient/friction coefficient shows values with minimal differences and a nearly horizontal trend as the pressure increases, because of the approximation of frictional forces to yield shear stress. The observed ratio is greater that Cullen's ratio, but lower than Plaza's ratio. The ratio shows the same trend as Cullen's trend. Differences with the Plaza's ratio seem to be caused by the design of the platens, and roughness. Plaza used grooved platen whose depth was only 5 mm. compare to this thesis whose value were from flat to 91 mm.

6.2   The maximisation of the friction coefficient

From Figures 5.5 through 5.22 it would appear that there is an optimum combination of levels which result in a maximum friction coefficient. Table 6.1 gives results from exercising Equation (5.2) across the three variables over the range low to high pressure. The objective was to determine the maximum friction coefficient across levels.

Table 6.1 *The effect of the variables roughness, groove angle, and compaction on the maximum friction coefficient value.*

Solution	roughness (mm)	groove angle (degree)	compaction (kg/m³)	maximum friction coefficient
1	4.50	125	400	0.81
2	4.26	152	400	0.78
3	4.05	97	700	0.36
4	3.38	150	700	0.34
5	2.20	106	1000	0.22
6	3.00	104	1000	0.21
7	1.25	67	1000	0.21

These predicted combinations suggest that obtuse angles result in the highest friction coefficient. For the particular case of a groove angle equal to 35° (a popular groove angle in the majority of the Australian milling units) the maximum predicted values for the friction coefficient that may be achieved is shown in Table 6.2.

Table 6.2 *The combination for roughness and compaction for predicted maximum friction coefficient at a fixed 35° groove angle.*

Solution	roughness (mm)	groove angle (degree)	compaction (kg/m³)	friction coefficient
1	4.14	35	702	0.19
2	0.13	35	787	0.17
3	1.65	35	966	0.17
4	1.72	35	979	0.17
5	3.89	35	512	0.31
6	3.79	35	623	0.21
7	4.26	35	472	0.40
8	2.12	35	985	0.15
9	4.49	35	741	0.20
10	0.09	35	787	0.17

6.3   The dewatering of bagasse

The results indicate that high compaction is required to reduce the bagasse volume (volumetric strain) in order to increase extraction. An increment of extraction can also be achieved by widening the groove angle of the contact surface. Wider groove angles resulted in a reduction in shear strain and failure of the material by shear at the region of high pressure (apex of the tooth).   A maximum value of extraction was achieved with

groove angles between 100° and 125°. A negative response for extraction with groove angles less than 120° conflicts with the fact that greater volumetric strain must occur, and consequently, more extraction. It is likely that a lower permeability at high compaction or unknown factors is contributing to the reduction in extraction. Further investigation is needed into the effect of groove angles on the extraction. Table 6.3 shows a comparison of extraction between 35° and 100°.

Table 6.3 *Comparison in percentages of extracted liquid between 35° and 100° groove angles at three compaction levels, at 52% moisture bagasse*

Compaction	Moisture in Bagasse (%)		
(kg/m³)	35 º	100 º	Difference
400	52.00	52.00	0.00
700	46.23	44.01	-2.22
990	40.00	38.24	-1.76

Overall the experimental results suggest that bagasse moisture has a minimal effect on the friction coefficient and coefficient of internal shear. However, these findings should be treated with reserve since the level of juice loading is considered low compared with factory environments. More work is required to better understand this important problem.

Summary

The following observations are made:

1) It is argued that the reduction in friction coefficient with increasing compaction is due to the apparent alignment of fibres orthogonal to the maximum principle stress. This alignment is caused by the densification process (seepage induced consolidation).

2) When the groove angle of a contact surface is widened, a reduction of normal forces may be produced. This reduction may cause less deformation and densification of the material. This behaviour causes a positive effect on the maximum shear strength, increasing the friction coefficient.

3) It was observed that shear failure in the bagasse occurred near the apex of asperities, regardless of the height of the asperity.

4) Wider groove angles may enhance dewatering for compactions up to 1000 kg/m^3.

7

CONCLUSIONS

Abstract: In this final chapter the conclusions and recommendations of the investigation into the effect of interface friction on bagasse compaction between steel grooved platens are presented.

Sugar mill managers throughout the world strive for maximum throughput and maximum juice extraction in milling trains. These two objectives depend on many factors. Some factors are difficult to define. There is a general agreement amongst mill practitioners that circumferential grooves on rolls are a necessity for good juice drainage. However, the geometric configurations employed vary. In addition, practitioners firmly agree on the need for some degree of roll roughness to be applied to the apex and flanks of grooves. Once again, the level and specification vary enormously. The principal variable of importance here is the friction coefficient. A systematic experimental investigation has been undertaken in this thesis to explore the primary factors which influence friction between roughened grooved surfaces and compacted bagasse.

The results of the investigation have led to the following conclusions and implicit observations:

- Roughness, groove angle and compaction are key variables which influence the interface friction between bagasse and steel grooved platens.

- The static friction coefficient across the entire population of all tests undertaken in this thesis (compaction: 400 – 1000 kg/m3; groove angles: 35° – 180°; roughness: smooth to rough) ranged from 0.149 to 0.601.

- Compaction was shown to affect the friction coefficient in a negative fashion. The friction coefficient reduces by 300% when compaction increases from 400 kg/m^3 to 1000 kg/m^3.

- Groove angles positively affect the friction coefficient. The friction coefficient increases by 120%, when the groove angles increase from 35° to 100°.

- Roughness positively affects the friction coefficient. The friction coefficient increases by 16% when the roughness varies from "smooth" to "rough

- Roughness, groove angle, and compaction are variables which interact to influence friction coefficient.

- The shear coefficient is negatively affected when compaction increases from 400 kg/m^3 to 1000 kg/m^3.

- The bagasse moisture influences neither the friction coefficient nor the shear coefficient.

- The developed empirical model for the friction coefficient, in terms of roughness, groove angle and compaction, can predict 97% of the observed responses.

- The groove angle and compaction exhibit a positive response on dewatering of bagasse. Roughness does not appear to influence dewatering over the range tested.

- The dewatering of bagasse is maximum when the groove angle is between 100° and 120°. A 100° groove angles extracts 2% more liquid than a 35° groove angle at the same compaction and roughness.

7.1   Future investigations

With respect to future research direction, the following suggestions are proposed:

- More work is required to assess the effect of roughness on friction coefficient and internal shear of the spatial location of asperities on the apex and groove flank.

- Because of conflicting results regarding the effect of friction on bagasse moisture and shear coefficient, more work is required to assess friction and juice loading on final bagasse moisture.

- More work using bagasse higher than 52% moisture content is required. Furthermore, groove angles containing juice channels at the root of teeth need to be carried out.

- Bagasse undergoes very large strain deformation when it is compressed between groove platens. There is a need to quantify this deformation experimentally and to compare the results with theoretical coupled finite element models.

References

Adam, C. J. 1997. Application of Computational Porous Media Mechanics to the Rolling of Prepared Sugar Cane. James Cook University. Australia. Ph.D. Thesis.

Adam, C.J., Loughran, J.G. 2004. Multivariate Analysis of Frictional Interaction between Grooved Rollers and Prepared Sugar Cane. Transaction of the American Soc. of Agric. Engineers (ASAE). Vol. 47 (5), pp. 1611-1618.

Allan, C.J. 1958. Roller Surface and the Efficient Operation of Mills. Proc. QSSCT, 25th Conference, pp. 65-73.

Anon., 1958. Sugar Research Institute. *Milling Studies*. Experimental Mill. 7. The influence of degree of preparation on N_o 1 Mill Performance. Technical Report N_o 49.

Anon., 2001. Bureau of Sugar Experiment Station. The Laboratory Manual for Australian Sugar Mills. *Analytical Methods and Tables, Vol.2*. BSES Publications, Brisbane, Australia.

Anon., 2001. Chapman Instruments. Performance Plus Software. Parameter Definition. Technical Note – TG-5. Rochester, NY.

Anon., 2004. THK. General Catalogue N^o300-4E. Friction Coefficient THK-A-6. www.thk.com/technical. Accessed 15 October 2004.

Arvanitis, C.L. and Portier, K.M. 1997. Sample Size Estimation in Simple Random Selection. University of Florida. http://www.ifasstat.ufl.edu/nrs98/SRSsam.htm. Accessed 10 November 2003.

Atkinson, J. 2002. Shear Strength. Compression and Shear. http://fbe.uwe.ac.uk/public/geocal/SoilMech/shear.htm . Accessed 20 Jan. 2005.

Aysen, A. 2002. *Soil Mechanic: Basic Concepts and Engineering Applications*. A.A. Balkema Publisher. The Netherlands.

Barnes, A.C. 1974. *Agriculture of the Sugar Cane*. 2nd Edit. Wiley Pub. New York.

Barnes, G.E. 2000. *Soil Mechanics. Principles and Practice*. 2nd Edit. Macmillan Press Ltd. London.

Belz, M.H. 1973. *Statistical Methods for the Process Industries*. The Macmillan Press Ltd. London.

Box, G.E.P., Hunter, W.G., and Hunter J.S. 1978. *Statistic for Experimenters: An Introduction to Design, Data Analysis, and Model Building*. Wiley Pub., New York.

Brunelly, Sydney 1994. Capacidad de Molienda y Extracción. Sociedade do Tecnicos Acucareiros e Alcooleiros do Brasil. STAB, Set-Oct, Vol.13 #1, pp. 19-23.

Budinski, K.G. and Budinski, M.K. 2002. *Engineering Materials and Properties*. 7th Ed. Pearson Education, Inc., N.J.

Bullock, K. J. 1957. An Investigation into the Crushing and Physical Properties of Sugar Cane and Bagasse. University of Queensland. Australia. Ph.D. Thesis.

Bullock, K. J. and Murry, C. R. 1958. Coefficient of Friction of Bagasse on Iron Surfaces. The International Sugar Journal. Vol. 37, pp. 162-164.

Cochran, W.G. and Cox, G.M. 1966. *Experimental Design*. 2nd. Edit. Wiley Pub. New York.

Cullen, R.N. 1965. An Investigation of the Shear Strength of Bagasse. University of Qld., Australia, M. Eng. Sc. Thesis.

Cullen, R.N. 1987. The Influence of Shredder Design on Cane Preparation. The International Sugar Journal. Vol. 84, No 1065, pp 166-168.

Deerr, N. 1905. *Sugar and the Sugar Cane: An Elementary Treatise on the Agriculture of the Sugar Cane and on the Manufacture of Cane Sugar*. N. Rodger Pub. London.

Downing, C.M., Loughran, J.G. and Domanti, S.A. 1999. Crushing Soil Contaminated Sugar cane. Proc. of Australian Society of Sugar Cane Technol. 21st Conf., pp. 294-300.

Downing, C.M. 1999. Investigation of the Effects of Soil Contamination on the Crushing of Comminuted Sugar Cane. James Cook University, Australia, Ph.D. Thesis.

Ford, I.J. 1993. Roughness Effect on Friction for Multi-asperity Contact between Surfaces. J. Physic D. App. Phys. Vol. 26, pp. 2219-2225.

Gambley, C. 2003. CSIRO's Diversity in Sugar Research: Molecular to Macro. Australian Sugar Cane. Vol. 7 N_o SA, pp.58.

Hicks, C.R. and Turner, K.V. 1999. *Fundamental Concepts in the Design of Experiments*. 5th Edit. Oxford University Press, New York.

Hogan, M. 2001. Assessment of Cane Behaviour at the "Factory" Roll/Blanket Interface. BE. Hon. Thesis, James Cook University.

Hugot, E. 1986. *Handbook of Cane Sugar Engineering*. 3rd Edit. Elsevier Publishing. Amsterdam.

Jenkins, G.H. 1953. Some Factors Involved in the Feeding of the Cane Mill. Proc. Q.S.S.C.T., 20th Conf., pp. 169-174.

Jenkins, G.H. 1966. *Introduction to Cane Sugar Technology*. Elsevier Publishing. Amsterdam.

Kannapiran, A. 2002. Computational and Experimental Modelling of the Crushing of Prepared Sugar Cane. James Cook University. Australia. Ph.D. Thesis.

Kaupilla, D.J. and Loughran, J.G. 2000. An Experimental Investigation into the Effect of Mill Orientation Angle on Reabsorption. Proc. Aust. Soc. Sugar Cane Technol. Conf., Vol. 22, pp. 423-428.

Kaupilla, D.J., Loughran, J.G. and Kent, G.A. 2001. Fundamental Studies into the Dewatering of Prepared Cane and Bagasse between Groove Surfaces. Proc. Aust. Soc. Sugar Cane Technol. Conf., Vol. 23, pp. 437-443.

Kaupilla, D.J., Britton, P.F, Kent, G.A. and Loughran, J.G. 2003. Grooving and its Effect on Bagasse Moisture Content. Proc. Aust. Soc. Sugar Cane Technol. Conf., Vol. 25:(CD-ROM).

Kaupilla, D.J., Kent, G.A. and Loughran, J.G. 2003. Preliminary Experimental Studies into the Flow of Juice in Roller Groove Conduits. Proc. Aus. Soc. Sugar Cane Technol., Vol. 25:(CD-ROM).

Kent, G.A. and Delfini, P. 2000. High-Speed Milling – A Low Cost Avenue for Increasing Milling Capacity? Proc. Aust. Soc. of Sugar Cane Technol., 22nd. Conf., pp. 416-422.

Kroes, S. 1999. Enhanced Roll Life. Proc. Aus. Soc. Sugar Cane Technol., 21st Conf., pp. 307-312.

Lamiatre, J and Chaboche, J.L 2000. *Mechanic of Solid Materials.* 3rd edition. Cambridge University Press, UK.

Loughran, J.G., Ivin, P.C., McCarthy, W. and Vidler, T.L. 1988. A New Method and Apparatus for determining of Fibre in Cane. Proc. Aust. Soc. Sugar Cane Technol. 10th Conf., pp. 89-98.

Loughran, J.G 1990. Mathematical an Experimental Modelling of the Crushing of Prepared Sugar Cane. University of Queensland. Australia. PhD. Thesis.

Ludema, C.K. 1996. *Friction, Wear and Lubrication.* CRC Press Ltd., New York.

Mendenhall, W. 1968. *The Design and Analysis of Experiments*. Wadsworth Publishing Company, Inc., California.

Morrow, R, Grant, A, Jackson, D.P. 1999. A Strange Behaviour of Friction. The Physics Teacher. Vol. 37, pp. 412-415.

Murry, C.R. 1960. The Mechanics of Crushing Prepared Sugar Cane. University of Queensland. Australia. Ph.D. Thesis.

Murry, C.R. and Holt, J.E. 1967. *The Mechanics of Crushing Sugar Cane*. Elsevier Publishing, Amsterdam.

Neale, M.J. 1995. *The Tribology Handbook*. 2nd Edit. Butterworth Heinemann, Oxford.

Nicklin, D.J. and Nix, K.J. 1979. An Unsuccessful of a New Concept in Juice Grooves. Proceedings of Australian Society of Sugar Cane Technologist Conference, 2nd Conf.

Ott, L. 1984. *An Introduction to Statistical Methods and Data Analysis.* PWS-KENT Publishing Company, Boston.

Owen D.R.J.; Zhao S.Y.; and Loughran J.G. 1994. An Overview of Crushing Theory Investigation at Swansea. Part 1 – Testing and Constitutive Relation. Proc. Aust. Soc. Sugar Cane Technol.,16th Conf., pp. 244-247.

Plaza, F. and Edwards, B.P. 1994. Shear, Friction, and the Required Roll Roughness. Proc. Aust. Soc. Sugar Cane Technol.,16th Conf., pp. 264-270.

Plaza, F. and Kent, G.A 1997. Using Soil Shear Test to Investigate Mill Feeding. Proc. Aust. Soc. Sugar Cane Technol.,19th Conf., pp. 380-340.

Plaza, F. and Kent, G.A. 2000. Drainage Requirements of the Crushing Roll Surface. Proc. Aust. Soc. of Sugar Cane Technol., 22nd Conf., pp. 368-373.

Plaza, F. 2002. Measurement, Modelling and Understanding the Mechanical Behaviour of the Bagasse. University of Queensland. Australia. Ph.D. Thesis.

Plaza, F., Kirby, J.M. and Harris, H.D. 2003. Modelling Sugar Cane Bagasse Behaviour in a Modified Direct Shear Test Using and Elastic-Plastic Critical State Model. 2003 ABAQUS Users' Conference, pp. 1-15.

Solomon, T. J. 1967. Theoretical and Experimental Studies in the Mechanics of Crushing Sugar Cane. University of Queensland. Australia. Ph.D. Thesis.

Stolarsky, T.A. 1990. *Tribology in Machine Design.* Butterworth-Heinemman, Oxford.

Vass, N.1999. Experimental and Numerical Investigation of Bagasse Compression Between Grooved Surfaces. BE.H. Thesis, James Cook University.

Waddell, C.W. 1963. Prepared Cane Sampling for Individual Fibres. Proc. Qld. Soc. Sugar Cane Technol. 30th, Conf., pp 27-35.

Williams, J.A. 1994. *Engineering Tribology.* Oxford University Press. N.Y.

Yong, R. and Warkentin, B.P. 1966. *Introduction to Soil Behaviour.* The Macmillan Company, N.Y.

Zlokarnick, M. 1991. *Dimensional Analysis.* Spring-Verlag. Berlin.

Appendices

Appendix A

Example of calculations

A.1 Example of calculation of cane/bagasse mass and volume and dimensions of the shear box

a) The following parameters are considered:

Fibre/cane content, %	:	*15.00*
Fibre/bagasse content, %	:	*47.00*
Particle density, kg/m³	:	*1530.00*
Juice density, kg/m³	:	*1080.00*
Compaction, kg/m³ (max)	:	*1000.00*
Set opening, mm	:	*40.00 (fixed)*
Work opening, mm	:	*94.00 (maximum)*
Cell area (228mm x 100 mm), m²	:	*0.0342*
Bagasse/cane, %	:	*31.00*

b) Formulas employed

$$Specific\ volume = \frac{Volume\ of\ final\ bagasse}{Volume\ of\ cane\ particle}$$

$$Compaction = \frac{1530}{Specific\ Volume}$$

$$Cane\ Volume = \frac{Fibre\ mass}{Fibre\ density} + \frac{Juice\ mass}{Juice\ density}$$

c) Calculation of the cell height for cane

Calculation of the cell height respect to a known area

Cell area: 100 mm x 228 mm

$$Compaction = \cfrac{1530}{\left(\cfrac{\cfrac{Cell\ area \times final\ height\ bagasse}{Fibre \times Bagasse\ mass}}{1530}\right)} = \frac{1530 \times 0.47 \times BagasseMass}{1530 \times 0.094 \times 0.228 \times 0.100}$$

$$Bagasse\ mass = \frac{Compaction \times 0.094 \times 0.0228}{0.47} = \frac{1000 \times 0.094 \times 0.0228}{0.47} = 4.56\ kg.$$

$$Cane\ Mass = \frac{Bagasse\ mass}{Bagasse/cane} = \frac{4.56}{0.31} = 14.71\ kg.$$

Juice mass = Cane mass – Fibre mass

Juice mass = 14.71 - 0.15×14.71 = 12.50 kg.

$$\text{Cane volume no-void} = \frac{0.15 \times 14.71}{1530} + \frac{12.50}{1080} = 0.013\ m^3$$

$$\text{Cane volume and void} = \frac{0.013}{0.7} = 0.01859\ m^3$$

$$Cell\ Height_{effective} = \frac{Cane\ volume}{Cell\ area} = \frac{0.01859}{0.0228} \times 1000 = 816\ mm.$$

Cell height = cane + platen heights + bearing height

Required cell height = 816 + 2×87 + 79 = 982 mm

d) Calculation of the cell height for bagasse

Juice mass = Bagasse mass – Fibre mass

Juice mass = 4.56 - 0.47×4.56 = 2.42 kg

$$\text{Bagasse volume no-void} = \frac{0.47 \times 4.56}{1530} + \frac{2.42}{1080} = 0.00364\ m^3$$

$$\text{Bagasse volume and void} = \frac{0.00364}{0.7} = 0.0052\ m^3$$

$$Cell\ height_{effective} = \frac{Bagasse\ volume}{Cell\ area} = \frac{0.0052}{0.0228} \times 1000 = 228\ mm$$

Cell height = cane bagasse + platen heights + bearing height

Required cell height (Bagasse) = 228 + 2×87 + 79 = 481mm

A.2 Example of calculation for friction coefficient

Friction coefficient was calculated by Equations (2.40). The average friction coefficient value is the sum of the friction coefficient on each flank and the tip of the tooth. There are two similar inclined planes and one flat where frictional force is produced.

Compressive force, kN   :   *69.994*

Shear Force, kN   :   *19.500*

Flank angle, degree   :   *100.00*

Tip angle. degree   :   *180.00*

a) Friction coefficient on the flanks of the tooth

$$\mu_f = \frac{\frac{f}{N} \cdot sin\frac{\theta}{2}}{1 - \frac{f}{N} \cdot cos\frac{\theta}{2}} = \frac{\frac{19.50}{69.994} \cdot sin\left(\frac{100}{2}\right)}{1 - \frac{19.50}{69.994} \cdot cos\frac{100}{2}} = 0.2601$$

b) Friction coefficient on the tip of the tooth

$$\mu_f = \frac{\frac{f}{N} \cdot sin\frac{\theta}{2}}{1 - \frac{f}{N} \cdot cos\frac{\theta}{2}} = \frac{\frac{19.50}{69.994} \cdot sin\left(\frac{180}{2}\right)}{1 - \frac{19.50}{69.994} \cdot cos\frac{180}{2}} = 0.2910$$

c) The average friction coefficient action on the tooth

$$\mu_{ave} = \frac{\mu_{f100} + \mu_{f100} + \mu_{t180}}{3} = \frac{0.2601 + 0.2601 + 0.2910}{3} = 0.2704$$

A.3 Example of calculation for shear coefficient

Shear coefficient was calculated as the ratio of the horizontal force to the vertical force. The horizontal force recorded was that which caused failure in a plane other than the interface

Compressive force, kN   :   *69.994*

Shear Force, kN   :   *19.500*

$$Shear\ coeff = \frac{f}{F} = \frac{19.50}{69.994} = 0.2786$$

A.4 Example of calculation for extracted liquid ratio (SRI, 1958)

Mass of liquid extracted, gr   :   *64.00*

Dry fibre in bagasse, %   :   *47.20*

Mass of bagasse, gr   : *587.00*

$$Dewatering\ ratio = \frac{Mass\ of\ liquid}{Mass\ of\ bagsse\left(1 - \dfrac{fibre\%bagase}{100}\right)} \times 100$$

$$Dewatring\ ratio = \frac{64}{587 \cdot \left(1 - \dfrac{47.20}{100}\right)} \times 100 = 20.65$$

A.5 Example of calculation of average roughness

The average roughness was calculated based on the Equation 2.52. Seven measurements were taken at 1 mm apart. The average length of the asperity was 7 mm. For nodule, the length was 20 mm.

     n = 7

     y1 = 0.90   *y5 = 3.50*   *y4 = 1.00*

     y2 = 2.00   *y6 = 2.75*

     y3 = 2.60   *y2 = 1.95*

$$R_a = \frac{|y_1| + |y_2| + |y_3| + \ .\ \ .\ \ .\ \ + |y_7|}{n} = \frac{0.90 + 2.00 + 2.60 + 3.50 + 2.75 + 1.95 + 1.00}{7} = \frac{14.8}{7}$$

$$R_a = 2.11\ mm$$

A.6 Example of calculation of canonical equation and contours for response surface experiment on friction coefficient.

The following developed empirical model was used (Equation 5.2)

$$FC_{pred} = 0.28 + 0.13r + 0.12g - 0.16c - 0.040r^2 - 0.066g^2 + 0.10c^2 - 0.020rg$$
$$- 0.14\,rc - 0.124\,gc - 0.13\,r^2g - 0.026\,r^2c - 0.12\,rg^2 \qquad \textbf{(C.1)}$$

To convert Equation C.1 into canonical form, a stationary point, O, is calculated. By deriving FC_{pred} respect to their variables, $\dfrac{\partial FC}{\partial r} = 0,$ $\dfrac{\partial FC}{\partial g} = 0,$ $\dfrac{\partial FC}{\partial c} = 0$. The equations for determining a stationary point are

$$-0.16 - 0.14r + 0.00g + 0.20c - 0.026r^2 = 0$$
$$0.12 - 0.02r - 0.132g - 0.124c - 0.13r^2 - 0.24rg = 0$$
$$0.13 - 0.08r - 0.02g - 0.14c - 0.12g^2 - 0.26rg - 0.052rc = 0$$

There are six solutions for the above equation. Taking the first solution gives

$$FC' = 0.1259 \qquad r' = -0.8798 \qquad g' = -0.7296 \qquad c' = -0.1676$$

The canonical form for the equation of a response surface is thus

$$FC_{pred} = FC' + \lambda_1 \cdot R^2 + \lambda_2 \cdot G^2 + \lambda_3 \cdot C^2 \qquad \textbf{(C.2)}$$

where $\lambda_1, \lambda_2,$ and λ_3 are the eigenvalues. From Equation C.1, making $|A - \lambda I| = 0$, then the solution is

$$\lambda_1 = -0.1068 \qquad \lambda_2 = -0.0422 \qquad \lambda_3 = 0.1430$$

The canonical form is then

$$FC_{pred} = 0.1259 - 0.1068R^2 - 0.0422G^2 + 0.143C^2 \qquad \textbf{(C.3)}$$

where

$$R = (r + 0.8798) \cdot x_{11} + (g + 0.7296) \cdot x_{12} + (c + 0.1676) \cdot x_{13}$$
$$G = (r + 0.8798) \cdot x_{21} + (g + 0.7296) \cdot x_{22} + (c + 0.1676) \cdot x_{23}$$
$$C = (r + 0.8798) \cdot x_{31} + (g + 0.7296) \cdot x_{32} + (c + 0.1676) \cdot x_{33}$$

.

If $\bar{V}$ is a vector which components are *R, G* and , C. Then $\bar{V}$ can be writing in the following way

$$\bar{V} = \begin{pmatrix} x_{11} & x_{12} & x_{13} \\ x_{21} & x_{22} & x_{23} \\ x_{31} & x_{32} & x_{33} \end{pmatrix} \cdot \begin{pmatrix} r + 0.8798 \\ g + 0.7296 \\ c + 0.1676 \end{pmatrix}$$

The values for $x_{11}, x_{12}, \ldots x_{32}$, and x_{33} are calculated from coefficients of Equation C.1. Then, it results in homogenous equations. The calculated values for the first group of solutions is

$$\bar{V} = \begin{pmatrix} 0.7143 & 0.2790 & 0.6400 \\ 0.9947 & 0.1018 & 0.0167 \\ -0.3395 & -0.7871 & 0.7592 \end{pmatrix} \cdot \begin{pmatrix} r + 0.8798 \\ g + 0.7296 \\ c + 0.1676 \end{pmatrix}$$

The contour plots are represented in two-dimensions. It can be plotted by making one of the variables equals to zero.

Appendix B

Calculation of samples

B.1 Calculation of the number of samples

Table B1 shows values of friction coefficients reported by Cullen (1965). Both static and dynamic coefficients, at two replications are shown. These values were required to determine the parameters required to calculate the number of tests.

Table B1 *Friction coefficients values for four variables reported by Cullen (1965)*

				P_1			P_2			P_3			P_4		
				G_1	G_2	G_3	G_1	G_2	G_3	G_1	G_2	G_3	G_1	G_2	G_3
Static coefficient of friction	S_1	p_1	R_1	.256	.347	.334	.117	.233	.219	.088	.149	.153	.082	.111	.120
			R_2	.249	.296	.291	.129	.234	.219	.092	.160	.163	.083	.128	.097
		p_2	R_1	.227	.299	.252	.104	.251	.211	.076	.126	.126	.072	.166	.090
			R_2	.239	.276	.298	.122	.232	.219	.076	.126	.126	.094	.104	.104
	S_2	p_1	R_1	.214	.315	.291	.112	.211	.176	.067	.140	.140	.071	.127	.101
			R_2	.234	.289	.259	.112	.214	.234	.076	.145	.145	.065	.124	.102
		p_2	R_1	.220	.236	.244	.108	.182	.149	.062	.129	.129	.060	.105	.082
			R_2	.234	.277	.272	.114	.178	.195	.072	.146	.146	.070	.111	.099
Dynamic coefficient of friction	S_1	p_1	R_1	.256	.274	.322	.117	.233	.219	.088	.153	.153	.070	.111	.120
			R_2	.222	.259	.261	.108	.234	.219	.079	.163	.163	.071	.119	.094
		p_2	R_1	.199	.299	.234	.104	.251	.211	.070	.123	.123	.072	.166	.090
			R_2	.209	.276	.279	.112	.232	.219	.069	.126	.126	.094	.098	.104
	S_2	$p1$	R_1	.196	.263	.229	.104	.197	.157	.067	.129	.129	.068	.117	.076
			R_2	.228	.209	255	.102	.214	.209	.076	.121	.121	.065	.102	.088
		$p2$	R_1	.204	.204	.230	.105	.182	.147	.062	.119	.119	.060	.092	.080
			R_2	.184	.252	.252	.102	.178	.195	.065	.127	.127	.070	.100	.089

where

P pressure at four levels: P_1: 400 psi; P_2: 1200 psi; P_3; 2000 psi; P_4 2800 psi

G grooved angle at three levels: G_1: 45°; G_2: 55°; G_3: flat plate(180°)

S speed at two levels: S_1: 1.76 ft/min; S_2: 8.22 ft/min

p cane preparation at two levels: p_1: 47.9 lb/cu.ft at 750 rpm/15 s; p_2: 39.2
    lb/cu.ft at 500 rpm/20 s,

Table B2: Statistical parameters to estimate the number of samples.

Parameters	Static friction coefficient	Dynamic friction coefficient
Number of samples	96	96
Mean, μ	0.167	0.156
Standard deviation, σ	0.0757	0.0690
Standard error ξ	0.00773	0.007042
Margin of error e %	9.17	8.94
Student's t distribution, t @ 95%	1.98	1.98

The equation to estimate the sample size and the margin of error

$$n = \frac{n_o}{1 + \dfrac{n_0}{N}} \quad \text{(B.1)}$$

where,

$$n_o = \left(\frac{\sigma.t}{me.\mu} \right)^2 \quad \text{(B.2)}$$

and

$$e = \frac{100.\xi.t}{\mu} \quad \text{(B.3)}$$

Assuming that N, the population size, is too large or infinite, and the margin of error 9%, equation (B.2) gives:

$$n_{sfc} = \left(\frac{0.076 \times 1.98}{0.09 \times 0.167} \right)^2 = 100 \text{ tests for static friction coefficient}$$

$$n_{dfc} = \left(\frac{0.069 \times 1.98}{0.09 \times 0.156} \right)^2 = 95 \text{ tests for dynamic friction coefficient}$$

The ideal number of test required for this experiment was expected to be 108, because of limitation of resources and time, the experiment was adjusted to 72 tests

Appendix C

Shear box design

A design of the shear box used for the experiments is shown on the following page.

Horizontal. ram frame

Load cell

25.40

101.00

400.00 141.80

225.00

200.00

356.00

100.00

ram

128.00

64.00

128.00

136.00

100.00

65.00

Linear bearing

528.00

Upper platen

72.00

68.00

2" diam.

50.00

46.99

76.00

76.00

366.99

453.99

590.99

25.00

180.00

358.00

bottom platen

Appendix D

Set of steel grooved platens used for the experiments

35° 60° 100° 180^0
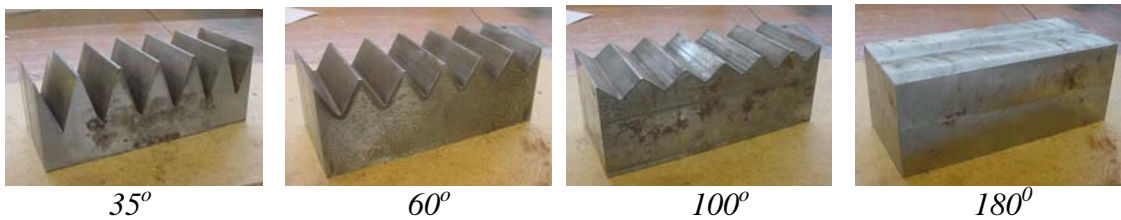
Figure C1. *Set of smooth steel grooved platens. Roughness assumed zero mm.*

35° 60° 100° 180°
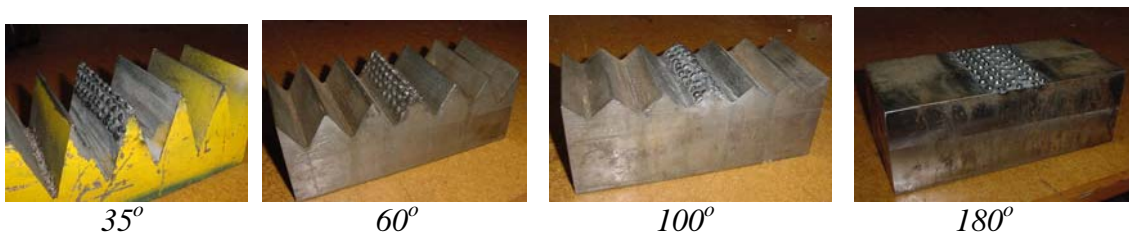
Figure C2. *Set of roughened steel grooved platens with 2.25 mm average asperities*

35° 60° 100° 180°

Figure C3. *Set of roughened steel grooved platens with 4.50 mm average nodules*

Appendix E

Miscellanea

E.1 Photographs of friction coefficient tests

(a)   *(b)*
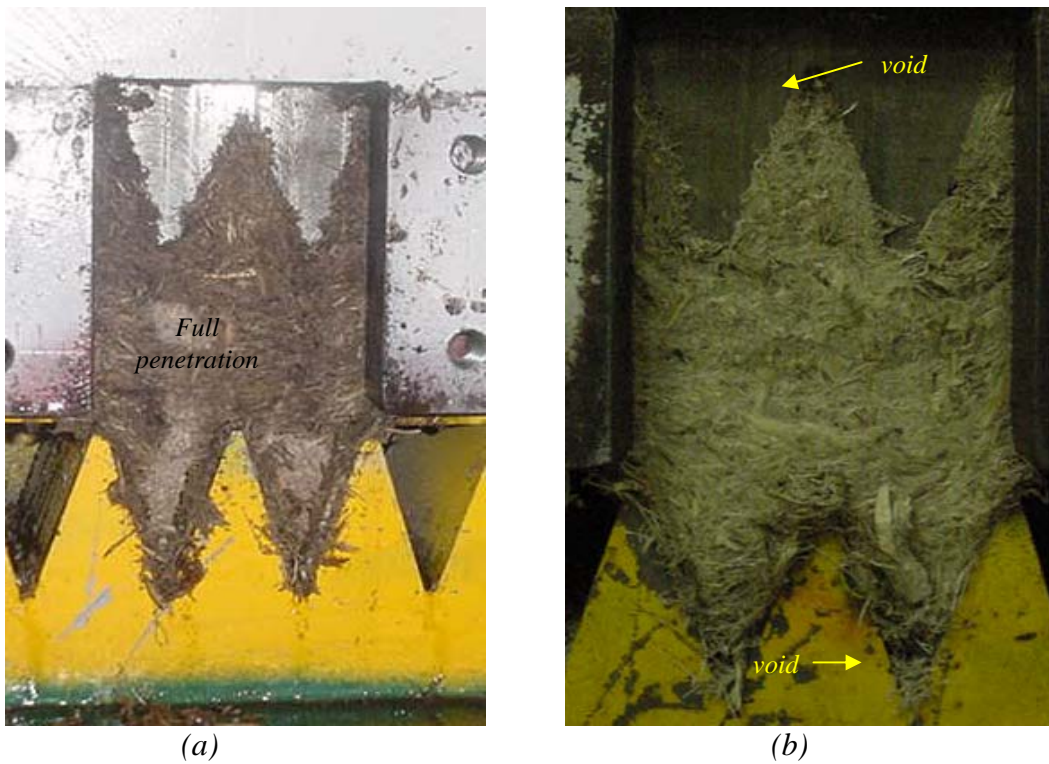
Figure E.1 *Bagasse compacted at 35° groove angle at different levels: (a) 1000 kg/m^3 and (b) 700 kg/m^3.*

Figure E.2 *Grooved platen roughened by nodules. Fibre forming a curvature radius around the nodule; (a) 60° and (b) 35°.*

Figure E.3 *(a) Traces of the nodules indented in bagasse without signs of causing ploughing. (b) Platen roughened with nodules after being pushed about 14 mm.*

(a)   (b)

Figure E.4 *(a) Flat smooth platen pushed at 1000 kg/m³. (b) Flat roughened platen pushed at 700 kg/m³.*

(a)   (b)

Figure E.5 *(a) Flat platen with nodules pushed at 1000 kg/m. (b) Platen with asperities showing fibre attached around the roughened flank of the teeth*
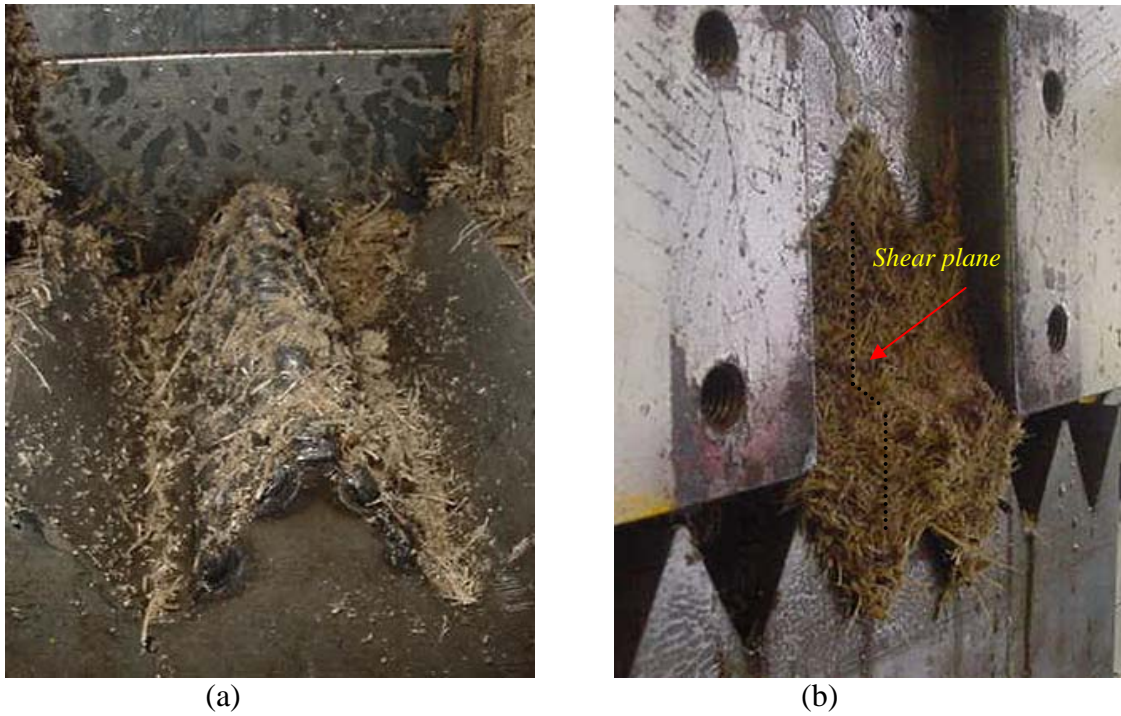
Figure E.6 *(a) Roughened platens after having taken the bagasse out. (b) Shear test for internal shear coefficient. Test run without scraper.*
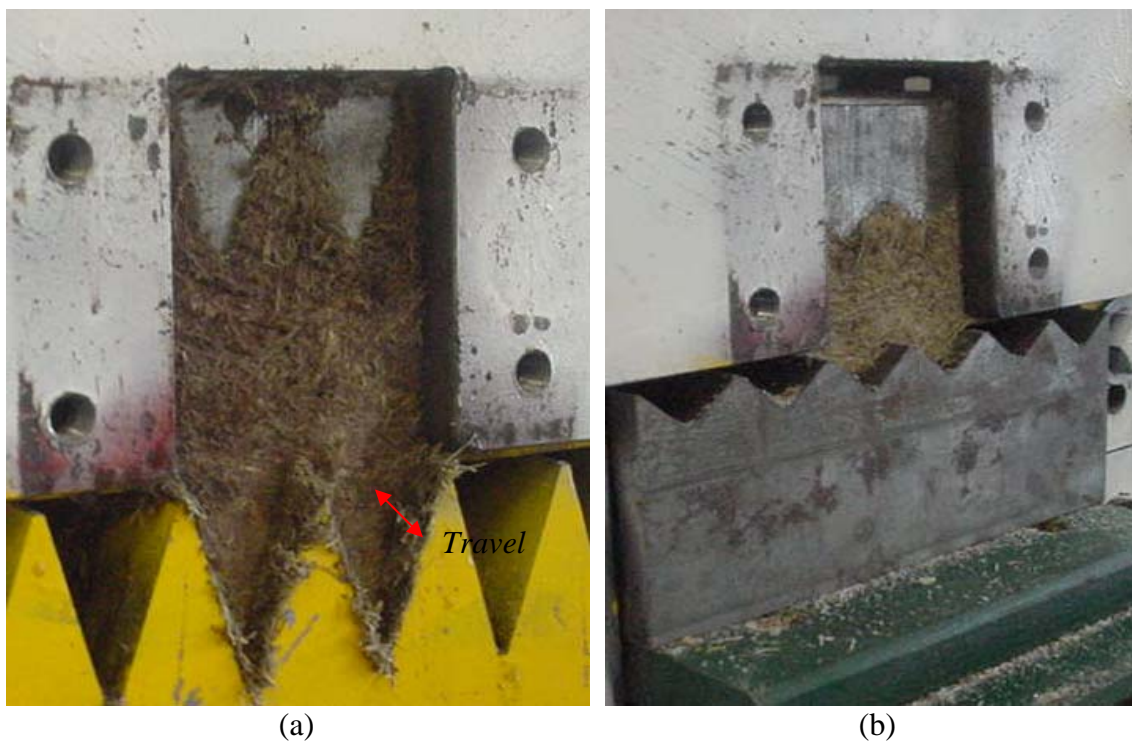
Figure 6.7 *Mass of bagasse fixed. Platen pushed to cause shear stress at the interface friction. (a) smooth surface, 35°, 1000 kg/m^3; (b) smooth surface, 100°, 700 kg/m^3.*

Appendix F

Laboratory measurements

The following two sets of data have been recorded for measurements of tangential force, compressive force, and fibre contained in bagasse:

1.   Bagasse fibre analysis
2.   Shear box test data

Can Fibre Analysis Sheet

Date: 17 Nov, 2004   Material: Bagasse

First can N₀	B1	Second Can N₀	3A
Sample mass (g)	196,2	Sample mass (g)	200,0
Dry mass (g)	1414,7	Dry mass (g)	1399,2
1st check weight (g)	1411,2	1st check weight (g)	1398,7
2nd check weight (g)	1411,1	2nd check weight (g)	1398,7
3rd check weight (g)		3rd check weight (g)	
4th check weight (g)		4th check weight (g)	
Mass of hot, dry can (g)	1323,4	Mass of hot, dry can (g)	1307,4
Mass of fibre (g)	87,7	Mass of fibre (g)	91,3
Fibre fraction (-)	0,447	Fibre fraction (-)	0,457
Average fibre fraction		0,452	

Date: 18 Nov, 2004   Material: Bagasse

First can N₀	B1	Second Can N₀	3A
Sample mass (g)	200,0	Sample mass (g)	200,0
Dry mass (g)	1422,3	Dry mass (g)	1396,9
1st check weight (g)	1412,6	1st check weight (g)	1396,4
2nd check weight (g)	1412,0	2nd check weight (g)	1396,4
3rd check weight (g)	1411,8	3rd check weight (g)	
4th check weight (g)	1411,8	4th check weight (g)	
Mass of hot, dry can (g)	1323,4	Mass of hot, dry can (g)	1307,4
Mass of fibre (g)	88,4	Mass of fibre (g)	89,0
Fibre fraction (-)	0,442	Fibre fraction (-)	0,445
Average fibre fraction		0,444	

Date: 19 Nov, 2004   Material: Bagasse

First can N₀	3A	Second Can N₀	B1
Sample mass (g)	200,0	Sample mass (g)	200,0
Dry mass (g)	1406,4	Dry mass (g)	1461,4
1st check weight (g)	1397,4	1st check weight (g)	1413,3
2nd check weight (g)	1396,7	2nd check weight (g)	1413,3
3rd check weight (g)	1396,6	3rd check weight (g)	
4th check weight (g)		4th check weight (g)	
Mass of hot, dry can (g)	1307,4	Mass of hot, dry can (g)	1323,3
Mass of fibre (g)	89,2	Mass of fibre (g)	90,0
Fibre fraction (-)	0,446	Fibre fraction (-)	0,45
Average fibre fraction		0,448	

JCU
Mechanical Eng.
Department

Can Fibre Analysis Sheet

Date: _22, Nov. 2004_   Material: _Bagasse_

First can N$_o$	3A	Second Can N$_o$	B1
Sample mass (g)	200,0	Sample mass (g)	200,0
Dry mass (g)	1404,4	Dry mass (g)	1413,0
1st check weight (g)	1347,9	1st check weight (g)	1412,2
2nd check weight (g)	1397,8	2nd check weight (g)	1412,2
3rd check weight (g)	1397,8	3rd check weight (g)	1412,2
4th check weight (g)		4th check weight (g)	
Mass of hot, dry can (g)	1307,4	Mass of hot, dry can (g)	1323,4
Mass of fibre (g)	90,4	Mass of fibre (g)	88,8
Fibre fraction (-)	0,452	Fibre fraction (-)	0,444
Average fibre fraction		0,448	

Date: _23 Nov. 2004_   Material: _Bagasse_

First can N$_o$	3A	Second Can N$_o$	B1
Sample mass (g)	200,0	Sample mass (g)	200,0
Dry mass (g)	1397,6	Dry mass (g)	1414,7
1st check weight (g)	1397,7	1st check weight (g)	1415,3
2nd check weight (g)		2nd check weight (g)	1415,3
3rd check weight (g)		3rd check weight (g)	
4th check weight (g)		4th check weight (g)	
Mass of hot, dry can (g)	1307,4	Mass of hot, dry can (g)	1323,4
Mass of fibre (g)	90,3	Mass of fibre (g)	91,9
Fibre fraction (-)	0,452	Fibre fraction (-)	0,458
Average fibre fraction		0,455	

Date: _24 Nov. 2004_   Material: _Bagasse_

First can N$_o$	3A	Second Can N$_o$	B1
Sample mass (g)	200,0	Sample mass (g)	200,0
Dry mass (g)	1398,5	Dry mass (g)	1413,9
1st check weight (g)	1398,1	1st check weight (g)	1413,6
2nd check weight (g)	1397,9	2nd check weight (g)	1413,5
3rd check weight (g)		3rd check weight (g)	
4th check weight (g)		4th check weight (g)	
Mass of hot, dry can (g)	1307,4	Mass of hot, dry can (g)	1323,4
Mass of fibre (g)	90,5	Mass of fibre (g)	90,1
Fibre fraction (-)	0,453	Fibre fraction (-)	0,451
Average fibre fraction		0,452	

JCU
Mechanical Eng.
Department

Can Fibre Analysis Sheet

Date: _25 Nov. 2004_   Material: _Bagasse_

First can N$_o$	3A	Second Can N$_o$	B1
Sample mass (g)	200,0	Sample mass (g)	200,0
Dry mass (g)	1400,7	Dry mass (g)	1412,4
1st check weight (g)	1400,7	1st check weight (g)	1412,4
2nd check weight (g)		2nd check weight (g)	
3rd check weight (g)		3rd check weight (g)	
4th check weight (g)		4th check weight (g)	
Mass of hot, dry can (g)	1309,1	Mass of hot, dry can (g)	1321,5
Mass of fibre (g)	91,6	Mass of fibre (g)	90,9
Fibre fraction (-)	0,458	Fibre fraction (-)	0,455
Average fibre fraction		0,456	

Date: _26 Nov. 2004_   Material: _Bagasse_

First can N$_o$	3A	Second Can N$_o$	B1
Sample mass (g)	200,0	Sample mass (g)	200,0
Dry mass (g)	1399,4	Dry mass (g)	1412,2
1st check weight (g)	1399,3	1st check weight (g)	1411,5
2nd check weight (g)		2nd check weight (g)	1411,5
3rd check weight (g)		3rd check weight (g)	
4th check weight (g)	1309,3	4th check weight (g)	
Mass of hot, dry can (g)	90,0	Mass of hot, dry can (g)	1321,7
Mass of fibre (g)	0,45	Mass of fibre (g)	89,8
Fibre fraction (-)		Fibre fraction (-)	0,449
Average fibre fraction		0,45	

Date: _24 Nov. 2004_   Material: _Bagasse_

First can N$_o$	3A	Second Can N$_o$	B1
Sample mass (g)	200,0	Sample mass (g)	200,0
Dry mass (g)	1402,4	Dry mass (g)	1406,1
1st check weight (g)	1400,3	1st check weight (g)	1406,1
2nd check weight (g)	1400,0	2nd check weight (g)	
3rd check weight (g)	1400,0	3rd check weight (g)	
4th check weight (g)		4th check weight (g)	
Mass of hot, dry can (g)	1309,2	Mass of hot, dry can (g)	1321,6
Mass of fibre (g)	90,8	Mass of fibre (g)	84,5
Fibre fraction (-)	0,454	Fibre fraction (-)	0,423
Average fibre fraction		0,438	

JCU
Mechanical Eng.
Department

Can Fibre Analysis Sheet

Date: 30 Nov. 2004   Material: Bagasse

First can N$_0$	3A	Second Can N$_0$	B1
Sample mass (g)	200,0	Sample mass (g)	200,0
Dry mass (g)	1396,9	Dry mass (g)	1407,6
1st check weight (g)	1394,6	1st check weight (g)	1407,5
2nd check weight (g)	1394,5	2nd check weight (g)	
3rd check weight (g)		3rd check weight (g)	
4th check weight (g)		4th check weight (g)	
Mass of hot, dry can (g)	1309,1	Mass of hot, dry can (g)	1321,6
Mass of fibre (g)	85,4	Mass of fibre (g)	85,9
Fibre fraction (-)	0,427	Fibre fraction (-)	0,428
Average fibre fraction		0,428	

Date: 01 Dic, 2004   Material: Bagasse

First can N$_0$	3A	Second Can N$_0$	B1
Sample mass (g)	200,0	Sample mass (g)	196,0
Dry mass (g)	1396,7	Dry mass (g)	1411,5
1st check weight (g)	1396,4	1st check weight (g)	1411,4
2nd check weight (g)	1396,4	2nd check weight (g)	
3rd check weight (g)		3rd check weight (g)	
4th check weight (g)		4th check weight (g)	
Mass of hot, dry can (g)	1309,3	Mass of hot, dry can (g)	1321,6
Mass of fibre (g)	87,1	Mass of fibre (g)	89,8
Fibre fraction (-)	0,436	Fibre fraction (-)	0,458
Average fibre fraction		0,447	

Date: 02 Dic, 2004   Material: Bagasse

First can N$_0$	3A	Second Can N$_0$	3A
Sample mass (g)	200,0	Sample mass (g)	200,0
Dry mass (g)	1398,0	Dry mass (g)	1401,5
1st check weight (g)	1397,6	1st check weight (g)	1401,4
2nd check weight (g)	1397,7	2nd check weight (g)	
3rd check weight (g)		3rd check weight (g)	
4th check weight (g)		4th check weight (g)	
Mass of hot, dry can (g)	1309,3	Mass of hot, dry can (g)	1309,3
Mass of fibre (g)	88,4	Mass of fibre (g)	92,1
Fibre fraction (-)	0,442	Fibre fraction (-)	0,461
Average fibre fraction		0,451	

Can Fibre Analysis Sheet

Date: __14 Dic 2004__   Material: __Bagasse__

First can N$_o$	51	Second Can N$_o$	3A
Sample mass (g)	200,0	Sample mass (g)	200,0
Dry mass (g)	1409,1	Dry mass (g)	1393,5
1st check weight (g)	1409,7	1st check weight (g)	1393,1
2nd check weight (g)	1409,6	2nd check weight (g)	1393,0
3rd check weight (g)		3rd check weight (g)	
4th check weight (g)		4th check weight (g)	
Mass of hot, dry can (g)	1321,8	Mass of hot, dry can (g)	1309,2
Mass of fibre (g)	87,8	Mass of fibre (g)	83,8
Fibre fraction (-)	0,439	Fibre fraction (-)	0,419
Average fibre fraction		0,429	

Date: _____   Material: _____

First can N$_o$		Second Can N$_o$	
Sample mass (g)		Sample mass (g)	
Dry mass (g)		Dry mass (g)	
1st check weight (g)		1st check weight (g)	
2nd check weight (g)		2nd check weight (g)	
3rd check weight (g)		3rd check weight (g)	
4th check weight (g)		4th check weight (g)	
Mass of hot, dry can (g)		Mass of hot, dry can (g)	
Mass of fibre (g)		Mass of fibre (g)	
Fibre fraction (-)		Fibre fraction (-)	
Average fibre fraction			

Date: _____   Material: _____

First can N$_o$		Second Can N$_o$	
Sample mass (g)		Sample mass (g)	
Dry mass (g)		Dry mass (g)	
1st check weight (g)		1st check weight (g)	
2nd check weight (g)		2nd check weight (g)	
3rd check weight (g)		3rd check weight (g)	
4th check weight (g)		4th check weight (g)	
Mass of hot, dry can (g)		Mass of hot, dry can (g)	
Mass of fibre (g)		Mass of fibre (g)	
Fibre fraction (-)		Fibre fraction (-)	
Average fibre fraction			

SHEAR BOX TEST DATA

Location:	MATERIAL TESTING LABORATORY					Combination test:	R - G - C		
Operator:	W. F. VILLARREAL					Replications:	02		
Type of test:	Shear tests					Date:	November 2004		
Bagasse description:	Final Bagasse					Test box area:	7605,0 mm²		
Type of specimen:						Linear Bearing:	THK - SHS65L		

Machine:	MTS	capacity:	1000,00	kN	Fibre density	1530,0	kg/m3	Sheet #
		Rate displact:	1,00	mm/s	Set Openinig, S	40,0	mm	01
Cyld.	ENERPAC	capacity:	20,00	ton	Fibre	~ 45,0	%	
pump:		Rate displact:	9,0	mm/s	Moisture	~ 52,0	%	

Test order No	Day of the test	Combination	Vertical displcm. (mm)	Horzntl displcm. (mm)	Vertical Load (kN)	Horizntl Load (kN)	Static firction coeff.	Shear coeff.	Mass of Bagasse, (g)	Remarks
01	2/11	1000-035	76,10	10,0	231,196	34,50		—	1442,0	B: smooth
02	22/11	700-035	103,0	10,0	105,424	26,00		—	1014,0	@ 400 kg/m3
03	22/11	400-035	40,98	10,0	31,056	15,00		—	580,0	Bagasse no
04	22/11	700-035	102,98	10,0	108,645	27,60		—	1014,0	saturated
05	22/11	400-035	45,81	12,0	32,247	9,50		—	580,0	@ 700 kg/m3
06	22/11	1000-035	82,02	12,0	293,994	60,00		—	1442,0	Bagasse is
07	23/11	400-0100	78,51	13,0	9,196	3,00		—	348,0	saturated
08	23/11	1000-0100	94,48	13,0	267,393	44,00		—	870,0	@ 1000 kg/m3
09	23/11	700-0100	51,98	13,0	83,965	26,00		—	609,0	Bagasse is
10	23/11	1000-0100	89,86	13,0	266,963	47,50		—	870,0	dried out
11	23/11	700-0100	47,92	13,0	89,969	21,00			609,0	
12	23/11	400-0100	31,61	13,0	9,472	2,00		—	348,0	Scraper is
13	24/11	1000-060	127,52	8,0	269,379	71,50		—	1090,0	installed
14	24/11	400-060	61,97	12,0	32,325	11,50		—	436,0	for friction
15	24/11	700-060	72,39	12,0	85,035	27,00		—	763,0	coefficient
16	24/11	400-060	51,98	12,0	16,756	9,10		—	436,0	tests.
17	24/11	1000-060	116,97	10,0	291,995	56,00		—	1090,0	
18	24/11	700-060	64,23	12,0	83,372	25,00		—	763,0	
19	25/11	700-0180	51,97	12,0	111,712	16,00		—	466,0	
20	25/11	1000-0180	71,98	12,0	320,946	38,80		—	666,0	
21	25/11	400-0180	85,97	12,0	6,894	10,50		—	266,0	
22	25/11	400-0180	74,43	12,0	6,824	9,50		—	266,0	
23	25/11	700-0180	69,99	12,0	109,225	20,50		—	466,0	
24	25/11	1000-0180	73,98	12,0	335,187	44,10		—	666,0	

SHEAR BOX TEST DATA

Location:	MATERIAL TESTING LABORATORY						Combination test:	L-G-C	
Operator:	W. F. VILLARREAL						Replications:	02	
Type of test:	Shear tests						Date:	NOV - DIC 2004	
Bagasse description:	Final bagasse						Test box area:	7605,0 mm2	
Type of specimen:							Linear Bearing:	THK-SHS65L	

Machine:	MTS	capacity:	1000,0	kN	Fibre density	1530,0	kg/m3	Sheet #
		Rate displact:	1,00	mm/s	Set Openinig, S	40,00	mm	02
Cyld. pump:	ENERPAC	capacity:	20,0	ton	Fibre ~	45,00	%	
		Rate displact:	9,00	mm/s	Moisture	52,00	%	

Test order No	Day of the test	Combi-nation	Vertical displcm. (mm)	Horzntl displcm. (mm)	Vertical Load (kN)	Horizntl Load (kN)	Static firction coeff.	Shear coeff.	Mass of Bagasse, (g)	Remarks
25	26/11	700-N60	73,99	12,0	85,102	28,00		-	790,0	N: nodule
26	26/11	400-N60	43,47	12,0	30,267	13,10		-	450,0	scraper
27	26/11	400-N60	46,98	12,0	23,291	10,50		-	450,0	installed
28	26/11	1000-N60	126,97	12,0	277,509	56,00		-	1130,0	during test
29	26/11	1000-N60	120,98	12,0	267,203	54,10		-	1130,0	for friction
30	26/11	700-N60	69,98	12,0	84,836	27,50		-	790,0	Coeffcient
31	29/11	400-N35	60,34	12,0	35,905	11,80		-	574,0	.
32	29/11	700-N35	96,87	12,0	80,539	30,00		-	1005,0	
33	29/11	1000-N35	68,00	12,0	236,468	62,00		-	1436,0	Tests at
34	29/11	700-N35	92,00	10,0	89,875	29,90		-	1005,0	1000 kg/m3
35	29/11	1000-N35	72,39	10,0	248,085	63,30		-	1436,0	were pre-
36	29/11	400-N35	47,93	12,0	36,726	10,60		-	574,0	compressed
37	30/11	700-N100	61,48	12,0	90,588	25,40		-	649,0	
38	30/11	400-N100	71,34	14,0	11,805	13,20		-	371,0	
39	30/11	400-N100	61,47	14,0	12,46	7,90		-	371,0	
40	30/11	1000-N100	92,78	14,0	290,047	50,00		✓	922,0	
41	30/11	1000-N100	90,48	14,0	289,187	45,50		-	922,0	
42	30/11	700-N100	64,23	14,0	90,588	25,40		-	649,0	
43	01/12	400-N80	66,00	14,0	9,034	5,50		-	281,0	
44	01/12	700-N80	74,43	15,0	121,884	19,80		-	493,0	
45	01/12	1000-N80	73,95	14,0	289,779	41,90		-	704,0	
46	01/12	700-N80	71,98	14,0	112,598	17,70		-	493,0	
47	01/12	1000-N80	80,54	14,0	301,300	43,60		-	704,0	
48	01/12	400-N80	64,23	14,0	8,876	5,60		-	281,0	

JCU
Mechanical Engineering
Departm.

SHEAR BOX TEST DATA

Location:	MATERIAL TESTING LABORATORY					Combination test:	R - G - C	
Operator:	W.F. JILLBREAL					Replications:	O2	
Type of test:	Shear Tests					Date:	DiCember 2004	
Bagasse description:	Final Bagasse					Test box area:	7605,0 mm²	
Type of specimen:						Linear Bearing: THK · SHS GSL		

Machine:	MTS	capacity:	1000,0	kN	Fibre density	1530,0°	kg/m3	Sheet #
		Rate displact:	1,00	mm/s	Set Openinig, S	40,00	mm	03
Cyld. pump:	ENERPAC	capacity:	20,00	ton	Fibre ~ 46,0		%	
		Rate displact:	9,00	mm/s	Moisture 53,0		%	

Test order No	Day of the test	Combi-nation	Vertical displcm. (mm)	Horzntl displcm. (mm)	Vertical Load (kN)	Horizntl Load (kN)	Static firction coeff.	Shear coeff.	Mass of Bagasse, (g)	Remarks
49	02/12	400-a180	68,31	12,0	8,542	6,50		~	281,0	a. aspevity
50	02/12	400-a180	66,28	12,0	9,800	6,50		~	281,0	Non-Saturated
51	02/12	700-a180	70,35	12,0	119,045	21,40		~	443,0	Saturated Bg
52	02/12	1000a180	71,98	12,0	248,555	43,70		-	704,0	Nearly dried
53	02/12	700-a180	71,98	12,0	104,988	24,00		-	443,0	
54	02/12	1000a180	71,98	12,0	203,115	47,00		-	704,0	
55	03/12	400-a100	76,46	12,0	9,411	7,00		~	344,0	.
56	03/12	400-a100	66,28	12,0	7,161	6,00		~	344,0	
57	03/12	700-a100	63,47	12,0	65,748	19,00		-	603,0	
58	03/12	1000a100	84,48	12,0	207,445	42,00		-	861,0	
59	03/12	1000-a100	75,48	12,0	253,448	42,00		~	861,0	
60	03/12	700-a100	56,08	12,0	69,994	19,50		-	603,0	
61	06/12	1000-a35	76,48	12,0	251,136	65,50		-	1449,0	
62	06/12	700-a35	101,98	12,0	100,104	32,00		-	1014,0	
63	06/12	400-a35	39,77	12,0	30,518	11,15		-	580,0	
64	06/12	1000-a35	75,77	12,0	234,124	60,00		-	1449,0	
65	06/12	400-a35	37,72	12,0	29,820	11,25		-	580,0	
66	06/12	700-a35	99,91	12,0	92,164	29,00		-	1014,0	
67	07/12	1000-a60	120,97	14,0	241,136	50,50		-	1095,0	
68	07/12	1000-a60	115,22	14,0	234,895	52,0		-	1095,0	
69	07/12	400-a60	43,34	14,0	13,878	10,50		-	738,0	
70	07/12	400-a60	48,97	14,0	16,321	9,00		~	438,0	
71	07/12	700-a60	64,27	14,0	78,696	24,50		-	767,0	
72	07/12	700-a60	68,28	14,0	80,234	26,50		-	767,0	

JCU
Mechanical Engineering
Departm.

SHEAR BOX TEST DATA

Location:	MATERIAL TESTING LABORATORY					Combination test:	Compretion			
Operator:	W.F. VILLARREAL					Replications:	0 2			
Type of test:	shear tests					Date:				
Bagasse description:	final bagasse					Test box area: 7605,0 mm				
Type of specimen:						Linear Bearing: THK -SHS 65L				

Machine: MTS	capacity: 1000,0	kN	Fibre density		kg/m3	Sheet #
	Rate displact: 1,00	mm/s	Set Openinig, S	40,0	mm	04
Cyld. pump: ENERPAC	capacity: 20,0	ton	Fibre ~ 44,0		%	
	Rate displact: 9,00	mm/s	Moisture 13,0		%	

Test order No	Day of the test	Combi-nation	Vertical displcm. (mm)	Horzntl displcm. (mm)	Vertical Load (kN)	Horizntl Load (kN)	Static friction coeff.	Shear coeff.	Mass of Bagasse, (g)	Remarks
01	29 11	400+0	52,00	12,0	16,585	8,50	–		438,0	No- scraper
02	28 11	1000-60	124,00	12,0	266,679	28,50	–		1095,0	No scraper
03	29 11	700-60	67,316	12,0	79,858	15,20	–		767,0	No scraper
04	01 12	1000 60	98,868	12,0	288,919	26,50	–		1095,0	No scraper
05	01 12	700-60	65,484	12,0	94,039	16,50	–		767,0	No scraper
06	01 12	400-60	39,763	12,0	12,058	8,40	–		438,0	No scraper
07	08 12	700-60	24,631	14,0	83,342	24,00		–	390,0	
08	8 12	400-60	39,346	14,0	18,215	6,50		–	223,0	holding 45-
09	08 12	1000-60	63,983	14,0	225,165	71,00		–	557,0	perities Cte.
10	08 12	700-100	75,481	14,0	83,337	24,00		–	312,0	fibre @
11	08 12	400-100	55,479	14,0	15,317	6,20		–	178,0	11% moisture
12	08 12	1000-100	115,227	14,0	205,078	57,50		–	445,0	↑
13	08 12	700-180	74,435	14,0	68,767	23,00		–	261,0	
14	08 12	400-180	74,436	14,0	14,857	4,50		–	149,0	↓
15	08 12	1000-180	91,971	14,0	282,706	76,00		–	373,0	
17	09 12	700-60	40,340	14,0	98,259	24,50	–		390,0	shear test
18	09 12	1000 60	88,711	14,0	260,794	84,00	–		557,0	with mois-
19	09 12	400-60	37,096	14,0	27,99	9,50	–		223,0	ture @ 11%

JCU
Mechanical Engineering
Departm.

SHEAR BOX TEST DATA

Location:	MATERIAL TESTING LABORATORY					Combination test:	R- G- C	
Operator:	W. F. VILLORILEAL					Replications:	12	
Type of test:	Shear test					Date:	December 2004	
Bagasse description:	final bagasse					Test box area:	7605,0 mm	
Type of specimen:						Linear Bearing:	THK SHS 65L	

Machine: MTS	capacity: 1000,0		kN	Fibre density	1530,0	kg/m3	Sheet #
	Rate displact: 1,0		mm/s	Set Openinig, S	40,00	mm	05
Cyld. pump: Enerpac	capacity: 20,0		ton	Fibre ~ 48		%	
	Rate displact: 9,00		mm/s	Moisture ~ 52		%	

Test order No	Day of the test	Combi-nation	Vertical displcm. (mm)	Horzntl displcm. (mm)	Vertical Load (kN)	Horizntl Load (kN)	Static firction coeff.	Shear coeff.	Mass of Bagasse, (g)	Remarks
01	13/12	700-a/00	58,121	13,0	63,907	21,00		—	628,0	Data re-
02	13/12	700-a/00	62.197	13,0	72,857	22,50		—	628,0	quired for
03	13/12	700-a/00	60.157	13,0	77,713	22,50		—	628,0	applying
04	13/12	700-a/00	61.968	13,0	76,262	22,00		—	628,0	Box-Behnken
05	13/12	700-a/00	70.553	13,0	69,230	22,50		—	628,0	design.
06	13/12	700-a/00	56.079	13,0	79,315	22,60		—	628,0	(Additional)
07	13/12	700-a/00	57.478	13,0	68,736	22,00		—	628,0	
08	13/12	700-a/00	55.478	13,0	72,384	20,60		—	628,0	
09	13/12	700-a/00	59.481	13,0	80,738	23,00		—	628,0	
10	13/12	700-a/00	57.480	13,0	91,038	22,10		—	628,0	
11	13/12	700-c/00	62.975	13,0	96,407	24,50		—	628,0	
12	13/12	700-c/00	57.471	13,0	72,812	20,50		—	630,0	
13	15/12	700-a/00	61,479	13,0	82,387	22,30		—	630,0	
14	15/12	700-c/00	56,079	13,0	74,357	22,00				